# Doctoral Thesis
# (博士論文)

# Interfacial Properties, Phase and Rheological Behavior of Nonionic Fluorinated Amphiphiles in Water
# (非イオンフッ素系両親媒性物質の水溶液系における界面物性、相挙動およびレオロジー特性の研究)


Graduate School of Environment and Information Sciences
Yokohama National University
横浜国立大学大学院　環境情報学府

Suraj Chandra Sharma
スラジ　チャンドラ　シャーマ




March 2007
平成19年3月

# Interfacial Properties, Phase and Rheological Behavior of Nonionic Fluorinated Amphiphiles in Water

# (非イオンフッ素系両親媒性物質の水溶液系における界面物性、相挙動およびレオロジー特性の研究)

**Doctoral Thesis**

**(博士論文)**

**Suraj Chandra Sharma**

スラジ　チャンドラ　シャーマ

**Student Number: 04TB903**

**Academic Supervisor:**

**Associate Prof. Kenji Aramaki**

**Graduate School of Environment and Information Sciences**

**Yokohama National University**

**横浜国立大学大学院　環境情報学府**

**March 2007**

**平成 19 年 3 月**

## Contents

## Abstract

This thesis covers the extensive investigation on the interfacial properties of aqueous solutions of fluorinated amphiphiles, phase behavior of fluorinated amphiphiles or mixed fluorinated amphiphiles in water and temperature induced viscosity growth in a water-surfactant binary system of a nonionic fluorinated surfactant at various concentrations.

Phase behavior and surface tension of aqueous solutions of fluorinated random copolymers [perfluorinatedalkylacrylate]–[poly(ethyleneoxide)methacrylate], [$C_m$Rf-acrylate]-[$EO_n$-methacrylate] with fluroalkyl carbon number, *m* and number of ethyleneoxide unit, *n* were investigated as a function of composition and different combinations of *m* and *n*. Isotropic solutions are formed at lower temperatures over wide concentration range of copolymer but at higher temperature phase separation occurs. The cloud point of copolymer decreases with decreasing *n* as well as *m*, and also with decreasing the number of poly(ethyleneoxide)methacrylate chain per perfluorinatedalkylacrylate chain, suggesting that the copolymers become more hydrophobic on decreasing *m* and *n*. Equilibrium and dynamic surface tension measurements show that copolymers become increasingly surface active as *m* as well as *n* decrease but the adsorption at the air / water interface is very slow due to bulkiness of the molecules. No clear evidence of the formation of micellar aggregates could be obtained from surface tension-composition curves.

The equilibrium, dynamic surface tensions and surface dilatational elasticity of aqueous solutions of nonionic fluorocarbon surfactant are reported. The critical micellar concentration, CMC (0.023mM) and equilibrium surface tension (24.6mN.$m^{-1}$) at CMC were measured by Wilhelmy plate method for aqueous solution of $C_8F_{17}SO_2N(C_3H_7)(C_2H_4O)_nH$ ($n = 20$), abbreviated as EF122A. The surface tension decay is slower for $C_8F_{17}SO_2N(C_3H_7)(C_2H_4O)_nH$ ($n = 10$) system, abbreviated as EF122B compared to the EF122A system over short time region, which indicates the slow transport of the surfactant molecules to the surface. The relaxation time for surface tension decay is estimated by fitting a series of exponentials to the dynamic surface tension data and it decreases with temperature for EF122A. Slow exchange of monomers between bulk and interface is reflected in the high elasticity value of the

air-liquid interface for EF122B compared with EF122A within measured frequency window (0.125-1.25Hz).

The phase behavior and formation of self-assemblies in the ternary water / fluorinated surfactant ($C_8F_{17}EO_{10}$) / hydrophobic fluorinated polymer $(C_3F_6O)_nCOOH$ system have been investigated by means of phase study, small angle X-ray scattering and rheology. Hexagonal ($H_1$), bicontinuous cubic ($V_1$) with Ia3d symmetry and polymer rich lamellar ($L'_\alpha$) are observed in the ternary diagram. $C_8F_{17}EO_{10}$ molecules are dissolved in polymer rich aggregates, whereas $(C_3F_6O)_nCOOH$ molecules are practically insoluble in the surfactant lamellar phase due to packing restrictions. Hence, two types of lamellar phases exist: one with surfactant rich ($L_\alpha$) and the other with polymer rich ($L'_\alpha$) in the water / $C_8F_{17}EO_{10}$ / $(C_3F_6O)_nCOOH$ system. As suggested by rheological measurements, worm-like micelles are present in $C_8F_{17}EO_{10}$ aqueous solutions but a rod-sphere transition takes place by solubilization of $(C_3F_6O)_nCOOH$.

The formation and rheological behavior of a viscoelastic wormlike micellar solution in an aqueous solution of a nonionic fluorinated surfactant, perfluoroalkyl sulfonamide ethoxylate, of structure $C_8F_{17}SO_2N(C_3H_7)(CH_2CH_2O)_{10}H$ was studied. Temperature-induced viscosity growth is observed even at low-surfactant concentration (~1wt%), and viscosity reaches the maximum at a temperature $T_{\eta\text{max}}$. Upon successive increase in the temperature, the viscosity decreases, and ultimately a phase separation occurs. The nonionic fluorinated surfactant forms flexible cylindrical aggregates at low temperature, which undergo continuous one-dimensional growth with increasing temperature, and ultimately, an indication of slight lamellar like structural pattern is observed, which probably comes from the formation of micellar joints or branching. Such changes in the microstructure result in a decrease in the viscosity and stress relaxation time, while the network structure is retained; the trends in the evolution of shear modulus ($G_o$) and relaxation time ($\tau_R$) with temperature are in agreement with this. With increased surfactant concentration, the temperature corresponding to the viscosity maximum ($T_{\eta\text{max}}$) in the temperature-viscosity curve shifts to lower values, and the viscosity at temperatures below or around $T_{\eta\text{max}}$ increases sharply. A viscoelastic solution with Maxwellian type dynamic rheological behavior at low shear-frequency is formed, which is typical of entangled wormlike micelles. Rheological parameters, $\eta_o$ and $G_o$, show scaling relationships with

surfactant concentrations with exponents slightly greater than the values predicted by living-polymer model, but the exponent of $\tau_R$ is in agreement with the theory.

The content of the thesis is based on the following papers:

1. Sharma, S.C.; Acharya, D.P.; Garcia-Roman, M.; Itami, Y.; Kunieda, H. " Phase Behavior and Surface Tensions of Amphiphilic Fluorinated Random Copolymer Aqueous Solutions" *Colloids Surf. A* **2006,** *280*, 140-145, (Chapter 3).
2. Sharma, S.C.; Shrestha, L.K.; Aramaki, K. " Interfacial properties of aqueous nonionic fluorocarbon surfactant solutions" *J. Dispersion Sci. & Technol.* Accepted. (Chapter 4).
3. Sharma, S.C.; Kunieda, H.; Esquena, J.; Rudriguez-Abreu, C. "Phase Behavior and Preparation of Mesoporous Silica in Aqueous Mixtures of Fluorinated Surfactant and Hydrophobic Fluorinated Polymer" *J. Colloid Interface Sci.* **2006**, *299*, 297-304. (Chapter 5).
4. Acharya, D.P.; Sharma, S.C.; Rodriguez-Abreu, C.; Aramaki, K. "Viscoelastic Micellar Solutions in Nonionic Fluorinated Surfactant Systems" *J. Phys. Chem. B* **2006**, 110, 20224-20234. (Chapter 6).

The structure of thesis is shown below.

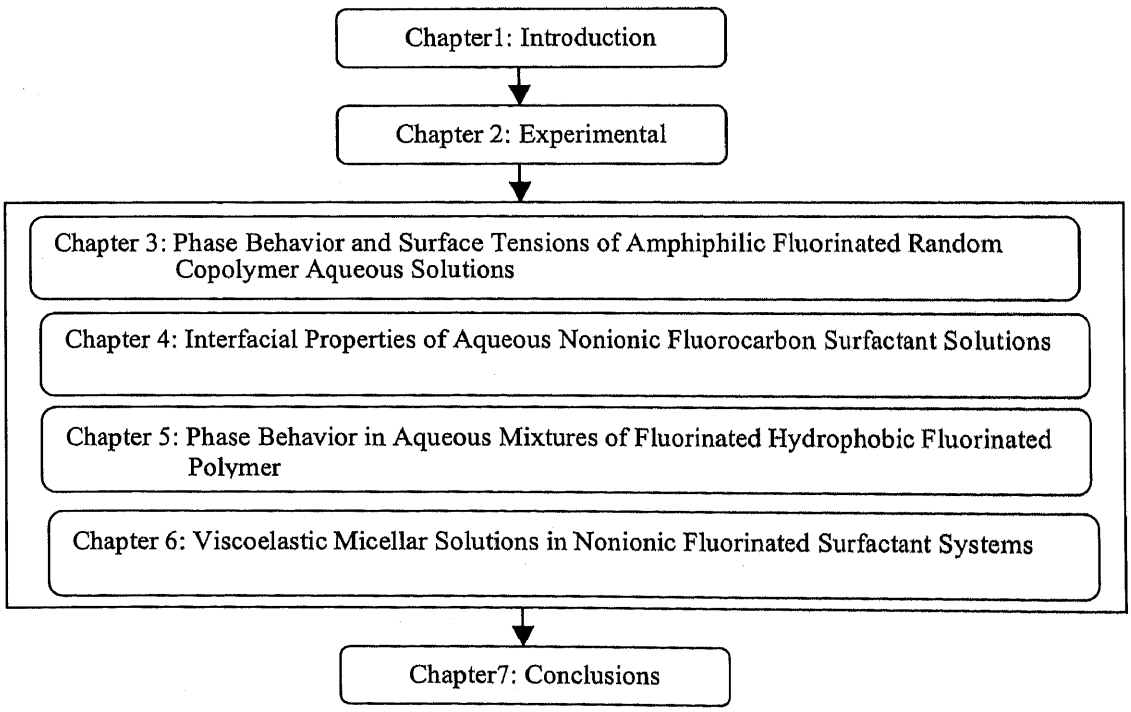

# Chapter 1: Introduction

## 1.1 Amphiphilic molecules and copolymers

Amphiphilic molecules consist of two parts with opposing character. One part is hydrophilic (polar) and the other is hydrophobic (nonpolar). The hydrophobic group is usually a long- chain hydrocarbon covalently bonded to hydrophilic moiety. Due to the presence of these polar and nonpolar parts, amphiphiles can spontaneously adsorb at surfaces or interfaces and hence they are also called surfactants, an abbreviation for surface active agents. Low molecular weight synthetic amphiphiles are called surfactants while large amphiphilic molecules are called polymers.

Amphiphiles are mainly classified on the basis of the charge on the polar head group as follows[1,2]:

1. Anionics: They contain anionic group such as carboxylate, sulfate, sulfonate, phosphate as a polar group coupled with a posititive counterion (cation) such as sodium, potassium, ammonium, calcium and protonated alkyl amines. They are used in greater volume than any other surfactants.
2. Cationics: They contain cationic group coupled with a negative counterion ion (anion). Both amine and quaternary ammonium-based products bearing a halogen atom (Cl, Br) counterion are common. They are used in surface modification due to strong adsorption to most surfaces.
3. Zwitterionics: They contain two oppositely charged groups within single molecule. The cationic group is mostly ammonium ion and anionic varies, although carboxylate is the most common.
4. Nonionics: They contain nonionic polar group such as polyether or polyhydroxyl as a hydrophilic part. The polyether moiety consists of oxyethylene units, formed by polymerization of ethyelene oxide. Ethoxylation is usually carried out under alkaline conditions. Any material containing an active hydrogen can be ethoxylated, but most commonly used starting materials are fatty alcohols, fatty acids, fatty amines and alkylphenols.

Polymers are long molecules consisting of repeating sequences of small units, monomers, connected by covalent chemical bonds. If the monomers are identical, the polymer is called a homopolymer. The polymers that incorporate more than one kind of monomer into their chain are called copolymers. There are three important types of

copolymers. A random copolymer contains a random arrangement of the multiple monomers. A block copolymer contains block of monomers of the same type. Finally, a graft copolymer contains a main chain polymer consisting of one type of monomer with branches made up of other monomers.

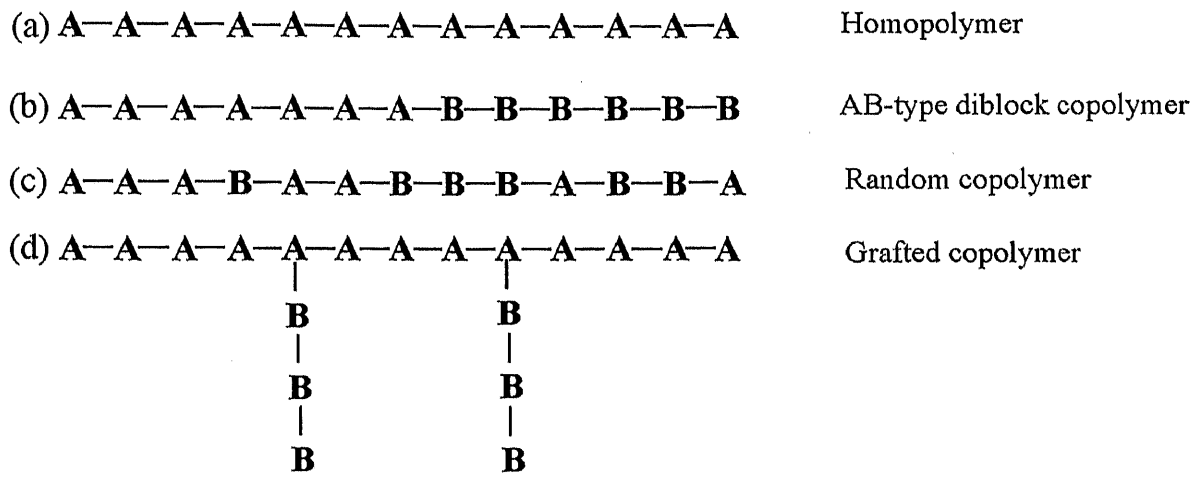


Figure 1-1: Schematic drawing of different types of polymers: (a) homopolymer, $A_{13}$; (b) diblock copolymer, $A_7B_6$; (c) random copolymer, $(A/B)_{13}$; (d) grafted copolymer, $A_{13}B_6$.

**1.2 Fluorinated amphiphiles**

In fluorinated amphiphiles, the hydrophobic part of the molecule contains fluorine. At least one hydrogen atom in the hydrophobic segment of an amphiphile has been replaced by fluorine. Both the extent of fluorination and the position of fluorine atoms in the molecule affect the characteristics of the amphiphle. Hence, fluorinated amphiphiles can be classified as perfluorinated amphiphiles or partially fluorinated amphiphiles. In partially fluorinated amphiphiles, the hydrophobic part of the molecule contains both fluorine and hydrogen atoms while in perfluorinated amphiphiles, all hydrogens in the hydrophobic segment have been replaced by fluorine. The location and the number of fluorine atoms in the partially fluorinated hydrophobe are important. Partially fluorinated amphiphiles with a terminal $CF_3$ group differ in their characteristics from partially fluorinated amphiphiles with a hydrogen-containing terminal group. The presence of fluorine atoms alters the properties of amphiphiles and particularly its hydrophobicity and its critical micellar concentration, CMC[3]. It was reported that for nonionic surfactants one $CF_2$ group is equivalent to $1.7CH_2$ groups[4]. Fluorinated amphiphiles are much more surface active than their hydrocarbon counterparts. Fluorinated amphiphiles can lower the surface tension of aqueous systems to below 20 mN/m and are effective at a low concentration. Only 10ppm of a fluorinated amphiphile may be needed to lower the

surface tension of water to 40 mN/m.The hydrophobic part of the fluorinated amphiphile not only repels water but repels oil and fat as well. Hence, fluorinated amphiphiles exhibit both water and oil repellency when adsorbed on substrates such as textiles or paper. The carbon-fluorine bond is amongst the most stable known covalent bonds with the heat of formation of the C-F bond in $CF_4$ being 486 KJ/mol[5]. This high bond strength is thought to result from an excellent match between the 2s and 2p orbitals of fluorine and the corresponding orbitals of carbon. Fluorine atoms (atomic radius 0.072 nm when covalently bound) are close to the optimum size to shield carbon atoms without steric stress. These factors combine to make fluorocarbon chains very thermally and chemically stable relative to hydrocarbons. The good chemical stability of fluorinated amphiphiles is an important consideration when choosing amphiphiles to operate in harsh environments such as extremes of pH, high temperatures or in combination with strong oxidizing or reducing agents. The main disadvantage with fluorinated amphiphiles, besides high price, is their poor biodegradability. The relatively high price of fluorinated surfactants limits their use to applications where hydrocarbon-based surfactants are inadequate. However, fluorinated surfactants are cost-effective because their high price is compensated by the low concentration needed. Because of their unique properties, fluorinated surfactants are irreplaceable in many applications and justifies Kissa's claim in his 1994 text on the subject that fluorinated surfactants are truly 'super surfactants'[6].

### 1.3 Interfacial phenomena

#### 1.3.1 Adsorption of surfactants at interfaces[1,2]

A fundamental characteristic of surfactants is their tendency to adsorb at interface in an oriented fashion. In dilute solutions of surfactants, the amount of change in any interfacial phenomenon produced by the adsorption of surfactant at the interface is a function of the concentration of surfactant adsorbed at the interface. Thus the efficiency of surfactant is determined by the ratio of surfactant concentration at the interface to that in the bulk (liquid) phase, $C_{interface}$ / $C_{bulk}$. This ratio is determined by the free energy change $\Delta G$ involved in the transfer of a surfactant molecule from the interior of the bulk phase to the interface by the equation $C_{interface}$ / $C_{bulk} = \exp\left(-\Delta G/RT\right)$, where $R$ =1.99cal (or 8.31J) $deg^{-1}mol^{-1}$ and $T$ = absolute temperature; therefore, efficiency is related to the free energy change associated with that transfer. Since the effect of a surfactant on an interfacial phenomenon is a

function of the concentration of surfactant at the interface, we can define the effectiveness of a surfactant in adsorbing at an interface as the maximum concentration that the surfactant can attain at the interface, i. e., the surface concentration of surfactant at surface saturation. The effectiveness of adsorption is related to the interfacial area occupied by the surfactant at the interface, the greater its effectiveness of adsorption. Effectiveness of adsorption, therefore, depends on the structural groupings in the surfactant molecule and its orientation at the interface. Another parameter characterizing the performance of surfactants, important in high-speed interfacial phenomena such as wetting and spreading, is the rate of adsorption of the surfactant at the relevant interface(s).

The surface tension of water is depressed remarkably with the addition of a surfactant at low (usually less than 1 wt%) concentrations. The change of surface tension by dissolution surfactants originates from the adsorption of surfactant molecules onto the surface of the solution. The amount of surfactant adsorbed per unit area of interface can be readily be calculated by use of the Gibbs adsorption equation. The Gibbs adsorption equation, in its most general form is given as

$$d\gamma = -\sum_i \Gamma_i d\mu_i \tag{1-1}$$

where $d\gamma$ is the change in surface or interfacial tension of the solvent, $\Gamma_i$ is the surface excess concentration of any component of the system, $d\mu_i$ is the change in chemical potential of any component of the system. This equation is fundamental to all adsorption processes where monolayers are formed. At equilibrium between the interfacial and bulk phase concentrations, $d\mu_i = RTd\ln a_i$, where $a_i$ is the activity of any component in the bulk (liquid) phase, $R$ is gas constant, and $T$ is the absolute temperature. Thus,

$$d\gamma = -RT\sum_i \Gamma_i d\ln a_i \tag{1-2}$$

$$= RT\sum_i \Gamma_i d\ln x_i f_i \tag{1-3}$$

$$= RT\sum_i \Gamma_i d(\ln x_i + \ln f_i) \tag{1-4}$$

where $x_i$ is the mole fraction of any component in the bulk phase and $f_i$ its activity coefficient. For solutions consisting of the solvent and only one solute, $d\gamma = -RT(\Gamma_o d\ln a_o + \Gamma_1 d\ln a_1)$, where subscripts 0 and 1 refers to the solvent and the solute, respectively. For dilute solutions ($10^{-2}M$) or less containing only one

nondissociating surface-active solute, the activity of the solvent and the activity coefficient of the solute can both be considered to be constant and the mole fraction of the solute $x_1$ may be replaced by its molar concentration $C_1$. Thus

$$d\gamma = -RT\Gamma_1 d\ln C_1 \qquad (1\text{-}5)$$

Thus, the surfactant adsorption is obtained from the slope of a plot of the surface tension versus the logarithm of concentration as shown in Figure 1-2.

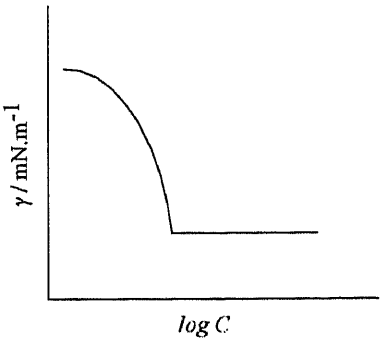


Figure 1-2: A typical plot of surface tension versus concentration of an aqueous solution of surfactant.

Note that the curve suddenly breaks at a certain concentration and shows constant values of surface tension above this concentration. The break point above which the surface tension becomes constant is called the critical micelle concentration, abbreviated as CMC.

### 1.3.2 Dynamic surface tensions

Dynamic surface tensions are defined as any nonequilibrium values of surface tension that arise when the surface of a solution is extended or contracted. Rapidly expanding liquid surfaces occur in several processes, such as spraying, painting, and coating, and in the generation of foams. The surface tension of a pure liquid is established almost immediately on creation of the surface. Solutes with low surface activity, such as short-chain alcohols, reach equilibrium after formation of a fresh interface in about a millisecond; for some high-molecular weight surfactants, this time approaches a day. To reach equilibrium the molecules have to rearrange to a preferred orientation at the created surface.

The pioneering theoretical work of Ward and Tordai formulated a time-dependent relationship between the surface density of surfactants adsorbed at an interface and their concentration at the subsurface layer of solution, assuming a diffusive transport from the bulk solution. To explain non-equilibrium states of the surface they introduced the three-zone model for the structure of a liquid solution. The first zone is the monomolecular surface layer. The next layer below the surface,

called the sublayer, extends to a depth of some hundred molecular diameters. The third one, being further below the surface and called the bulk, is assumed to be semi-infinite. Sometimes the top molecular plain of the sublayer is called the subsurface, and is defined as a region separating the anisotropic pressure from the region of isotropic (normal) pressure in the liquid. If a surface of a surfactant solution is newly created, the dissolved molecules being near the surface will be quickly adsorbed. Thus, a strong concentration gradient between domains close to the bulk and those close to the surface arises. This is what diffusion tries to compensate. As the demand for dissolved molecules to saturate the surface layer is negligible compared to the total amount of dissolved molecules, the bulk concentration is assumed constant and only the sublayer concentration covers the demand for molecules of the surface. For very dilute surfactant solutions the property of the surface is characterized by the surface excess concentration. Ward and Tordai[7] found the following equation to describe the time-dependent surface excess concentration:

$$\Gamma(t) = \left(\frac{4D}{\pi}\right)^{\frac{1}{2}}\left[C_0 t^{\frac{1}{2}} + \int_0^t C_s(\tau)d(t-\tau)^{\frac{1}{2}}\right] \tag{1-6}$$

where $t$ is time , $\Gamma(t)$ the surface excess concentration. $D$ the monomer diffusion coefficient, $C_0$ the bulk concentration, $C_S$ $(t)$ the concentration at the subsurface, and $\tau$ a dummy time-delay variable. Applying the Ward and Tordai equation to the experimental data from the short-to long-time region, however, is a complicated task. To get information from the experimental data, the following asymptotic equations are used for short- and long-time adsorption behavior, respectively[8-10]

$$\gamma = \gamma_0 - 2RTC_0\left(\frac{Dt}{\pi}\right)^{\frac{1}{2}} \tag{1-7}$$

$$\gamma = \gamma_e + \frac{RT\Gamma^2}{2C_0}\left(\frac{\pi}{Dt}\right)^{\frac{1}{2}} \tag{1-8}$$

where $\gamma_0$ is interfacial tension at the moment the interface is created, that is, the interfacial tension of the solvent, and $\gamma_e$ is the equilibrium surface tension of the solution.

### 1.3.3 Interfacial rheology[11,12]

Interfacial rheology is the study of deformation and flow of thin films of material at a liquid / gas or liquid / liquid interface, where interface indicates the boundary between two phases. Inerfacial rheology technology provides information

on the behavior and interaction of molecules at interfaces, which is important for the application and processing of many materials of the general type: foods, beverages, pharmaceuticals, coatings, household and personal care products. There are two primary methods for measuring the interfacial rheological properties of adsorbed (soluble) and deposited (insoluble) layers of surface active materials at an interface. Interfacial shear rheology [Figure 1-3(b)] involves a change of shape of the interface as it is sheared, which gives a direct measure of the mechanical strength of the adsorbed layer. Interfacial dilatational rheology [Figure 1-3(a)] is determined by measuring the change in interfacial tension due to a specific change in interfacial area. This is a measure of the resistance to compression and expansion of the adsorbed layer.

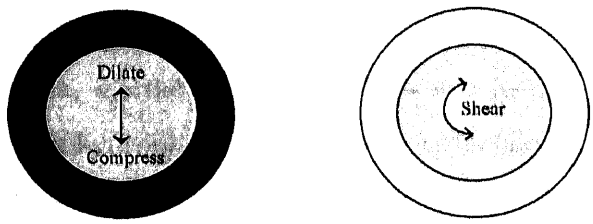


Figure 1-3: Interfacial dilatational (a), and interfacial shear (b) rheology.

Surface dilatational elasticity $|E^*|$ of an air-liquid interface of area, A undergoing a periodic dilatation is given by the equation

$$\left|E^*\right| = \frac{d\gamma}{d\ln A} \tag{1-9}$$

where $d\gamma$ is the small change in surface tension due to small change in area $dA$. Surface dilatational elasticity $|E^*|$ may be taken as a measure of the ability of an interface to resist deformation such as stretching. Higher the $|E^*|$ value, (that is, greater the change in interfacial tension for a change in area), greater is the tendency of the film to minimize the surface tension and hence higher is the rigidity (or elasticity) of the interface. However, if the surfactant molecules from the bulk can exchange to the interface and adsorb/desorb quickly, the interfacial tension doesn't fluctuate significantly during the bubble oscillation, and the interface becomes flexible (low $|E^*|$).

### 1.4 Surfactant self-assembly

Surfactants possess unique ability to self-assemble to form organized structures in solvent (water or oil). Usually, above certain relatively low concentration

called the critical micellar concentration (CMC), surfactant molecules start to form aggregates called micelles. This property can be explained in terms of the change in the free energy, $dG$

$$dG = \gamma\, dA \tag{1-10}$$

Where $\gamma$ is the surface tension and $dA$ is the change in surface area. A process which leads to a reduction in the surface area $A$ is energetically favoured, therefore, the surfactant molecules tend to associate in aggregates so that the contact area between their solvophobic parts and the solvent decreases.

Self-aggregation of amphiphilic molecules in aqueous medium is favored by the hydrophobic effect, which tends to reduce the hydrocarbon-water interfacial area, whereas several other interactions oppose it. These opposing forces are the collective force involving several repulsive interactions including hydration and steric contribution, and also electrostatic contributions in case of charged headgroups. At the optimal surface area, $a_s$, the total interaction energy per molecule attains its minimum. Assuming that hydrophobic chain of the surfactant molecules in aggregates behave as an incompressible liquid, that is, they have a constant volume $v$ at defined temperature, a dimensionless parameter called " critical packing parameter" (*cpp*) is defined as $v/a_s l_c$, where $l_c$ is the maximum extended length of the hydrophobic chain the amphiphile can assume in the aggregate, also known as critical length. The fully extended length of the chains for a saturated hydrocarbon with $n$ carbon atoms, $l_{max}$, and volume $v$ is estimated by Tanford's equation[13].

$$l_c \leq l_{max} \approx 0.154 + 0.1265n \text{ nm} \tag{1-11a}$$

$$v \approx (27.4+26.9n)\text{x}10^{-3} \text{ nm}^3 \tag{1-11b}$$

The extended length $l_c$ is approximately 80% of the *lmax* value. Once the cpp of a surfactant molecule is roughly estimated from the molecular diamensions, it gives a rough idea about the shape of the aggregates into which it is packed as shown in Figure 1-4.

$cpp \leq 1/3$ : spherical aggregate;

$1/3 < cpp \leq 1/2$ : rod-like aggregate;

$1/2 < cpp \leq 1$ : bilayer and planner aggregate

$cpp > 1$ : reversed aggregates.

The hydrophilic head group on the side of water interface and hydrophobic tail on the other side of the interface determines an optimal curvature, also, known as

spontaneous curvature, which in turn determines geometry of the aggregates. The principle curvatures, $c_1$ and $c_2$, define the mean ($H = (c_1 + c_2)/2$) and the Gaussian ($K = c_1 c_2$) curvatures. Aggregates enclosing polar head groups and water are said to have negative curvatures while aggregates with interior filled with lipophilic chains have positive curvatures. By convention, aggregates with interior filled with lipophilic chains (with cpp < 1) have a normal or positive curvatures, while aggregates enclosing polar headgroups and water (with cpp >1) are considered to have reversed or negative curvatures. A simple general expression relates the dimensionless packing parameter to the curvature of the interface:

$$CP = \frac{v}{a_s l_c} = 1 - H l_c + \frac{K l_c^2}{3} \qquad \text{(1-12a)}$$

$$\text{Alternately, } CP = \frac{v}{a_s l_c} = 1 - \frac{1}{2}\left(\frac{1}{R_1} + \frac{1}{R_2}\right) l_c + \frac{l_c^2}{3R_1 R_2} \qquad \text{(1-12b)}$$

where $R_1$ (=$1/c_1$) and $R_2$ (= $1/c_2$) are the radii of local curvatures.

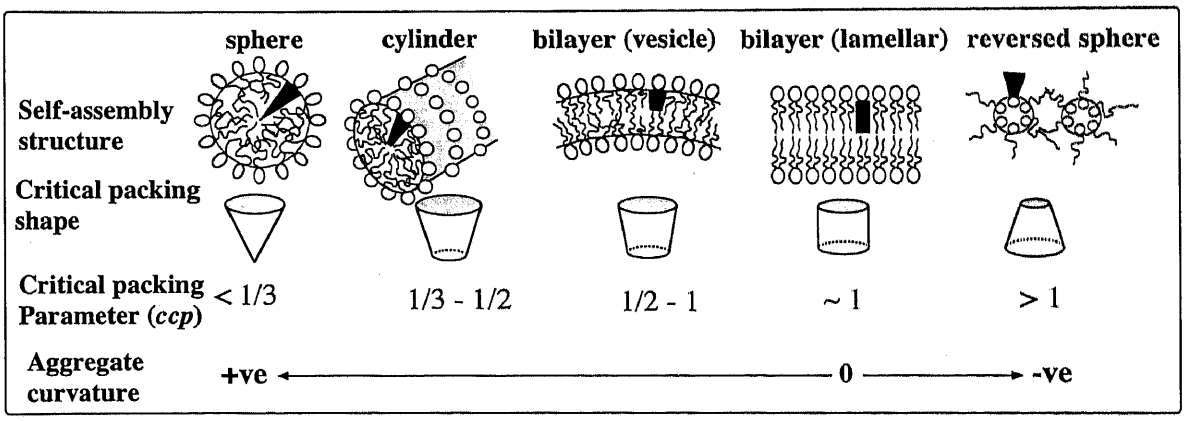


Figure 1-4: Variation of surfactant aggregates with the critical parameter, *ccp*.

## 1.5 Lyotropic liquid crystals

At concentrations well above the CMC, a variety of self-organising structures can be found in a liquid crystalline state[14]. Various kinds of liquid crystals are found in surfactant systems. They are present mainly as lyotropic liquid crystals (namely, they are formed upon addition of solvent) but also thermotropic liquid crystals can be formed in the absence of solvent. Most of the surfactant lyotropic liquid crystals are of the smectic type, with both orientational and positional order, although in some systems nematic type with only orientational order are also formed. Liquid crystal regions exist in equilibrium state only above the so-called Krafft temperature, namely,

the upper boundary of the surfactant solid crystal[14]. The following phases are commonly formed in surfactant systems:

a) Lamellar phase ($L_\alpha$, $L_\beta$, $P_\beta$): This phase is built up of bilayers of surfactant molecules alternating with solvent layers. There are several types of lamellar phases[15-18] indicated by $L_\alpha$, $L_\beta$, $P_\beta$ according to their structures. The $L_\alpha$ phase consists of one-dimensional lamellar lattice with hydrocarbon chains in liquid-like (disordered) state and oriented perpendicular to the lamellar plane (Figure 1-5a). The $L_\beta$ phase is built up with a one-dimensional lamellar lattice with hydrocarbon chains in solid-like (ordered) state, sometimes interdigitated or tilted (Figure 1-5b). Finally, the $P_\beta$ the phase consists of two-dimensional monoclinic lattice with the belayed distorted by a periodic ripple (Figure 1-5c).

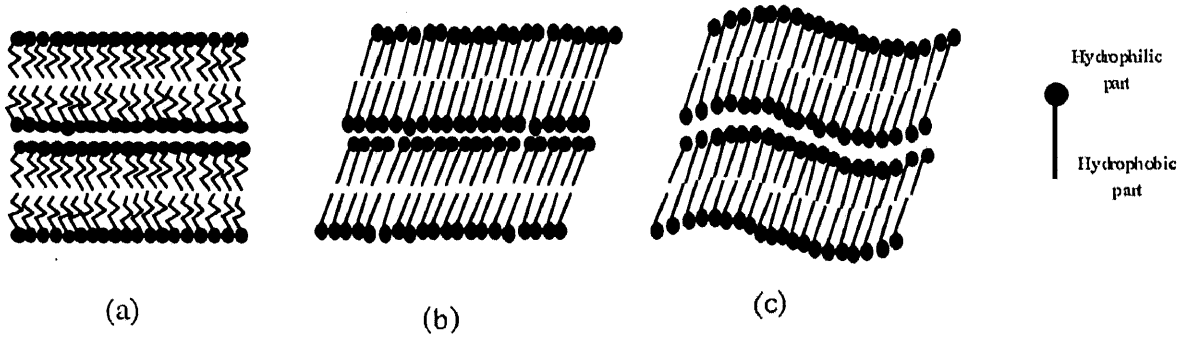


Figure1-5: Lamellar phases (a) $L_\alpha$ (b) $L_\beta$ (c) $P_\beta$

b) Hexagonal phases ($H_1$, $H_2$): The $H_1$ phase is composed of long cylindrical micelles with a lipophilic core arranged in a hexagonal pattern[19]. In the normal hexagonal phase ($H_1$), the hydrophobic chains form the core of the cylinders while the hydrophilic chains face the polar solvent (Figure 1-6a), whereas in the inverse hexagonal phase ($H_2$), the core of the cylinders consists of the hydrophilic chains with the hydrophobic chains directed towards a non-polar solvent (Figure 1-6b).

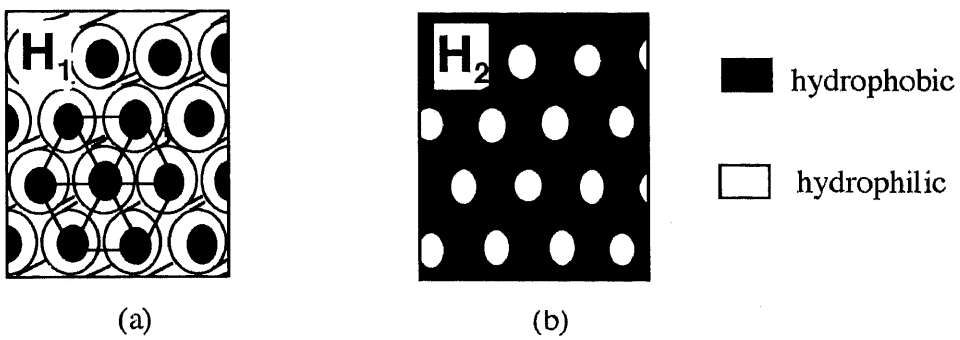


Figure 1-6: Hexagonal phases (a) normal hexagonal (b) inverse hexagonal

c) Cubic phases ($I_1$, $I_2$, $V_1$, $V_2$): On the basis of the morphology cubic phase is divided to two types: discontinuous (micellar) and bicontinuous. The discontinuous micellar

cubic phases are formed of discrete aggregates packed in a three-dimensional array[20]. The normal discontinuous cubic phase ($I_1$) is built up with discontinuous hydrocarbon regions embedded in continuous aqueous medium, namely, normal micellar aggregates in water (Figure 1-7a). The inverse discontinuous cubic phase ($I_2$) consists of discontinuous water regions embedded in a continuous lipid medium, namely, reversed micellar aggregates in hydrocarbon (Figure 1-7b).

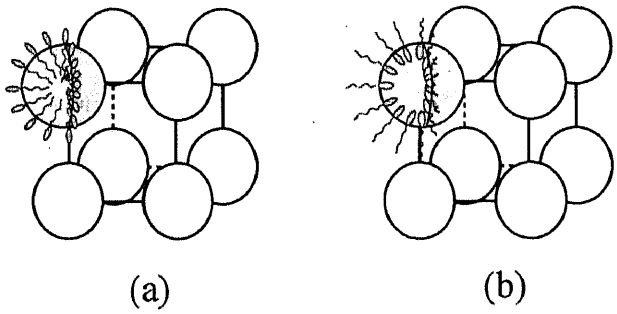


Figure 1-7: Discontinuous cubic phases: (a) normal micellar cubic ($I_1$) and (b) reverse micellar cubic ($I_2$).

In bicontinuous cubic phase the surfactant molecules form an interconnected network with a three dimensional porous structure. In this structure, the curvature of aggregates is at all points positive and negative (as in a saddle), giving a net curvature equal to zero[21].

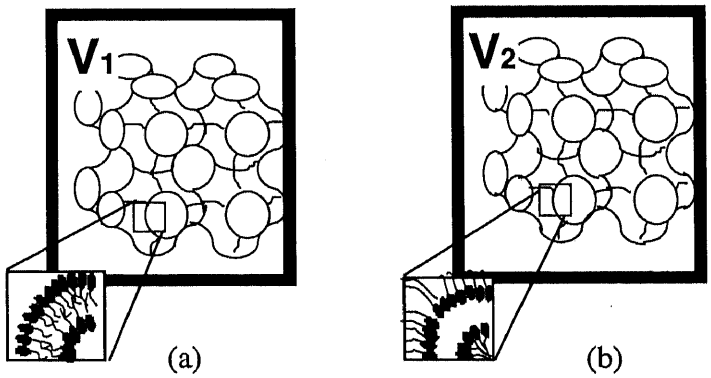


Figure 1-8: Bicontinuous cubic phases (a) normal bicontinuous ($V_1$) (b) reverse bicontinuous ($V_2$)

The bicontinuous cubic phase is described as a multiply connected bilayer separating two distinguishable and continuous domains of the same solvent. In the $V_1$ phase (Figure 1-8a), a polar film consisting of the hydrophilic groups and the polar solvent divides two apolar domains. On the other hand, the $V_2$ phase (Figure 1-8b) can be described as a non-polar film consisting of the hydrophobic groups dividing two polar domains.

## 1.6 Rheological behavior of micellar solutions

In aqueous media, surfactants molecules self-assemble to form aggregates of different microstructures and shape depending on the composition, temperature and type of the amphiphile. At a surfactant concentration just above critical micelle concentration (CMC), micelles are usually spherical. The micellar solutions with globular aggregates always have a low viscosity, often comparable to the viscosity of the solvent ($\eta_s$). The viscosity ($\eta$) varies linearly with the volume fraction of the globular particles, $\phi$, according to the Einstein's equation:

$$\eta=\eta_s(1+2.5\phi) \tag{1-13}$$

The sphere-rod transition in the micellar shape can be induced by different ways such as increasing surfactant concentrations, saltinity or temperature, depending on the type of the surfactant. However, in certain conditions, the micelles undergo enormous elongation and form very long and highly flexible aggregates, called " worm-like" or " thread-like" micelles. In the rod-like micelles, the curvature of the end-caps is higher than the spontaneous curvature of the aggregate at the cylindrical part. One-dimensional (1D) micellar growth may be considered as an effort of the system to minimize the excess free energy by reducing the number of end-caps in spite of the counteracting entropy factor.

Figure 1-9: Schematic diagram of unentangled (*concentration*<$c^*$) and entangled (*concentration*>$c^*$) worm-like micelles.

Above a certain surfactant concentration, called overlap concentration ($c^*$), the wormlike micelles begin to overlap with each other and viscosity becomes much higher than that predicted by the Einstein's equation. However, in some surfactant solutions, the viscosity may be very high even at low concentrations (about 1 wt%) suggesting a supramolecular three-dimensional network structure. Formation of such structure is attributed to the tendency of the micellar aggregates to arrange them into a long thread-like or worm-like aggregates, which are connected and interwoven or entangled to form a transient network (Figure 1-9). The viscoelastic behavior of the

worm-like micelles arises due to entanglement of the flexible aggregates to form transient network analogous to the polymer network.

The worm-like micelles have an equilibrium conformation in the networks. The micelles constantly undergo translational diffusion process, and they also break and recombine. If the network is deformed or an equilibrium conditions are suddenly changed, the relaxation occurs within a definite time and the equilibrium condition is restored again. If the network is deformed by a small perturbative shear stress σ in a shorter time than it can reach equilibrium, the system exhibits an elastic property characteristics of a solid material with a Hookean constant $G_o$, which is called the shear modulus and we obtain a simple relation between stress (σ) and strain ($\gamma$)[22]:

$$\sigma = G_o \gamma \tag{1-14a}$$

If, on the other hand, the network is deformed slowly, it behaves like a viscous fluid with a zero-shear viscosity $\eta_o$ and the shear stress is given by

$$\sigma = \eta_o \frac{d\gamma}{dt} \tag{1-14b}$$

where ($d\gamma/dt$) is the shear rate.

The dynamic rheological behavior of viscoelastic micellar solution is described by the mechanical model, called Maxwell model, consisting of an elastic component (spring) with the Hookean constant $G_o$ and a viscous component (dashpot) with the viscosity $\eta_o$ [Figure1-10(a)] . When a sudden strain is applied to the system for a short time, the stress relaxes exponentially with a time constant $\tau_R$

$$\sigma = \sigma_o \exp(-t/\tau_R) \tag{1-15}$$

$$\tau_R = \eta_o / G_o \tag{1-16}$$

It is possible to obtain different rheological parameters by following the stress decay as a function of time. Alternatively, the rheological properties of a viscoelastic material can be investigated by applying a sinusoidal deformation of angular frequency $\omega$. From the phase angle between sinusoidally varying stress and strain signals, the elasticity (storage) modulus $G'$, the viscous (loss) modulus $G''$, and the magnitude of complex viscosity $|\eta^*|$ can be calculated. For a Maxwell fluid, following relations are obtained[23]:

$$G'(\omega) = \frac{\omega^2 \tau_R^2}{1+\omega^2 \tau_R^2} G_o \tag{1-17}$$

$$G''(\omega) = \frac{\omega\tau_R}{1+\omega^2\tau_R^2} G_o \tag{1-18}$$

$$|\eta^*| = \frac{(G'^2 + G''^2)^{1/2}}{\omega} = \frac{\eta_o}{\sqrt{1+\omega^2\tau_R^2}} \tag{1-19}$$

where $\omega$ is the frequency of oscillatory-shear. $G_o$ is called shear (plateau) modulus. At low $\omega$, and $\omega\tau_R << 1$, $G'$ becomes proportional to $\omega^2$ whereas $G''$ is proportional to $\omega$, with $G'' > G'$. This region is called terminal zone, and the system behaves as a simple liquid (Figure 1-10(b)). It can be seen that for $\omega\tau_R >> 1$, $G'$ approaches a constant limiting plateau value equal to shear modulus ($G_o$), with $G' > G''$ and the system behaves as an elastic material. The $G_o$ is the material property and is related to the number density of entanglement ($\nu$) at a temperature $T$, according to the following relation:

$$G_o = \nu\, kT \tag{1-20}$$

Where $k$ is the Boltzmann constant.

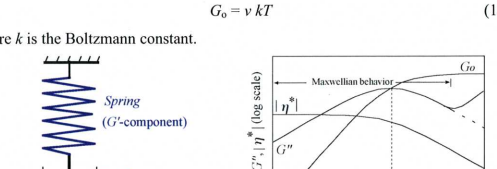


Figure 1-10: (a) Mechanical model for a viscoelastic behavior described by Maxwell equations. (b) The rheological behavior shown by a typical worm-like micellar solution. At low oscillatory-shear frequency the system shows Maxwellian behavior. However, at high frequency deviation from Maxwellian behavior is observed.

The relaxation time, $\tau_R$ is given by the inverse of the $\omega$ (expressed in rad.s$^{-1}$) corresponding to $G'$-$G''$ cross-over in a $G'$,$G''$-$\omega$ plot. In addition to equation (1-9), equation (1-12) allows one to estimate $\eta_o$ from the oscillatory-shear measurement by extrapolating $|\eta^*|$ to the zero oscillatory frequency.

Although the Maxwell equations predict a monotonous decrease of $G''$ at high frequency region [shown by a broken line in Figure 1-10(b)], the worm-like micelles deviates from this behavior, showing an upturn of $G''$ in high-frequency region

[shown by solid line in Figure 1-10(b)]. This deviation is often associated with the transition of relaxation mode from 'slower' reptation to other 'faster' processes such as Rouse modes of cylindrical micelles, analogous to polymer chain. The minimum value of $G''$ at high-frequency region is related to the micellar contour length according to the following relation[24]:

$$\frac{G''_{min}}{G_o} \approx \frac{l_e}{\bar{L}} \tag{1-21}$$

where $l_e$ is the entanglement length and $\bar{L}$ is the contour length of the worm-like micelle.

Living polymer model proposed by Cates *et al*[24,25]describes the viscoelastic behavior of the entangled worm-like micelles by considering two processes of stress relaxation – reptation or reptile-like motion of the micelle along its own contour, and reversible scission of micelles – taking place at two time scales, namely, reptation time $\tau_{rep}$ and breaking time $\tau_b$. When the time scale of breaking and recombination of micelles occurs in a very short time scale in comparison to the slow reptation process, that is, $\tau_{rep} >> \tau_b$, the viscoelastic behavior of such system at low shear frequency follows Maxwell model with single relaxation time $\tau_R$ given by $(\tau_b.\tau_{rep})^{1/2}$.

**1.7 Significance of the study of nonionic fluorinated amphiphiles**

A unique characteristic of fluorinated surfactants is the chemical stability of the fluorocarbon chain to strong acids, oxidizing agents, and concentrated alkalis. Hence, fluorinated surfactants can be used in media where hydrocarbon-based surfactants would degrade rapidly. The performance characteristics of fluorinated surfactants are related to the fluorocarbon segment in the surfactant molecule[26]. The fluorocarbon segments are hydrophobic as well as oleophobic and their interaction between fluorocarbon chains is weak. Consequently, fluorinated surfactants can lower the surface tension of water more than hydrocarbon-based surfactants. For many practical applications, the effectiveness of a surfactant is primarily dependent on the minimum value of the surface tension ($\gamma_{min}$) that is capable of achieving together with the surfactant together with the surfactant concentration required to achieve this. Substitution of the hydrocarbon chain in a conventional surfactant for a fluorocarbon chain affects both these parameters. When interfacial processes are proceeding at a rapid rate, such as in high speed spreading of aqueous surfactant solution over a substrate, the dynamic properties of the surfactant solution are more important in

determining the behavior of the system than its equilibrium properties. There are sufficient reports on the equilibrium surface properties[4,27-33,] of fluorinated surfactant solutions but only a few on the dynamic behavior of surface tension in these systems, especially at short times[26]. The behavior of dynamic surface tension is determined by several mechanisms[34,35] such as diffusional transport, reorientation, and adsorption of surfactant molecules, diffusional transport of micelles, and dissociation of micelles, so there is a need for robust quantitative analysis of experimental data.

Knowledge of the phase behavior of aqueous surfactants is a basis of understanding of the properties of these systems and is vital for the numerous industrial applications of surfactants. The surfactant-water mixtures attract the attention of investigators due to the variability of the phase structures formed by the amphiphilic molecules in water. In contrast to the extensive knowledge on hydrocarbon type surfactants, less is known about the fluorinated surfactant phase behavior. The greater rigidity, volume, and hydrophobicity of fluorocarbon chains, relative to hydrocarbon chains, enhance the self-association of fluorinated surfactants into micelles, as well as into the liquid crystal mesophases and vesicles[26]. The structures formed by fluorinated surfactants are as various as with hydrogenated surfactants. However, they tend to prefer to form structures based on bilayers[36]. Among fluorinated surfactants perflurocarboxylic acids and their alkali-metal and (alkyl) ammonium salts are widely investigated compounds[3,37-41]. The anionic fluorinated alkyl carboxylates continue to attract attention due to their ability to form the lyotropic nematic phases. Monduzzi et al. reported the counterion effect on the phase behavior of perfluropolyether carboxylates in water[42-44]. In spite of the growing study of phase behavior of nonionic fluorinated surfactants in water the incorporation of fluorinated oil into self–organized structures of fluorocarbon surfactant has rarely been considered[45].

The rheological behavior of surfactant solutions is the most fascinating subject and plays an important role in many formulations in industry. Fluorocarbon chains are bulkier than the hydrocarbon chain; hence to form spherical aggregate, fluorinated surfactants with very large head groups are needed to balance the effect of the bulky fluorocarbon chain[46]. Therefore, cylindrical micelles are often observed at solution conditions where spherical micelles are expected in hydrocarbon surfactant systems. These cylindrical micelles often undergo enormous one-dimensional growth and form flexible threadlike aggregates called "wormlike micelles". The formation and

properties of viscoelastic wormlike micelles have been studied extensively for hydrocarbon surfactants, mostly in long hydrophobic-chain ($C_{16}$ or longer) cationic surfactant in the presence of excess counterions[47-53] and, in some cases, even in absence of excess counterions if counterions are strongly bound at hydrophilic-hydrophobic interface[54-57]. Viscoelastic solutions of wormlike micelles have also been reported in cationic or anionic fluorinated surfactant aqueous systems even at a relatively short fluorocarbon chain length[58-60]. Only a few reports on the formation of viscoelastic wormlike micellar solution and the study of their rheological behavior are available in aqueous systems of nonionic hydrocarbon surfactants such as ethoxylated sterols[61-63] and sucrose alkanoates[64] but the knowledge of rheological behavior of wormlike micellar solution formed by a nonionic fluorinated surfactant at relatively low concentration is nil and therefore it demands more attention.

## References


1 Rosen, M. *Surfactants and Interfacial Phenomena*, John Wiley, New York, 2nd edition, **1989**.

2 Holmberg, K.; Jönsson, B.; Kronberg, B.; Lindman, B. *Surfactants and Polymers in Aqueous Solution*, John Wiley & Sons. New York, **1998**.

3 Shinoda, K.; Hato, M.; Hayashi, T. *J. Phys. Chem.* **1972**, 76 , 909.

4 Ravey, J.C.; Gherbi, A.; Stébé, M.J. *Prog. Colloid Polym. Sci.***1988**, *76*, 234.

5 Sidgewick, N.V. *The chemical elements and their compounds*, Vol. II, p. 1099, Oxford University Press, Oxford, **1951**.

6 Kissa, E. *Fluorinated surfactants: synthesis, properties, applications,* Surfactant Sciences Series, Volume 50, Marcel Dekker, New York, **1994**.

7 Ward, A.F.H.; Tordai, L. *J. Chem. Phys.* **1946**, *14*, 453.

8 Fainerman, V.B.; Makievski, A.V.; Miller R. *Colloids Surf. A* **1994**, *87*, 61.

9 Eastoe, J.; Dalton, J.S. *Adv. Colloid Interface Sci.* **2000**, *85*, 103.

10 Rillaerts, E.; Joos, P. *J. Phys. Chem.* **1982**, *86*, 3471.

11 Manual of Interfacial rheometer CIR-100, Camtel Ltd, Royston, UK, **1994-2000**.

12 Acharya, D.P.; Gutiérrez, J.M.; Aramaki, K.; Aratani, K.; Kunieda, H. *J Colloid and Interface Sci.* **2005**, *291*, 236.

13 Tanford, C. *J. Phys. Chem.* **1974**, *78*, 2471.

14 Laughlin, R.G. *The Aqueous Phase Behavior of Surfactants*, Academic Press Inc. San Diego, **1994**.

15 Janiak, M; Small, D.; Shipley, G. *J. Biol. Chem.* **1979**, *254*, 6068.

16 Ulmius, J.; Wennerström, H.; Lindblom, G.; Arvidson, G. *Biochemistry* **1977**, *16*, 5742.

17 Ruocco, M.; Shipley, G. *Biochimica et Biophysica Acta.* **1982**, *684*, 59.

18 Mädler, B.; Binder, H.; Klose, G. *J. Colloid Interface Sci.* **1998**, *202*, 124.

19 Luzzati, V. *Biological Membranes*, D. Chapman ed. Academic Press, New York, **1968.**

20 Fontell, K. *Colloid Polym. Sci.***1990**, *268*, 264.

21 Anderson, S.; Hyde, S.T.; Larsson, K.; Lidin, S. *Chem. Rev.* **1988**, *88*, 221.

22 Rehage, H.; Hoffmann, H. *Molecular Phys.* **1991**, *74*, 933.

23 Larson, R. G. *The Structure and Rheology of Complex Fluids,* Oxford University Press, New York, **1999**.

24 Granek, R.; Cates, M. E. *J. Chem. Phys.* **1992**, *96*, 4758.

25 Cates, M. E.; Candau, S. J. *J. Phys. Condens Matter* **1992**, *2*, 6869.

26 Kissa, E. *Fluorinated Surfactants and Repellants*, 2nd Ed., Surfactant Sciences Series, Volume 97, Marcel Dekker, New York, **2001**.

27 Eastoe, J.; Paul, A.; Rankin, A.; Wat, R.; Penfold, J.; Webster, J.R.P *Langmuir* **2001**, *17*, 7873.

28 Matos, L.; Ravey, J.-C.; Serratrice, G. *J. Colloid Interface Sci.* **1989**, 128, 341.

29 Kunieda, H.; Shinoda, K. *J. Phys. Chem.* **1976**, *80*, 2468.

30 Rodriguez-Abreu, C.; Kunieda, H. *J. Dispersion Sci. Technol.* **2005**, *26*, 435.

31 Rodríguez, C.; Kunieda, H.; Noguchi, Y.; Nakaya, T. *J. Colloid Interface Sci.* **2001**, *242*, 255.

32 Asakawa, T.; Ishikawa, K.; Miyagishi, S.; *J. Colloid Interface Sci.* **2001**, *240*, 365.

33 An, Y.-J.; Jeong, S.-W. *J. Colloid Interface Sci.* **2001**, *242*, 419.

34 Zhmud, B.V.; Tiberg, F.; Kizling, J. *Langmuir* **2000**, *16*, 2557.

35 Kjellin, U.R.M.; Reimer, J.R.; Hansson, P. *J. Colloid Interface Sci.* **2003**, *262*, 506.

36 Ravey, J.C.; Stébé, M.J. *Colloids Surf. A* **1994**, *84*, 11.

37 Hoffmann, H.; Würtz, J. *J. Mol. Liq.* **1997**, *72*, 191.

38 Fontell, K.; Lindman, B. *J. Phys. Chem.* **1983**, *87*, 3289.

39 Bucci, S.; Hoffmann, H.; Platz, G. *Prog. Colloid Polym. Sci.* **1990**, *81*, 87.

40 Downes, N.; Ottewil, G.A.; Ottewil, R.H. *Colloids Surf. A* **1995**, *102*, 203

41 LoNostro, P.; Choi, S.M.; Ku, C.Y.; Chen, S.H. *J. Phys. Chem. B* **1999**,*103*, 5347.

42 Caboi, F.; Chittofrati, A.; Lazzari, P.; Monduzzi, M.J. *Colloids Surf. A* **1999**, *160*, 47.

43 Monduzzi, M.; Chittofrati, A.; Boselli, V. *J. Phys. Chem.* **1994**, *98*, 7591.

44 Mele, S.; Ninham, B.W.; Monduzzi, M. *J. Phys. Chem. B* **2004**, *108*, 1751

45 Ropers, M.H.; Stébé, M.J. *Langmuir*, **2003**, *19*, 3137.

46 El Moujahid, C.; Ravey, J. C.; Schmitt, V.; Stébé, M. J. Colloid Surf. A **1998**, *136*, 289.

47 Rehage, H.; Hoffmann, H. *J. Phys. Chem.* **1988**, *92*, 4712.

48 Kern, F.; Lemarechal, P.; Candau, S.J.; Cates, M. E. *Langmuir* **1992**, *8*, 437.

49 Clausen, T. M.; Vinson, P. K.; Minter, J. R.; Davis, H. T.; Talmon, Y.; Miller, W.G. *J. Phys. Chem.* **1992**, *96*, 474.

50 Khatory, A.; Kern, F.; Lequeux, F; Appell, J.; Porte, G.; Morie, N.; Ott, A.; Urbach, W. *Langmuir* **1993**, *9*, 933.

51 Khatory, A.; Lequeux, F; Kern, F.; Candau, S. J. *Langmuir* **1993**, *9*, 1456.

52 Berret, J.-F.; Appell, J.; Porte, G. *Langmuir* **1993**, *9*, 2851.

53 Lin, Z.; Cai, J. J.; Scriven, L. E.; Davis, H. T. *J. Phys. Chem.* **1994**, *98*, 5984.

54 Soltero, J. F. A.; Puig, J. E.; Manero, O.; Schulz, P. C. *Langmuir* **1995**, *11*, 3337.

55 Soltero, J. F. A.; Puig, J. E.; Manero, O. *Langmuir* **1996**, *12*, 2654.

56 Narayanan, J.; Manohar, C.; Kern, F.; Lequeux, F.; Candau, S. J. *Langmuir* **1997**, *13*, 5235.

57 Hassan, P. A.; Candau, S. J.; Kern, F.; Manohar, C. *Langmuir* **1998**, *14*, 6025.

58 Wang, K.; Karlsson, G.; Almgren, M.; Asakawa, T. *J. Phys. Chem. B* **1999**, *103*, 9237.

59 Knoblich, A.; Matsumoto, M.; Murata, K.; Fujiyoshi, Y. *Langmuir* **1995**, *11*, 2361.

60 Hoffmann, H.; Würtz, J. *J. Mol. Liquids* **1997**, *72*, 191.

61 Acharya, D. P.; Kunieda, H. *J. Phys. Chem. B* **2003**, *107*, 10168.

62 Acharya, D. P.; Hossain, Md. K.; Jin-Feng, Sakai, T.; Kunieda H. *Phys. Chem. Chem. Phys.* **2004**, *6*, 1627.

63 Naito, N.; Acharya, D. P.; Tanimura, K.; Kunieda, H. *J. Oleo Sci.* **2004**, *53*, 599.

64 Maestro, A.; Acharya, D.P.; Furukawa, H.; Gutiérrez, J. M.; López-Quintela, M.A.; Ishitobi, M.; Kunieda, H. *J. Phys. Chem. B* **2004**, *108*, 14009.

# Chapter 2: Experimental

## 2.1 Materials

Fluorinated random copolymers, (perfluoroalkylacrylate)–[poly (ethyleneoxide) methacrylate], with product identification names NS-1620*x* ($x = a - i$) were kindly supplied by Daikin Industries, Ltd. (Japan) and were used without further purification. For the sake of simplicity, each of the copolymers will be denoted hereafter by the last alphabet of its name, for example, *a* stands for NS-1620*a*, *b* for NS-1620*b* and so on. Schematic molecular structure of the copolymer is shown in Figure 2-1 and the properties of the copolymers are shown in Table 2-1.

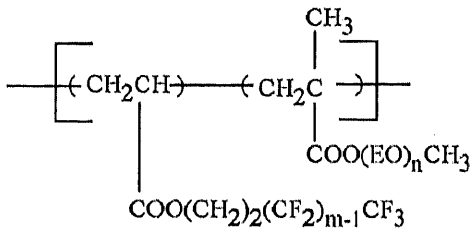


Figure 2-1: Schematic molecular structure of amphiphilic fluorinated random copolymer [$C_mRf$-acrylate]-[$EO_n$-methacrylate]. Copolymers with different combinations of $m$ (= 8, 6, 4, 2 for $C_8Rf$, $C_6Rf$, $C_4Rf$, $C_2Rf$) and $n$ (= 9 and 4.5) were studied.

Perfluorosurfactants, *N*-polyoxyethylene-*N*-propyl perfluorooctane sulfonamide, designated as $C_8F_{17}EO_n$ (where $n$ = 10 and 20) were obtained from Mistubishi Materials, Japan. Schematic molecular structure of the surfactant is shown in Figure 2-2.

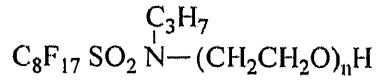


Figure 2-2: Schematic molecular structure $C_8F_{17}EO_n$

The surfactant $C_8F_{17}EO_{10}$ contains volatile components 1.34%. It was purified by placing it under vacuum for several days in order to remove volatile components until weight became constant. The surfactant $C_8F_{17}EO_{20}$ contains only 0.30% volatile components and was used as received. Perfluoropolyether oil [$F\text{-}(CF_2CF_2CF_2O)_n\text{-}CF_2CF_2COOH$] designated as $(C_3F_6O)_nCOOH$ was kindly supplied by Daikin Industries, Ltd. (Japan). The number average molecular weight of $(C_3F_6O)_nCOOH$ is 3600, which gives $n \approx 21$ and polydispersity 1.14. Millipore water was used in all the experiments.

Table 2-1: Properties of [$C_mRf$-acrylate]-[$EO_n$-methacrylate] fluorinated random copolymers.

| Copolymer | No. of $EO_n$ chain per $C_mRf$ chain ($R$) | Number average mol. wt | Fluorine content (wt%) | Apparent HLB |
|---|---|---|---|---|
| $m$=8, $n$=9 | | | | |
| *a* | 2 | 12000 | 18.7 | 10.5 |
| *b* | 3 | 12000 | 13.1 | 11.8 |
| *c* | 5 | 12000 | 9.25 | 13.2 |
| $m$=4, $n$=9 | | | | |
| *d* | 0.97 | 12000 | 18.7 | 9.6 |
| *e* | 1.5 | 12000 | 13.1 | 11.2 |
| *f* | 2.55 | 12000 | 9.20 | 12.8 |
| $m$=4, $n$=4.5 | | | | |
| *g* | 2 | 15000 | 16.4 | 8.7 |
| $m$=6, $n$=9 | | | | |
| *h* | 2.55 | 13000 | 13.4 | 12.0 |
| $m$=2, $n$=9 | | | | |
| *i* | 0.77 | 12000 | 11.9 | 10.2 |

## 2.2 Measurement of surface tension

The Laplace equation is the basis on which all the methods of measuring surface and interfacial tensions are founded:

$$\Delta p = \gamma\left(\frac{1}{R_1}+\frac{1}{R_2}\right) \tag{2-1}$$

where $\Delta p$ is the pressure difference across the curved interface, $\gamma$ is the surface tension, and $R_1$ and $R_2$ are the principal radii of curvature. In all experimental methods the pressure difference and radii of curvature are implicated in different ways.

### 2.2.1 Wilhelmy plate method[1]

The plate method, also known as Wilhelmy method, bases on a force measurement. The measuring device is a vertically hanged platinum plate with exactly known geometry (Figure 2-3). The surface of the plate is roughened to improve is

wettability. The lower edge of the plate is brought into contact with the liquid surface. It is to say the liquid jumps the plate and pulls it a little into it. This "Wilhelmy"-force results from the wetting. It is measured by moving up the plate to the level of the liquid surface. The measuring procedure is static, which means that the plate can hold on zero level any time. This makes possible a continuous measurement of the surface tension. Wilhelmy method has many advantages. It is absolute, simple to set up, and independent of the density of the fluid. The surface tension of the liquid is calculated from the measured force

$$\gamma = \frac{P_w}{l_w . \cos\theta} \tag{2-2}$$

where $\gamma$ is surface tension, $P_w$ is measured (Wilhelmy) force, $l_w$ is wetted length and $\theta$ is the contact angle between the tangent at the wetting line and the plate surface.

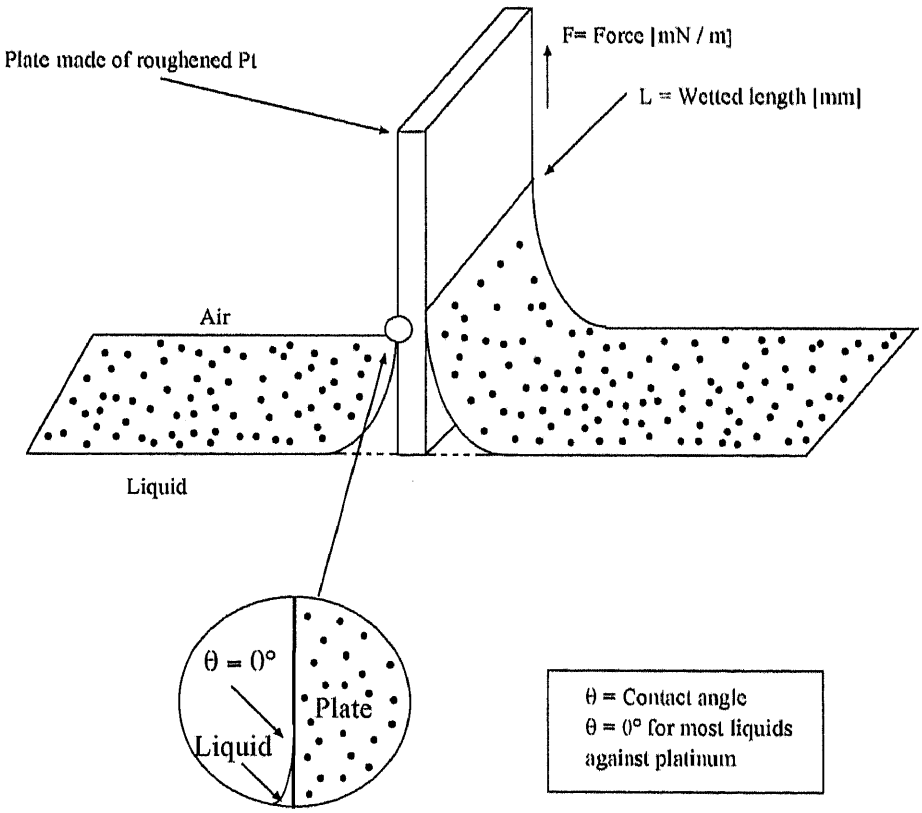


Figure 2-3: Cross-section of the wetted plate

To use the above mentioned equation for the determination of the surface tension the contact angle has to be zero which means $\cos\theta = 1$ (total wetting). The roughened and cleaned platinum plate used do fulfil this requirement.

### 2.2.2 Spinning drop method

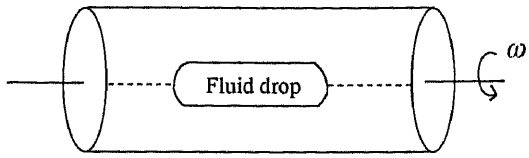


Figure 2-4: Schematic of the spinning drop method

This method relies on the fact that gravitational acceleration has little effect on the shape of a fluid drop suspended in a liquid, when drop and the liquid are contained in a horizontal tube spun about its longitudinal axis[2,3] as shown in Figure 2-4. At low rotational velocities ($\omega$), the fluid drop will take on an ellipsoidal shape, but when $\omega$ is sufficiently large, it will become cylindrical. Under this latter condition, the radius (r) of the cylindrical drop is determined by the interfacial tension, the density difference ($\Delta\rho$) between the drop and the surrounding fluid, and the rotational velocity of the drop. As the result, the interfacial tension is calculated from the following equation[4]

$$\gamma = \frac{1}{4} r^3 \Delta\rho\omega^2 \tag{2-3}$$

### 2.2.3 Maximum bubble pressure method

In processes such as foaming, cleaning, printing and coating the surfactant kinetics have a decisive influence. Depending on their chemical structure and concentration, various surfactants have different effects on the dependence of the surface tension as a function of surface age. The maximum bubble pressure method is an easy-to-use method for determining the dynamic surface tension.

This method is based on measuring the maximum pressure to force a gas bubble out of a capillary into a liquid[5,6]. The gas bubbles enter the liquid through a capillary made of silanized glass with known geometry. The instrument measures the maximum pressure which occurs during the bubble formation process (Figure 2-5). This is directly proportional to the surface tension

$$\gamma = \frac{(P_{max} - P_0)r}{2} \tag{2-4}$$

where $\gamma$ is surface tension gas/ liquid, $P_0$ is hydrostatic pressure in the capillary, $P_{max}$ is the maximum bubble pressure and $r$ is inner radius of capillary.

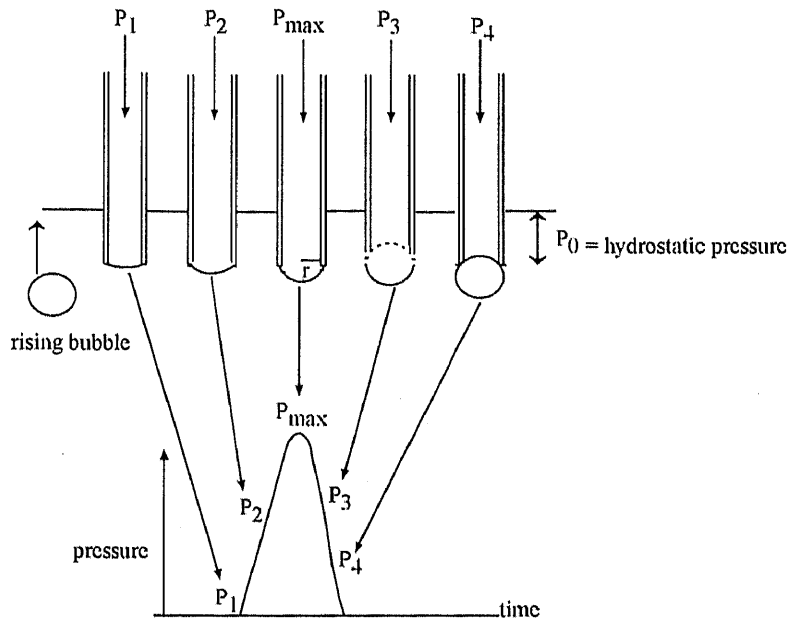


Figure 2-5: Pressure sequence during a measurement with the bubble pressure tensiometer.

Alterations to the surfactant concentration far above the CMC show no effect on the equilibrium surface tension. Dynamic measurements, which are always carried out beneath the liquid surface and thus directly in the solution, still show clear effects even at concentrations, which are equivalent to many times the CMC value.

**2.3 Phase diagram study**

Phase diagram is made by the direct visual observation as a basic procedure. The types of liquid crystal formed in the amphiphile system can also be distinguished from the presence or absence of the birefringence by observing the sample through a crossed polarizer. However, this classical method provides the rough information, and sometimes

it is difficult to decide the phase state especially at the phase boundary by this method. To obtain the correct experimental data, small-angle X-ray scattering (SAXS) is applied for analyzing the phase state.

**2.4 Calculation of volume fraction of hydrophobic part of surfactant in water-surfactant-polymeric oil system**

The volume fraction of hydrophobic part of surfactant, $\phi_L$, is calculated by

$$\phi_L = \frac{V_L \phi_S}{V_S} = \frac{V_L}{V_S + \frac{M_S}{\rho_W}\left(\frac{1-W_O}{W_S} - 1\right) + \frac{M_S}{\rho_O}\cdot\frac{W_O}{W_S}} \qquad (2\text{-}5)$$

where $V_S$, $\phi_S$ and $M_S$ are molar volume , volume fraction, molecular weight of surfactant, $V_L$ the molar volume of its hydrophobic part and $W_S$ and $W_O$ weight

fractions of surfactant and polymeric oil in the system, and $\rho_W$ and $\rho_O$ densities of water and oil respectively.

The molar volume of the surfactant, $V_s$, is calculated by

$$V_s = M_s / \rho_s \tag{2-6}$$

where $\rho_s$ is the density of the surfactant.

The volume fraction of surfactant, $\phi_S$, is calculated by

$$\phi_S = \frac{\frac{W_S}{\rho_S}}{\frac{W_S}{\rho_S} + \frac{W_W}{\rho_W} + \frac{W_O}{\rho_O}} \tag{2-7}$$

where $W_w$ is the weight fraction of water in the system.

**2.5 Small angle X-ray scattering (SAXS)**[7-11]

Small-angle scattering of X-ray is a widely used technique to determine size, shape and internal structures of colloidal particles in the size range from a few nanometers up to about a hundred nanometers. Information on such relatively large-scale structures is contained in the intensity of the scattered X-rays at small angles, typically at $2\theta$ within $0.2 \sim 4°$.

A characteristic property of waves is their interference with each other. The phenomenon of diffraction is the interference caused by an object in the path of waves. In X-ray scattering, the electrons present in the path of the x-ray beam will oscillate with the same frequency and amplitude as the original beam. The scattering contrast in a sample is provided by the variation in electron density therein. Periodic electron density fluctuations within the sample may give rise to constructive interference in certain discrete angles, which appear on the detector as scattered X-rays and thereby giving a diffraction pattern. From the scattering pattern we can learn about the structure of the individual scatters and the correlation between them.

In this study, SAXS has mainly been used for distinguishing between different phases, e.g., lamellar and hexagonal liquid crystalline phases, bicontinuous cubic phase and measuring the length scale of their periodicity.

**2.5.1 Basic theory in small angle scattering**[12]

The basic principals can be summarised as follows. The amplitude of the incident plane wave, $A_{in}$ can be written as

$$A_{in} = A_0 \exp(i\bar{k}_0 \bar{R}) \tag{2-8}$$

where $A_0$ is the scattering amplitude, $\bar{k}_0$ the wave vector which points in the direction of propagation and has the magnitude $\bar{k}_0 = 2\pi/\bar{\lambda}$, and $R$ the scattering position.

If this wave hits another atom, a fraction thereof will be scattered and the scattered wave radiates spherically around the scattering centre. With the atom not in the origin, the scattered wave will be phase shifted with a path difference $\bar{q}\bar{r}$. For elastic scattering $|\bar{k}| = |\bar{k}_0|$, and the scattering vector is defined as $\bar{q} = \bar{k} - \bar{k}_0$. From geometric considerations it can be shown that the magnitude of the scattering vector is

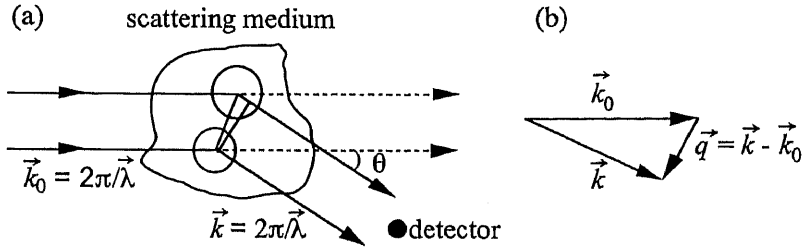


Figure 2-6: (a) scattering from a medium. (b) Definition of the scattering vector $q$.

$$|\bar{q}| = 2|\bar{k}_0|\sin\frac{\theta}{2} \Leftrightarrow \frac{4\pi}{\lambda}\sin\frac{\theta}{2} \tag{2-9}$$

The scattered wave radiates spherically around the scattered center and it is accordingly given by

$$A_{SC} = \frac{b}{r}A_0 \exp\left\{i\left(k_0 r - \bar{q}\bar{R}\right)\right\} \tag{2-10}$$

where $b$ is the scattering length, (a measure of the strength of the interaction with the atom). However, in the scattering medium there are not only two scattering centers but also a very large number, $N_a$, of atoms located at positions $R_j$. The total scattering amplitude is then written as

$$A_{SC} = \frac{A_0}{r}\exp(ik_0 r)\sum_{j=1}^{N_a} b_j \exp\left(-i\bar{q}\bar{R}_j\right) \tag{2-11}$$

The detectors are sensitive to the power flux instead of the phase of the scattered radiation. The interference pattern is controlled by terms, which measure the probability of finding an atom of scattering length $b_i$ and another atom of scattering length $b_j$ separated by a vector $\bar{r}_{ij} = \bar{R}_i - \bar{R}_j$. The normalized scattered intensity per solid angle then is given by

$$I(\bar{q}) = |A|^2 = \frac{r^2}{V}\frac{I_{SC}(\bar{q})}{I_{in}(\bar{q})} = \frac{1}{V}\sum_{i,j}^{N_a} b_i b_j \exp\left(-i\bar{q}\bar{r}_{ij}\right) \tag{2-12}$$

In order to obtain a physical understanding, an ensemble of $N_p$ colloidal homogeneous spherical particles of equal size, each containing $N_a$ scattering atoms is considered. To

describe the scattering from the colloidal objects one normally uses a continuum description where the sum in eq 2-12 is replaced by an integral of the scattering length density $\rho(\bar{r}) = \frac{1}{V}\sum_j b_j v(\bar{r} - \bar{r}_j)$, where the volume $v$ is larger compared with inter-atomic distances but small compared to the resolution of the experiment. The relevant scattering contrast is the difference in scattering in scattering length density between the particles $(\rho(\bar{r}))$ and the solvent ($\rho_{\text{solvent}}$), $\Delta\rho(\bar{r}) = \rho(\bar{r}) - \rho_{solvent}$. If the spheres are uncorrelated, the scattering results from only the intra-particle interference, the form factor, $P(q)$.

$$P(\bar{q}) = \left| \int_{V_{part}} d\bar{r}\Delta\rho(\bar{r})\exp(i\bar{q}\bar{r}) \right|^2 \tag{2-13}$$

where $V_{\text{part}}$ is the volume of particle. $P(q)$ can be expressed by using spherical polar co-ordinates as

$$P(\bar{q}) = \left(\Delta\rho\frac{4\pi r^3}{3}\right)^2 \left(3\frac{\sin(qr) - qr\cos(qr)}{(qr)^3}\right)^2 \tag{2-14}$$

However, if the sphere in the systems are correlated, the scattering can be divided into two terms, one that takes the intra-particle interference into account and one term that depends on the relative positions of the particles, i.e. on the inter-particle interactions, the structure factor, $S$(q).

$$I(\bar{q}) = \frac{1}{V}P(\bar{q})\left\langle \left| \sum_{i,j}^{N_p} \exp(i\bar{q}\bar{r}_{ij}) \right| \right\rangle \tag{2-15}$$

$$I(\bar{q}) = \frac{N_p}{V}P(\bar{q})S(\bar{q}) \tag{2-16}$$

Using an assumption that the particles interact as hard spheres gives an analytical expression of the structure factor.

### 2.5.2 The SAXS instruments[13]

The X-rays are electromagnetic waves, electrons released from a hot tungsten filament are accelerated toward a target material copper in an evacuated tube, and X-rays are generated on impact of electrons at the target. In a synchrotron, a beam of electrons is accelerated to nearly the speed of light and is made to circulate on a closed orbit under high vacuum in a storage ring. This is achieved by bending the path with a series of bending magnets. The flux of X-ray emitted by the accelerated

electrons is many orders of magnitude greater than that obtainable with conventional X-ray tubes, making the required time for any single measurement very short.

In order to obtain a scattering curve with high resolution, the incoming beam should be collimated and monochromatic. The radiation sources produce a wide spectrum of wavelengths, so that filters are used to eliminate the unwanted radiation. A Copper anode giving a $K_\alpha$ line (of the wave length 1.54 Å) and intense $K_\beta$ line; the $K_\beta$ line is filtered away with a nickel foil. Detection of the scattered radiation is recently performed by a one-dimensional photon position sensitive detector. An X-ray photon ionises the gas, and this ionisation is electronically measurable.

### 2.5.3 SAXS measurements in the liquid crystalline phases

Liquid crystals can be modelled as stacks of reflecting lattice planes separated by the distance $d$. When the path-length difference is an integral number of wavelengths (AB + BC = $n\lambda$, where $n$ = 1, 2, 3, ... $\lambda$ is the wavelength, and AB + BC = $2d\sin\theta$, where $\theta$ is the diffraction angle), the waves are in phase. When the diffraction angle satisfies the brag law, $n\lambda = 2d\sin\theta$, a constructive interference gives rise to peaks in the X-ray spectrum. These peaks are normally expressed as reflections. The brag law expressed in terms of the scattering vector $q$ is

$$q = n\frac{2\pi}{d_{hkl}} \tag{2-17}$$

where $h$, $k$, and $l$ are the Miller indices, denote the number of parallel planes that intersect with each unit axis and are therefore used to define the lattice planes in the crystal.

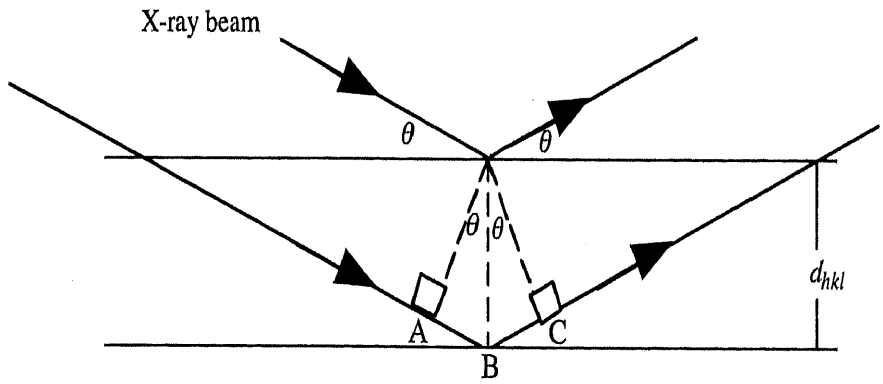


Figure 2-7: Parallel rays reflected from points on neighboring partially reflecting planes are in phase when Bragg's law is obeyed

Different diffracting planes produce reflections of characteristic patterns with peak ratios vary depending on the type of crystal, hence, different liquid crystalline phases can be identified according to these values.

(a) The cubic (micellar and bicontinuous) phases:

The cubic lattice spacing $d$ is related to the unit cell dimension as

$$d_{hkl} = \frac{a}{\sqrt{h^2 + k^2 + l^2}} \tag{2-18}$$

$$d_{hkl} = n\frac{2\pi}{q_{hkl}}$$

The cubic phase can be divided into three main families: primitive, body centered and face centered. For a tridimensional lattice, symmetry elements can be combined in groups and it can be shown that 230 distinctive elements (space groups) are possible. Each space group has its characteristic scattering pattern. Following are the spacing ratios corresponding to the space groups found so far in cubic liquid crystal phases (the notation follows the *International Tables for Crystallography*):

Pm3m $d_{100} : d_{110} : d_{111} : d_{200} : d_{210} : d_{211} : d_{220} = 1 : \frac{1}{\sqrt{2}} : \frac{1}{\sqrt{3}} : \frac{1}{2} : \frac{1}{\sqrt{5}} : \frac{1}{\sqrt{6}} : \frac{1}{\sqrt{8}}$

Im3m $d_{110} : d_{200} : d_{211} : d_{220} : d_{310} : d_{222} : d_{321} = 1 : \frac{1}{\sqrt{2}} : \frac{1}{\sqrt{3}} : \frac{1}{2} : \frac{1}{\sqrt{5}} : \frac{1}{\sqrt{6}} : \frac{1}{\sqrt{7}}$

Fm3m $d_{111} : d_{200} : d_{220} : d_{311} : d_{222} : d_{400} : d_{331} = 1 : \sqrt{\frac{3}{4}} : \sqrt{\frac{3}{8}} : \sqrt{\frac{3}{11}} : \sqrt{\frac{3}{12}} : \sqrt{\frac{3}{16}} : \sqrt{\frac{3}{19}}$

Pm3n $d_{110} : d_{200} : d_{210} : d_{211} : d_{220} : d_{310} : d_{222} = 1 : \frac{1}{\sqrt{2}} : \sqrt{\frac{2}{5}} : \frac{1}{\sqrt{3}} : \frac{1}{2} : \frac{1}{\sqrt{5}} : \frac{1}{\sqrt{6}}$

Ia3d $d_{211} : d_{220} : d_{321} : d_{400} : d_{420} : d_{332} : d_{422} = 1 : \sqrt{\frac{3}{4}} : \sqrt{\frac{3}{7}} : \sqrt{\frac{3}{8}} : \sqrt{\frac{3}{10}} : \sqrt{\frac{3}{11}} : \sqrt{\frac{3}{12}}$

Fd3m $d_{111} : d_{220} : d_{311} : d_{222} : d_{400} : d_{331} : d_{422} = 1 : \frac{1}{\sqrt{3}} : \frac{1}{\sqrt{8}} : \frac{1}{\sqrt{11}} : \frac{1}{\sqrt{12}} : \frac{1}{4} : \frac{1}{\sqrt{19}}$

(b) The hexagonal phase

For a hexagonal lattice, the Bragg positions corresponds to

$$d_{hk} = \frac{a\sqrt{3}}{2\sqrt{h^2 + hk + k^2}} \tag{2-19}$$

$$d_{hk} = n\frac{2\pi}{q_{hk}}$$

and the first reflections correspond to ($hk$) = (10), (11), (20), (21), related as 1:√3: 2: √7...

(c) The lamellar phase

The symmetry planes are parallel so that higher order reflections are simple multiples of that of the first-order, i.e. the reflections correspond to ($h$) = (1), (2), (3) ... related as 1:2:3...

### 2.5.4 Structural parameters of liquid crystals

Once the type of liquid crystal structure is identified, the structural parameters of aggregates in liquid crystals can be calculated from geometrical considerations.

1. Cubic phases ($I_1$,): Considering $n_c$ spherical micelles packed in a cubic lattice, the following equations can be derived for the radius of the hydrophobic part of micelle, $r_I$, and the effective cross sectional area of one surfactant molecule, $a_S$, in the $I_1$ phase:

$$r_I = d\left[\frac{3}{4\pi n_C}(\phi_L + \phi_O)\right]^{\frac{1}{3}} C \tag{2-20}$$

$$a_S = \frac{3v_L}{r_I}\cdot\frac{(\phi_L + \phi_O)}{\phi_O} \tag{2-21}$$

$d$ is the measured interlayer spacing, $v_L$ is the volume of the hydrophobic part per surfactant molecule, $\phi_L$ and $\phi_O$ are the volume fractions of hydrophobic parts of surfactant and polymeric oil in the system. $C$ is a constant: 2 for body-centered cubic, 3 for face-centered cubic, and 1 for simple-cubic structures respectively.

2. Hexagonal phase ($H_1$): We assumed that infinitely long rod micelles are packed in a hexagonal array in the $H_1$ phase. The radius of the hydrophobic part in the cylinders, $r_H$, as well as the effective cross sectional area per surfactant molecule for $H_1$ phase, $a_s$ are given by

$$r_H = \left\{\frac{2}{\sqrt{3}\pi}(\phi_L + \phi_O)\right\}^{\frac{1}{2}}\cdot d \tag{2-22}$$

$$a_S = \frac{2v_L}{r_H}\left(1 + \frac{\phi_O}{\phi_L}\right) \tag{2-23}$$

3. Lamellar phase ($L_\alpha$): Assuming that bimolecular layers are stacked in the $L_\alpha$ phase, the half-thickness of the hydrophobic part in the lamellar structure $d_L$ as well as the

effective cross sectional area per surfactant molecule for the lamellar phase, $a_s$ are given by

$$d_L = \frac{d}{2}(\phi_L + \phi_O) \tag{2-24}$$

$$a_S = \frac{v_L}{d_L}\left(1 + \frac{\phi_O}{\phi_L}\right) \tag{2-25}$$

## 2.6 Rheometry[14-16]

The rheological behavior of structured fluids, of polymer and surfactant solutions and of suspensions is a most fascinating subject. The basic principle of rheology (derives from the greek rheos = river) is the correlation of the deformation of a fluid with the occurring stresses, in particularly during flowing processes. Rheology is the study of the deformation and flow of matter. In a gross sense, a rheological measurement tells one how "hard" or "soft" a material is, or it indicates how "fluid-like" or solid-like" it is. These characteristics of a material depend on the time scale it is probed. A rheometer measures the rheological properties of a complex fluid (such as solutions of surfactant or polymer) as a function of rate or frequency of deformation.

### 2.6.1 Basic principle of rheology:

#### 2.6.1.1 Steady- shear rheology:

Simple steady-shear is the easiest flow to generate and is, therefore, of central importance in rheology. Let us consider a fluid between two plates as shown in Figure 2- 8. Suppose that both plates are initially at rest with no flow occurring. When a force F is applied to the upper plate, a shear stress $\sigma$ is generated in the fluid from the cohesive forces between the fluid molecules. It is assumed that the gap h is small and strain is the same at all points. The shear is given by

$$\sigma = F/S \tag{2-26}$$

where $S$ is the surface area of upper face. Alternately, $\sigma$ may be defined as the force that a flowing fluid exerts per unit area of its surface in a direction parallel to the flow. The rate of deformation or the shear rate is the first derivative of strain with respect to time.

$$\dot{\gamma} = \frac{d\gamma}{dt} = \frac{1}{h}\frac{da}{dt} \tag{2-27}$$

A shear viscosity is defined as

$$\eta = \frac{\sigma}{\dot{\gamma}} \tag{2-28}$$

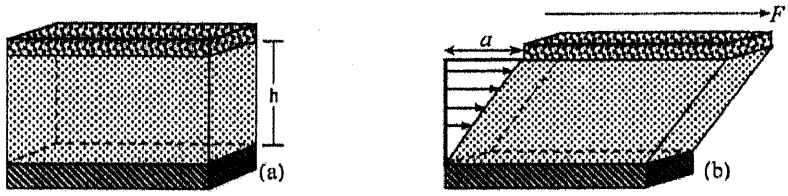


Figure 2-8: Test fluid between two parallel plates separated by a gap *h*. Steady shear (*a*/*h*) is applied to the fluid at rest (a) by sliding the upper plate at a constant velocity given by *da*/*dt* (b).

Note that this expression is analogous to Newton's law for simple liquids and the viscosity here is a function of shear rate and not a constant parameter.

Various kinds of flow curves, i.e., double logarithmic plots of viscosity versus shear –rate, observed in wormlike micellar systems are shown Figure 2-9.

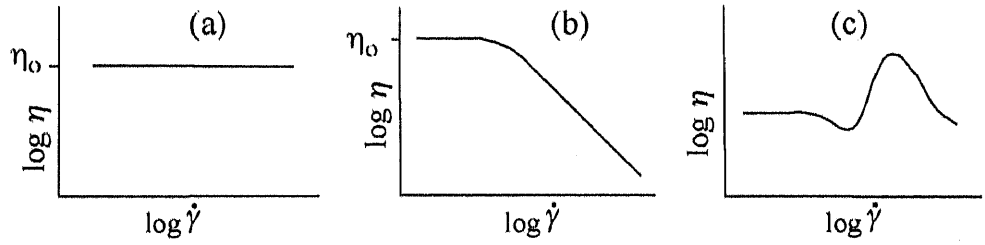


Figure 2-9: Various types of flow curves shown by the solution of surfactant systems.

The simplest type of steady-shear response is Newtonian behavior, where the viscosity is independent of the shear-rate [Figure2-9(a)]. This is also manifested as a linear relationship between shear stress and shear rate, with the slope of the line defining the viscosity. Most low molecular-weight liquids and gases show Newtonian behavior. Among the non-Newtonian phenomena, the most widely observed in the viscoelastic micellar systems is shear thinning. In the simplest case, the sample shows Newtonian behavior at low shear rate and shear thinning at higher shear rate [Figure 2-9(b)]. The zero-shear viscosity may be obtained by the extrapolation of the viscosity curve to zero shear-rate. Shear thickening [Figure 2-9(c)], which corresponds to the increase in viscosity over a range of shear-rate, is observed much less frequently.

### 2.6.1.2 Dynamic (oscillatory-shear) rheology:

In dynamic shear flow, a sinusoidally varying deformation (strain) is applied to the sample (Figure 2-10).

$$\gamma = \gamma_o sin\,(\omega t) \tag{2-29}$$

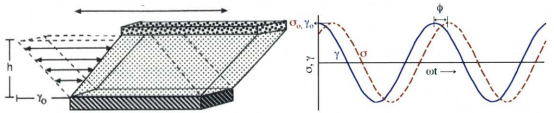


Figure 2-10: Oscillatory deformation of the viscoelastic material and variation of strain (solid line) and stress (dotted line) with time.

Where $\gamma$ is strain –amplitude (i. e. the maximum applied deformation) and w is the frequency of the oscillations. The shear stress generated by the oscillatory shear will again be sinusoidal but will be shifted by a phase angle ($\phi$) with respect to the strain wave form:

$$\sigma = \sigma_o \sin(\omega t + \phi) \tag{2-30}$$

The presence of phase angle term means that the maxima and minima of sinusoidally varying stress signals are not necessarily coincident with the maxima and minima in the strain. For perfect solid, stress is in phase with strain ($\phi$ =0). In case of purely viscous liquid, stress is in quadrature with strain ($\phi = \pi/2$). For viscoelastic materials $\phi$ has an intermediate value. At small strains and for a given viscoelastic material, the fluid structure is not much disturbed by the deformation and the stress measured during oscillatory deformation is controlled by the spontaneous rearrangements or relaxation. In this case, the shear stress produced by a small amplitude deformation is proportional to amplitude of the applied strain $\gamma_o$, and deformation ratio $\sigma_o/\gamma_o$ and the phase angle $\phi$ are the material properties at any frequency, which is the main feature of linear viscoelasticity.

Using trigonometric identities, the stress wave can be decomposed into two components, one in-phase with the strain and the other out-of –phase by 90 degrees:

$$\sigma = \sigma_o \cos(\phi) \sin(\omega t) + \sigma_o \sin(\phi) \cos(\omega t) \tag{2-31}$$

We can rewrite the above expression in terms of two material functions ($G'$ and $G''$) as

$$\sigma = \gamma_o [G' \sin(\omega t) + G'' \cos(\omega t)] \tag{2-32}$$

$$\text{Elastic or storage modulus, } G' = (\sigma_o/\gamma_o)\cos\phi \tag{2-33}$$

$$\text{Viscous or loss modulus, } G'' = (\sigma o/\gamma_o)\sin\phi \tag{2-34}$$

The elastic modulus ($G'$), which is related to the stress in phase with the imposed strain, provides information about the elastic nature of the material. Because elastic

behavior implies the storage of deformational energy in the system, this parameter is also called the storage modulus. The viscous modulus *(G'')*, on the other handle, is related to the stress component, which is completely out-of-phase with the displacement. This parameter characterizes the viscous nature of the material. Because viscous deformation results in the dissipation of energy, the *G''* parameter is also called the loss modulus. A purely elastic material would exhibit a non-zero elastic modulus and a viscous $G' = 0$. In contrast, a purely viscous material would show a zero elastic modulus. A viscoelastic material will exhibit non-zero values for both *G'* and *G''*.

The complex viscosity ($n^*$) is defined as:

$$\eta^* = \frac{\left(G'^2 + G''^2\right)^{\frac{1}{2}}}{\omega} \tag{2-35}$$

The variation of complex viscosity with frequency is analogous to the variation of steady viscosity versus shear-rate.

**2.6.2 Instrumentation**

Rheological measurements are typically performed on a rheometer. There are several categories of rheometers, with the most prominent being capillary rheometer (which utilize pressure-driven or poiseuille flows) and rotational rheometers (which use drag flows). Capillary rheometers are capable of measuring only the steady-shear properties of a fluid, not the dynamic rheological properties. For this reason, we will focus solely on rotational instruments. Two types of rotational rheometers exist: stress-controlled rheometers and strain-controlled rheometers. In a strain-controlled rheometer, a known deformation (strain or shear rate) is applied to the fluid, and the stress is detected. Typically, the strain is applied by rotating one segment of the geometry, and a transducer connected to the other segment measures the stress. A stress rheometer operates in the opposite fashion, by applying a controlled stress and measuring the resulting deformation. In the past few years, stress rheometers have become immensely popular because of great sensitivity and wide torque range.

In rheological measurements, depending on the property of the test material, test conditions to be maintained and type of the material property to be studied, various geometries such as parallel-plates, cone-and- plate, concentric cylinders, can be used to impose shearing flow. Schematic diagrams of cone-plate and couette (concentric cylinders) geometries are shown in Figure 2-11. The parallel-plate and cone-plate

geometries are common due to small amount of sample required and ease to load and clean. The advantage of the cone-plate geometry over the parallel-plate one is that the small cone angle $\theta$ (< 0.2rad) provides a uniform shear throughout the sample. Couette geometry is suitable for low-viscosity samples. Flow is generated in a rotational geometry by moving one of the systems in such a way that the fluid is dragged along the wall.

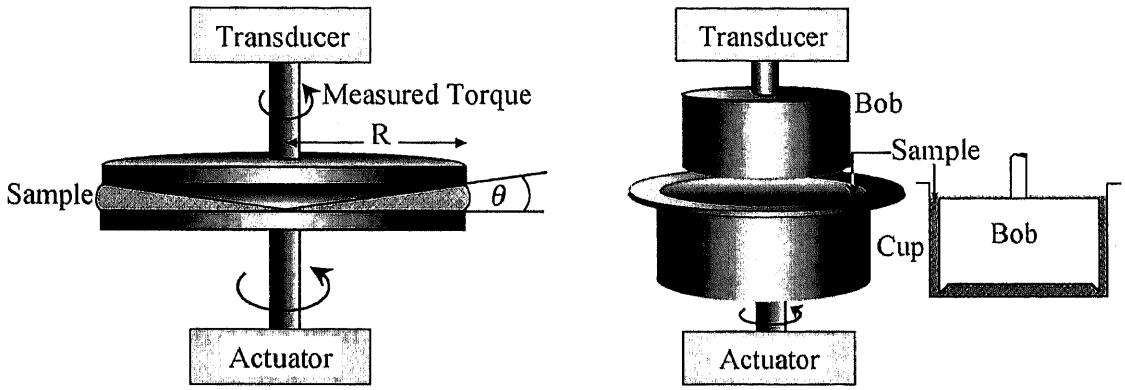


Figure 2-11: Schematic diagrams of cone-plate (left) and couette (right) geometries.

In a strain-controlled rheometer, input is the deformation and output is the torque. The raw data can be converted into rheologically significant quantities using the physical dimension of the geometry. On a cone-plate geometry with cone angle $\theta$ and radius of cone R, following equation relates the angular velocity $\Omega$ (rad.s$^{-1}$) of the lower plate induced by the actuator (as shown in Figure 2-9) to the shear-rate exerted on the sample:

$$\dot{\gamma} = \frac{\Omega}{\theta} \tag{2-36}$$

The response of the sample is measured by the transducer in terms of a torque (M), which is related to the shear-stress according to following relation:

$$\sigma = \frac{3M}{2\pi R^3} \tag{2-37}$$

The viscosity then can be obtained from equation (2-28).

In oscillatory-shear measurement, the plate is made to oscillate from its mean position, with a maximum displacement up to an angle $\varphi$ (in rad). The strain amplitude is then given by

$$\gamma_o = \frac{\varphi}{\theta} \tag{2-38}$$

The response of the sample is in terms of sinusoidal torque (M) with a phase lag ($\phi$) with respect to the input strain. The maximum stress amplitude ($\sigma_o$) is obtained from equation (2-37). The elastic and viscous moduli can then be calculated using equations (2-32) and (2-33) respectively. The final expressions are:

$$G' = \frac{3M\theta}{2\pi R^3 \varphi} \cos\phi \tag{2-39}$$

$$G'' = \frac{3M\theta}{2\pi R^3 \varphi} \sin\phi \tag{2-40}$$

**References:**


1 *Manual of the tensiometer K100*, Krüss GmbH, Hamburg, Germany, **2001**.

2 Vonnegut,B. *Rev. Sci. Instr.* **1942**, *13*, 6.

3 Princen, H.M.; Zia, I.Y.Z.; Mason, S.G. *J. Colloid Interface Sci.* **1967**, *23*, 99.

4 Couper, A.;Newton, R.; Nunn, C. *Colloid Polym. Sci.* **1983**, *261*, 371.

5 Sugden, S. J. Chem. Soc. **1922**, *121*, 858.

6 Rehbinder, P.A. *Z. Phys. Chem.* **1924**, *111*, 447.

7 Glatter, O. in *Modern Aspects of Small-Angle X-ray Scattering* (Brumberger, H., Ed.), Kluwer Academic Publishers, Dordrecht, **1995**.

8 Roe, R.J. Methods of X-ray and Neutron Scattering in Polymer Science, Oxford University Press, New York, **2000**.

9 Guinier, A. *X-ray Diffraction in Crystals, Imperfect Crystals and Amorphous Bodies*, Dover, New York, **1994**.

10 Woolfson, M.M. *An Introduction to X-ray Crystallography*, 2nd edition, Cambridge University Press, Cambridge, **1997**.

11 Glatter, O. In *Neutron, X-ray and Light scattering: Introduction to an Investigative Tool for Colloidal and Polymeric Systems* (Lindner, P.; Zemb, T., Ed.), North-Holland, Amsterdam, **1991**.

12 Cabane, B. *Small Angle Scattering Methods*, Marcel Dekker, New York, **1987**, Vol. 22, pp 57.

13 Pedersen, J.S. *Instrumentation for Small Angle Scattering*, Kluwer Academic Publishers, Amsterdam, **1995**, pp 57.

14 Larson, R.G. *The Structure and Rheology of Complex Fluids*, Oxford University Press, New York, **1999**.

15 Marin, G. in *Rheological Measurement* (Collyer, A. A.; Clegg, D. W.; Eds.), Chapman and Hall, UK, 2nd ed., **1998**.

16 Ferry, J.D. *Viscoelastic Properties of Polymers*, John Wiley & Sons, 3rd ed., **1980**.

# Chapter 3: Phase Behavior and Surface Tensions of Amphiphilic Fluorinated Random Copolymer Aqueous Solutions

## 3.1 Introduction

The fundamental property of surfactants as well as amphiphilic copolymers is their tendency to adsorb at the interface and form self-assemblies in solvent. The formation of self-aggregates and morphology of self-organized structures depend on the segregation tendency of hydrophilic and hydrophobic parts and their ratio in the molecules, which is often expressed as "hydrophilic-lipophilic-balance (HLB)". In block-type copolymers, where hydrophilic and hydrophobic groups are not randomly located, well-defined self-organized structure is formed[1,2]. However, in random copolymers where hydrophilic and hydrophobic groups are randomly distributed, the tendency of self-organization would be considerably reduced, especially when the segregation tendency of both groups is not very large.

Perfluorinated amphiphilic polymers are widely known for their large capability to reduce interfacial tension and their high thermal and chemical stability. The surface properties of such polymers are important for the function of materials. These polymers are used in industry for the production of various surface functional chemicals and possess potential applications such as water and oil repellents for textiles, surface modifiers for plastic, paper and metal, in coating, for antifogging, in cosmetics, in foams and defoaming, in graphic imaging, in greases and lubricants etc[3-6].

Among various types of hydrophobic groups (chains), perfluorinated carbon chain is the most hydrophobic and its tendency to separate from water or hydrophilic groups is the largest. It was reported that for nonionic surfactants one $CF_2$ group is equivalent to 1.7 $CH_2$ groups[7]. As a consequence of the high hydrophobicity of perfluorinated surfactant, the lowest surface tension is attained in aqueous solution. Due to low surface tension, fluorinated amphiphiles are used in many applications. On the other hand, understanding of dynamic surface tension behavior is important for the application of the surfactants in several processes, such as spraying, painting, coating, printing, foaming and wetting, where liquid surfaces expand rapidly.

There are many reports on the equilibrium surface properties[8-14] as well as dynamic surface properties[11,15,16] of fluorocarbon surfactants solutions, but to our knowledge, there are scarcity of report on the interfacial properties of amphiphilic fluorinated random copolymers, although there are some reports on the surface properties of the thin film of copolymer containing perfluoroalkyl and other hydrophobic side chains[3-19]. In this context, we studied the phase behavior, equilibrium surface tension, and dynamic surface tension of aqueous solutions of some amphiphilic fluorinated random copolymers.

## 3.2 Experimental

### 3.2.1 Materials

Fluorinated random copolymers, (perfluoroalkylacrylate)–[poly (ethyleneoxide) methacrylate], with product identification names NS-1620*x* ($x = a - i$) were kindly supplied by Daikin Industries, Ltd. (Japan) and were used without further purification. For the sake of simplicity, each of the copolymers will be denoted hereafter by the last alphabet of its name, for example, *a* stands for NS-1620*a*, *b* for NS-1620*b* and so on. The general chemical structure of the copolymer is shown in Figure 3-1 and the properties of the copolymers are shown in Table 2-1 (see page 25). The apparent HLB for each of the coplymers was estimated by relation[20]: Apparent HLB = (20 x mol wt of EO chain / mol wt of copolymer). Millipore deionized water was used.

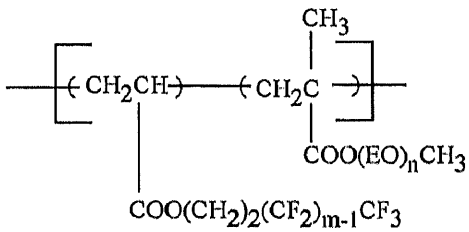


Figure 3-1: Schematic molecular structure of amphiphilic fluorinated random copolymer [$C_mRf$-acrylate]-[$EO_n$-methacrylate]. Copolymers with different combinations of $m$ (= 8, 6, 4, 2 for $C_8Rf$, $C_6Rf$, $C_4Rf$, $C_2Rf$) and $n$ (= 9 and 4.5) were studied.

### 3.2.2 Cloud point determination

Cloud points of fluorinated copolymer solutions were determined visually as the temperatures at which clear or slightly hazy polymer solutions suddenly turned

opaque on heating and clear on subsequent cooling. The sample was heated in such a way that rise in temperature was 0.2°C each time once the temperature reached a few degree below the pre-estimated cloud point. After the temperature crosses the cloud point, the sample was cooled below cloud point, and then it was heated again to see the reproducibility of the data. This procedure was repeated at least three times and cloud point values agreed within 0.2°C.

### 3.2.3 Equilibrium surface tension

The equilibrium surface tension of aqueous amphiphilic fluorinated copolymer solution was measured at 25°C by the Wilhelmy plate technique (K100 tensiometer, Krüss, Germany) and measurement was carried out until it deviated within ± 0.2 $mNm^{-1}$ for the last two readings. The copolymer solution was diluted with water and stirred for few minutes before each measurement. The values of equilibrium surface tension at 1 wt% and 0.1 wt% of aqueous solutions of copolymers were cross-checked using spinning–drop tensiometer (Site 400, Krüss) to see whether the results were affected by the wetting of the plate with solution or not in Wilhelmy plate method[12].

### 3.2.4 Dynamic surface tension

The dynamic surface tension of aqueous solutions of fluorinated random copolymers was measured at 25°C by the maximum–bubble pressure method using a Krüss BP2 tensiometer. A detailed description of measurement method is available elsewhere[21,22].

## 3.3 Results and discussion

### 3.3.1 Phase behavior

Figure 3-2 shows a phase diagram of fluorinated random copolymer-water binary system in wide concentration range. At the composition range studied, only isotropic solution exists at low temperatures. Upon increasing the temperature, clouding phenomenon is observed at temperatures depending on the concentration and the surfactant properties. The clouding phenomenon, which is commonly observed in aqueous nonionic surfactant systems, is related to the macroscopic separation of amphiphilic molecules from the solvent as the hydrophilic group become dehydrated due to increased temperature. In Figure 3-2, the domains of isotropic and turbid solution are separated by solid lines for each of the copolymers. Since clouding phenomenon is associated with the hydrophilicity of the amphiphiles, the trend in

cloud temperature of the fluorinated random copolymer aqueous solutions reflects the variation of the structure of the copolymer, such as the changes in the average number of [$EO_n$-methacrylate] chain per [$C_mRf$-acrylate] chain (*R*) in the molecule, number of EO units (*n*) in [$EO_n$-methacrylate] chain, number of fluorinated carbon (*m*) in the [$C_mRf$-acrylate] chain.

### 3.3.1.1 Variation of R at fixed m and n values

When the *R* value increases, that is, the number of $EO_n$ chain per $C_mR_f$ chain increases, for example among *a*, *b* and *c* copolymers with *m*=8 and *n*=9 (see Table 1) the cloud point shifts to higher temperatures. It is consistent with the fact that when an amphiphile becomes increasingly hydrophilic, the phase separation occurs at higher temperature because of the higher degree of hydration. Similar trend is observed in the systems *d*, *e* and *f* (*m*=4, n=9), but the effect of *R* on the cloud point is greater than that observed in the systems with longer hydrophobes (*a*, *b*, and *c*). For example, on increasing the *R* by more than 150%, the difference in the cloud point in the system *a* and *c* is only ~3 °C, where as it is ~12 °C in the systems *d* and *f*, with estimation of cloud point being made at composition around 40% copolymer solution. It shows that when the fluorocarbon chain becomes long, *R* has a little effect on the cloud point.

### 3.3.1.2 Variation of $EO_n$ chain length at fixed $C_mRf$ chain length

The effect of the variation of EO chain length on the cloud point at fixed fluorocarbon chain length can be seen by considering the systems *f* and *g* with comparable *R* values. With decreasing average *n* of $EO_n$ from 9 to 4.5, the cloud point decreases sharply (by ~34 °C). Even if comparison of cloud points of the system *g* is made with that of system *d* which has comparable fluorine content but has a lower *R* value, and therefore, is more hydrophobic, the effect of decreasing EO chain length in the cloud point is significantly wide (~20°C). This effect of doubling the EO chain length on the cloud points are significantly higher than that observed upon increasing the *R* value by 150% in the systems *d* and *f* discussed above. It indicates that when EO chain length is long, the EO units are better exposed to water and therefore better hydrated than in the case when the EO chain is short.

### 3.3.1.3 Variation of the $C_mRf$ chain length at fixed $EO_n$ chain length (n = 9)

The effect of the fluorocarbon chain length on the cloud point at fixed EO chain length and comparable *R* values can be investigated by comparing the cloud

point behavior of systems *a* (*m*=8), *h* (*m*=6), and *f* (*m*=4) and also the system *i* (*m*=2) with a fact in mind that *R* in *i* is comparatively low (more hydrophobic than other). It can be seen that with decreasing $C_mRf$ chain length, the cloud point gradually decreases, although extent of the decrease in cloud point is not uniform with respect to change in the value of *m*, which is attributed to the additional contribution of the *R* value which is not same in the each of the systems considered here, especially in the case of the system *i*, and to some extent in the system *a*. The observed trend of decreasing cloud point with decreasing lipophilic chain length contradict with the general trends observed for surfactant systems. It is reasonable to expect that when the $C_mRf$ chain length decreases, the hydrophobicity of the copolymer should also decrease, and therefore, the cloud point should increase. The reason for this anomalous behavior has not been understood, and further study is needed to explain the mechanism.

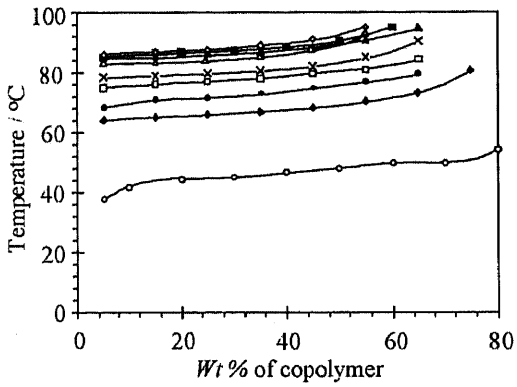


Figure 3-2: Cloud point versus concentration curves of the aqueous solution of random copolymers: *a* (▲), *b* (■), *c* (◇), *d* (●), *e* (□), *f* (×), *g* (○), *h* (△) and *i* (◆).

### 3.3.2 Equilibrium surface tension

The equilibrium surface tension ($\gamma$) versus concentration curves of fluorinated random copolymer aqueous solutions measured by Wilhelmy plate method are shown in Figure 3-3. The time taken to attain constant surface tension during measurement was very long, often 2-3 hours. The very long time needed to reach the equilibrium surface tension is most likely related to the conformational change at the air-water interface[23]. The surface tension values were cross-examined by spinning-drop technique at 0.1 and 1 wt% copolymer concentration. The surface tension values by both methods were in close agreement. Generally, critical micelle concentration (cmc) can be obtained from break point of the slope in the $\gamma$-composition curves.

However, in the present copolymer aqueous systems, there is no sharp break point in the slope. Therefore, no clear evidence for the formation of aggregate could be obtained. Existence of isotropic solution over wide composition range indicates that probably the copolymers do not form aggregate.

The tendency to decrease surface tension of water by the fluorinated copolymer appears to be dependent on both $C_mRf$ and EO chain length. The fluorinated copolymers *a*, *b* and *c* with $m$=8 show the highest surface tension among all the copolymers and the copolymers with shorter fluorocarbon chain but similar EO chain length, namely, *d*, *e*, *f* ($m$=4) show lower $\gamma$ values. Surface tension value of copolymer *h* ($m$=6) is almost same as that of the copolymers with $m$=4. Copolymer *i* with very short fluorocarbon chain ($m$=2), shows still lower $\gamma$, at least in low concentration region.

Thus, the observed trend in the surface tension shows that with increasing fluorocarbon chain length, the copolymer becomes less surface active which is consistent with the trend observed in the cloud point measurement because increase in the fluoroalkyl chain length make the copolymer more hydrophilic, therefore, less surface active. However, this trend is not consistent with the general trend observed in the surfactant systems. Normally, it is expected that as the lipophilic chain length decreases, surfactants become increasingly hydrophilic and their affinity for air-water interface should decrease, which is reflected in the decrease equilibrium $\gamma$ value. For conventional hydrocarbon surfactant systems it is known that the minimum $\gamma$ of the aqueous solution is dependent on the number of methyl groups located on the surface because bulky and less dense methyl groups achieve higher surface coverage and decrease the surface tension more effectively that the methylene groups can do[24]. In the present systems, however, observed surface tension does not seem to be related with the number of $-CF_3$ group per copolymer molecule, as evident from nearly similar value of surface tension for copolymers *a*, *b* and *c*, (or *d*, *e*, and *f*) which have identical value of $m$ and $n$ but differ in the number of hydrophilic chain per hydrophobic chain in the molecule ($R$), and therefore, differ in the number of $-CF_3$ groups per molecule.

The observed trend in the influence of fluorocarbon chain length on the surface tension may be related to orientation of the chain at interface. It is known that

the arrangement and orientation of fluorinated chain on surface depends on its chain length, long-chain fluorinated hydrophobe with $m > 8$ being in ordered and crystalline state whereas the short-chain hydrophobes are oriented randomly, and are in mobile state which results in the exposure of carbonyl group[3,17,19]. Possibly, when the long and rigid hydrophobes ($m = 8$) of single copolymer molecules are oriented randomly at the interface, they produce steric hindrance for the adsorption of other molecules, thereby reducing the adsorption of the copolymer but with decreasing hydrophobic chain length, the steric contribution would also be decreasing, thus resulting in the improved packing of the hydrophobes at the interface, and hence, lower surface tension.

Comparison of the surface tension values of *f* and *g* shows that with decreasing number of EO units (*n*) at similar value of *m*, the surface tension value of the copolymer decreases, because a decrease in EO chain length would make the molecule more lipophilic, and therefore more surface active.

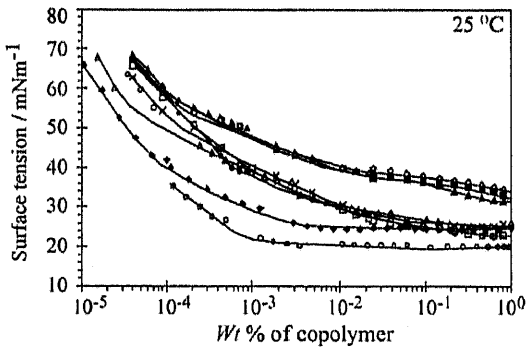


Figure 3-3: Equilibrium surface tension versus concentration curves of *a* (▲), *b* (■), *c* (◇), *d* (●), *e* (□), *f* (×), *g* (○), *h* (△) and *i* (◆) aqueous solutions.

### 3.3.3 Dynamic surface tension

The results of dynamic surface tension measurement of fluorinated random copolymer solutions at three different concentrations, viz., 0.01wt%, 0.1wt% and 1 wt% are shown in Figure 3-4. When a fresh interface is created surfactant molecules start to migrate at the interface and reduction of dynamic surface tension involved several mechanisms[25] such as (i) diffusional transport, reorientation, and adsorption of the surfactant molecules, (ii) diffusional transport of the micelles, and (iii) dissociation of the micelles. Since there is no clear evidence of the formation of aggregates in these systems, the dynamic surface tension of the aqueous solutions of

copolymers can be attributed to the diffusion of the monomers up to the sublayer below the air-water interface, followed by an adsorption at the interface.

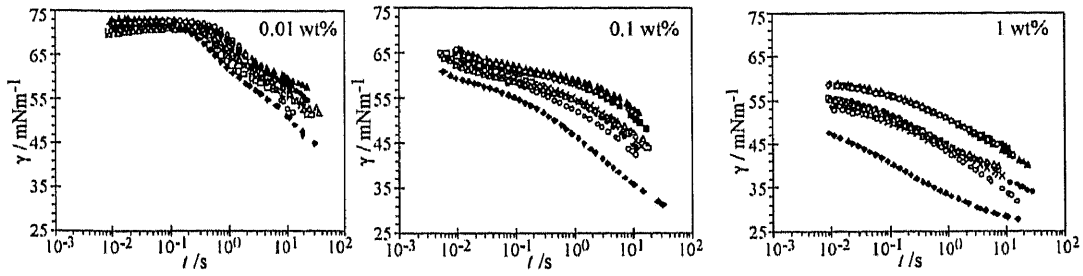


Figure 3-4: Dynamic surface tension of fluorinated random copolymer aqueous solutions at 25°C and different copolymer concentrations. Symbols for copolymers are: *a* (▲), *b* (■), *c* (◇), *d* (●), *e* (□), *f* (×), *g* (○), *h* (△) and *i* (◆).

The rate of solute adsorbed at a newly created surface in the absence of an energy barrier to adsorption, increases with concentration[26]. As can be seen from Figure 3-4, at low concentration (0.01wt%), there is a long induction time (~0.2–0.5 s), during which the surface tension of the solution is same as that of water. It indicates that the adsorption of the copolymer molecules at air-water interface is very slow, which is also evident from the surface tension values at the maximum range of measurement time which are far from the equilibrium values even after very long time (~30 s). At higher concentration (0.1 wt% copolymer), no induction period is seen in short time, but the effect of molecular structure on the surface tension decay can be clearly observed. Within the measured range, value and decay rate of surface tension is correlated to the fluorocarbon chain length of the copolymers, with the longest fluorocarbon chain, *a*, *b*, and *c* being the least surface active and slowest to reduce the surface tension which may be attributed to the steric hindrance due to random orientation of the long and rigid hydrophobes.

The trend of dynamic surface tension is consistent with that observed for equilibrium surface tension, except that the dynamic surface tension of copolymer *i* lower than that of *g* within the time range of measurement, which is very short in comparison to the time required to attain equilibrium value, but the decay curves of these copolymers at 1wt% indicates that after long time *g* tends to attain surface tension lower than the copolymer *i*. At 1wt% copolymer concentration, the effect of molecular structure on the decay of surface tension is more clearly visible. In consistence with the results from equilibrium surface tension measurements, dynamic surface tension data show that the variation of the hydrophilic-hydrophobic chain

ratio ($R$) of the copolymer at fixed hydrophobic and hydrophilic chain lengths has no effect on the dynamic surface tension decay.

### 3.4 Conclusions

The phase behavior and as well as static and dynamic surface tensions of aqueous solutions of fluorinated random copolymers [$C_m$Rf-acrylate]-[$EO_n$-methacrylate] with different combination of $m$ and $n$ and ratio of the numbers of hydrophilic to hydrophobic chain, $R$ were investigated. Isotropic solution is formed in aqueous copolymer solution at lower temperatures over wide composition range. The cloud point of copolymer decreases with decreasing $n$ as well as $m$, and also with decreasing $R$, suggesting that the copolymers become more hydrophobic on decreasing $n$ and $R$, which is as expected, but increasing hydrophobicity (decreasing cloud point) with decreasing fluorocarbon chain length ($m$) is opposite to what is generally observed in amphiphilic systems. Further study is needed to understand this behavior of the copolymer. Moreover, equilibrium and dynamic surface tension measurements show that copolymer become increasingly surface active as $m$ decrease which may have arisen due to restricted adsorption of the copolymer with long fluorinated chain at air/water interface. Surface tension results indicate that the random copolymers do not form micellar aggregates.

**Reference:**


1 Alexandridis, P.; Hatton, T.A. *Colloid Surf. A* **1995**, *96*, 1.

2 Wanka, G.; Hoffmann, H.; Ulbricht, W. *Macromolecules* **1994**, *27*, 4145.

3 Park, I.J.; Lee, S.-B.; Choi, C.K.; Kim, K.-J. *J. Colloid Interface Sci.* **1996**, *181*, 284.

4 Kissa, E. *Fluorinated Surfactants and Repellants*, 2nd Ed., Marcel Dekker, New York, **2001**.

5 Imae, T. *Curr. Opin. Colloid Interface Sci.* **2003**, *8*, 307.

6 Berret, J.-F.; Calvet, D.; Collet, A.; Viguier, M. *Curr. Opin. Colloid Interface Sci.* **2003**, *8*, 296.

7 Ravey, J.C.; Gherbi, A.; Stébé, M. J. *Prog. Colloid Polym. Sci.* **1988**, *76*, 234.

8 Eastoe, J.; Paul, A.; Rankin, A.; Wat, R.; Penfold, J.; Webster, J.R.P *Langmuir* **2001**, *17*, 7873.

9 Matos, L.; Ravey, J.-C.; Serratrice, G. *J. Colloid Interface Sci.* **1989**, *128*, 341.

10 Kunieda, H.; Shinoda, K. *J. Phys. Chem.* **1976**, *80*, 2468.

11 Rodriguez-Abreu, C.; Kunieda, H. *J. Dispersion Sci. Technol.* **2005**, *26*, 435.

12 Rodríguez, C.; Kunieda, H.; Noguchi, Y.; Nakaya, T. *J. Colloid Interface Sci.* **2001**, *242*, 255.

13 Asakawa, T.; Ishikawa, K.; Miyagishi, S.; *J. Colloid Interface Sci.* **2001**, *240*, 365.

14 An, Y.-J.; Jeong, S.-W. *J. Colloid Interface Sci.* **2001**, *242*, 419.

15 Hirt, D.E.; Prud'Homme, R.K.; Miller, B.; Rebenefeld, L. *Colloid Surf.* **1990**, *44*, 101.

16 Frømyr, T.; Hansen, F.K.; Kotzev, A.; Laschewsky, A. *Langmuir* **2001**, *17*, 5256.

17 Morita, M.; Ogisu, H.; Kubo, M. *J. Appl. Polym. Sci.* **1999**, *73*, 1741.

18 Kim, D.-K.; Lee, S.-B. *J. Colloid Interface Sci.* **2002**, *247*, 490.

19 Honda, K.; Morita, M.; Otsuka, H.; Takahara, A. *Macromolecules* **2005**, *38*, 5699.

20 Griffin, W.C. *J. Soc. Cosmet. Chem.* **1954**, *5*, 249.

21 Franses, E.I.; Basaran, O.A.; Chang, C.-H. Curr. Opin. Colloid Interface Sci. **1996**, *1*, 296.

22 Fainerman, V.D.; Miller, R.; Joos, P. *Colloid Polym. Sci.* **1994**, *272*, 731.

23 Folmer, B.M.; Svensson, M.; Holmberg, K.; Brown, W. *J. Colloid Interface Sci.* **1999**, *213*, 112.

24 Hill, R.M., Ed. *Silicone Surfactants*, Marcel Dekker, New York, Surfactant Sci. Series 86, **1999**.

25 Zhmud, B.V.; Tiberg, F.; Kizling, J *Langmuir* **2000**, *16*, 2557.

26 A.F.H. Ward, A.F.H.; Tordai, L. *J. Chem. Phys.* **1946**, *14*, 453.

# Chapter 4: Interfacial Properties of Aqueous Nonionic Fluorocarbon Surfactant Solutions

## 4.1 Introduction

Fluorinated surfactants are widely known for their higher capability to reduce surface tension of water to a very low value. Due to their outstanding thermal and chemical stability, fluorinated surfactants possess potential applications such as water and oil repellents for textiles, surface modifiers for plastic, paper, and metal, in coating, for antifogging, in foams and defoaming, in graphic imaging, in grease and lubricants[1-6]. The presence of fluorine atoms alters the properties of surfactants and particularly its hydrophobicity and its critical micellar concentration, CMC[4]. It has been reported that one $CF_2$ group in fluorinated surfactant system is equivalent to $1.7CH_2$ groups in hydrocarbon type nonionic surfactant system[7]. Usually, fluorinated surfactants are about 10 times more effective than silicones and 50-100 times more effective than hydrocarbon surfactants. The relatively high price of fluorinated surfactants limits their use to applications where hydrocarbon-based surfactants are inadequate. However, fluorinated surfactants are cost-effective because their high price is compensated by the low concentration needed[1].

There are several reports on the equilibrium surface tension properties[3,8-13]of aqueous fluorinated surfactant solutions, however, a little is known regarding the dynamic surface tension properties[10,14,15] of such systems. Understanding of dynamic interfacial properties such as dynamic surface tension and the surface dilatational elasticity are very important as it determines the application of the surfactants in several processes, such as formation and stability of foam, stability of emulsion, flotation and coating etc.

In this context we studied the equilibrium surface tension properties and then discussed the dynamic interfacial behavior of the nonionic fluorocarbon surfactants in water.

## 4.2 Experimental

### 4.2.1 Materials

Fluorinated surfactants, N-polyoxyethylene-N-propyl perfluorooctane sulfonamide $C_8F_{17}SO_2N(C_3H_7)(C_2H_4O)_nH$ ($n$ = 10 and 20) named as EF122B and EF122A were obtained from Mitsubishi Materials, Japan. Volatile components

present in EF122B surfactant was removed by keeping the surfactant under vacuum for several days until a constant weight is observed, and EF122A was used as received without further purifications. Millipore water was used in all the experiments.

### 4.2.2 Equilibrium surface tension

The equilibrium surface tension of aqueous fluorocarbon surfactant solution was measured at 25°C by the Wilhelmy plate technique (K100 tensiometer, Krüss, Germany). The surfactant solution was diluted with water and stirred for few minutes before each measurement. CMC was obtained from the break point in the surface tension versus logarithm of surfactant concentration.

### 4.2.3. Dynamic surface tension

The dynamic surface tension of aqueous solution of fluorocarbon surfactant was measured at different temperatures by the maximum-bubble pressure method using a Krüss BP2 tensiometer. Surface ages of bubbles can be measured between 5 ms to 50s.

### 4.2.4. Surface dilatational elasticity

Surface dilatational elasticity was measured at 25°C by the oscillating air bubble (rising drop) method, using Tracker (I. T. Concept, France). The size of air bubble formed inside the test solution was varied sinusoidally and the variation of the surface area of the bubble and the surface tension was measured from the image analysis of the bubble.

## 4.3 Results and discussion

### 4.3.1 CMC and equilibrium surface tension

The equilibrium surface tension versus concentration curve of EF122A aqueous solutions is shown in Figure 4-1. The surface tension of aqueous solutions decrease with increasing EF122A concentration reaching a break point, which is taken as the CMC. The surface tension obtained at CMC is 24.6mN.m$^{-1}$ and CMC is $2.3\times10^{-2}$ mM at 25°C. The surface excess, $\Gamma$ can be calculated from the surface tension-concentration plot (Figure 4-1) using the Gibbs equation,

$$\Gamma = -\frac{1}{RT}\frac{d\gamma}{d\ln C} \qquad (4\text{-}1)$$

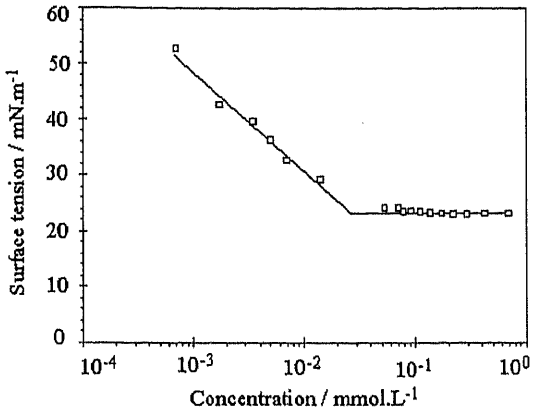


Figure 4-1: Equilibrium surface tension versus concentration curve of EF122A aqueous solution at 25°C.

and the surface area occupied by a surfactant molecule at the air-liquid interface, *a*, is calculated by the following equation

$$a = (\Gamma N_A)^{-1} \qquad (4\text{–}2)$$

where $R$ is the gas constant, $T$ the absolute temperature, $N_A$ the Avogadro number. Results are presented in Table 1 and compared with EF122B. Since EF122A is more hydrophilic than EF122B, so CMC for EF122A is higher than that of EF122B. Lower $\Gamma$ and higher $a$ values for EF122A indicate that it packs less tightly at the interface, which results in a higher surface tension value at the CMC.

Table 4-1: CMC, surface excess, area / molecule and surface tension at CMC at 25°C

| Surfactant | CMC/mM | $\Gamma$/ mol.m$^{-2}$ | $a$ / nm$^2$ | $\gamma_{cmc}$ / mN.m$^{-1}$ |
|---|---|---|---|---|
| EF122A | 0.023 | $0.92\times 10^{-6}$ | 1.81 | 24.6 |
| EF122B | 0.005[a] | $2.39\times10^{-6}$ [a] | 0.70[a] | 21[a] |

[a] Data from reference 10

### 4.3.2 Dynamic surface tension

#### 4.3.2.1 Effect of concentration

Dynamic surface tensions (DST) of aqueous solutions of EF122A were measured at different concentrations above CMC and the results are shown in Figure 4-2. When a fresh interface is created surfactant molecules start to migrate at the interface and reduction of surface tension involved several mechanisms[16] such as (i) diffusional transport, reorientation and adsorption of surfactant molecules, (ii) diffusional transport of the micelles, and (iii) dissociation of micelles. It is seen from Figure4-2 that the rate of surface tension decay becomes faster as the surfactant concentration increases, since the systems are above CMC, micelles act as a reservoir to supply monomeric molecules for the surface[17]. A detailed study of surface tension

properties of aqueous solution of EF122B is found elsewhere[10] but for comparison with EF122A we also measured dynamic surface tension of 1wt% EF122B. At a given concentration (1wt%), the aqueous solution of EF122B shows higher surface tension than that of EF122A within the time range of measurement, which is very short in comparison to the time required to attain equilibrium value, but the decay curve of EF122B indicates that after long time (~10s), 1 wt% aqueous solution EF122B tends to attain lower surface tension value than that of 1wt% of aqueous EF122A. This behavior could be explained by the presence of very stable micelles that slow down the diffusion process[18].

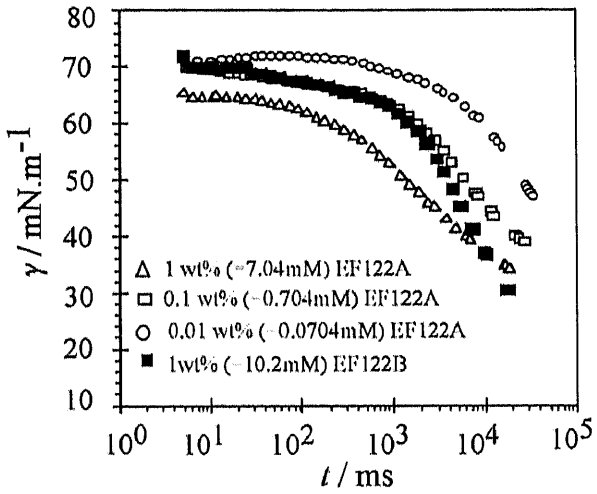


Figure 4-2: Dynamic surface tension (DST) of aqueous solutions of EF122A and EF122B at various concentrations above CMC at 25°C.

Ward-Tordai equation[19] can be used to describe the behavior of dynamic surface tension when the adsorption of surfactant at the interface is purely diffusion-controlled. Although dynamic surface tension is usually estimated by approximate relations for very short times ($t \rightarrow 0$) and very long times ($t \rightarrow \infty$)[20], it is not easy to solve the complete equation. Due to the presence of non-diffusive mechanisms or because of instrument limitations the model does not fit the experimental data. Here a simple approximation is taken into consideration. A normalized dynamic surface tension is defined as

$$\gamma_n = \frac{(\gamma_t - \gamma_\infty)}{(\gamma_0 - \gamma_\infty)} \tag{4-3}$$

where $\gamma_0$ $\gamma_t$, $\gamma_\infty$, are surface tensions at zero time , at time $t$, and after very long time when surface tension reaches to equilibrium values respectively. Following a common trend in dynamic surface process $\gamma_n$ is expressed by a series of exponentials of time

$$\gamma_n = \sum_{i=1}^{n} a_i e^{(-t/\tau_i)} \qquad (4\text{-}4)$$

where $a_i$ is constant and $\tau_i$ is a parameter having a unit of time related to the decay or relaxation of surface tension. A satisfactory fitting to the experimental data achieved using above equation involving two $\tau_i$ terms is presented in Figure 4-3. Two $\tau_i$ values, with $\tau_1 >> \tau_2$ indicates the presence of two mechanisms of widely different time scale for the adsorption of surfactant at the interface.

According to the theory of adsorption relaxation[21] when the diffusion time of surfactant monomers from the micelle ($t_m$) is much faster than that from the bulk solution ($t_d$) i.e. $t_m >> t_d$, then surface tension decays exponentially with time. This is generally occurs at higher surfactant concentration that is above CMC.

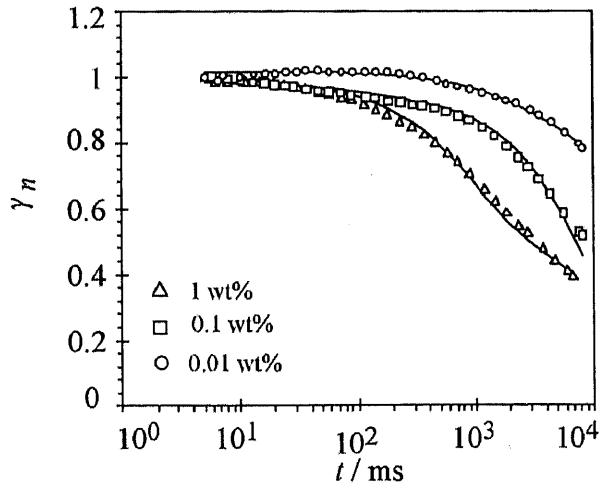


Figure 4-3: Normalized dynamic surface tension at 25°C of aqueous solutions of EF122A at various concentrations. Lines are best fits to experimental points.

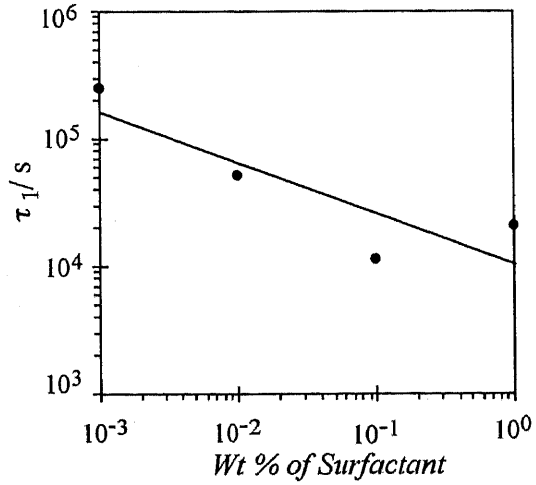


Figure 4-4: Variation of the parameter $\tau_1$ as a function of surfactant concentration for EF122A at 25°C. The solid line is the fit to the experimental point.

We have calculated the $\tau_1$ at different surfactant concentration using equation (4-4) and the results are given in Figure 4-4. The variation of $\tau_1$ with concentration follows a decreasing power law, which indicates that the diffusion is driven by concentration gradient between the bulk and the surface.

### 4.3.2.2 Effect of temperature

The plot of dynamic surface tension versus temperatures for 1wt% of aqueous solution of EF122A is shown in Figure 4-5.

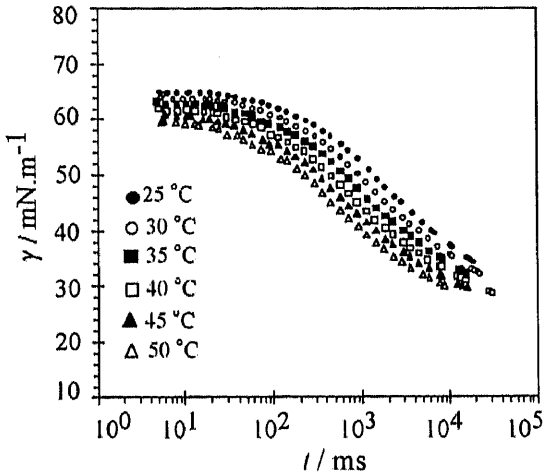


Figure 4-5: Dynamic surface tension behavior of 1wt% aqueous EF122A solutions at different temperatures.

With rise in temperature the diffusion of surfactant molecules increases and also the solubility of the nonionic surfactant decreases at higher temperature[14] and hence the surface tension decreases rapidly. The plot of normalized dynamic surface is shown in Figure 4-6. A double exponential equation fits well the experimental data suggesting more than one relaxation mechanism.

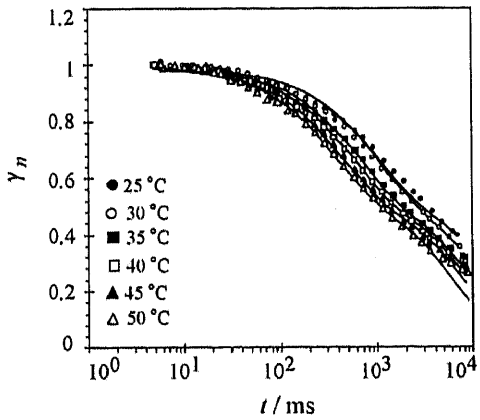


Figure 4-6: Normalized dynamic surface tension of 1wt% aqueous EF122A solutions at different temperatures. Lines are the best fits to experimental points.

The $\tau_1$ shows a good correlation with temperature, most probably corresponds to a diffusive mechanism. The poor correlation of $\tau_2$ with temperature may be due to

other non-diffusive mechanisms of surface tension decay, and partly due to instrumental restrictions of not measuring sufficient data points at long time, which is beyond the working range of instrument.

The plot of $1/\tau_1$ versus $1/T$ for EF122A at 1wt% is shown Figure 4-7. The plot shows the Arrhenius–type behavior with $1/\tau_1$ being the first-order kinetic constant, which decreases with temperature. The slope of the line in Figure 4-7 is proportional to activation energy barrier of adsorption at the interface.

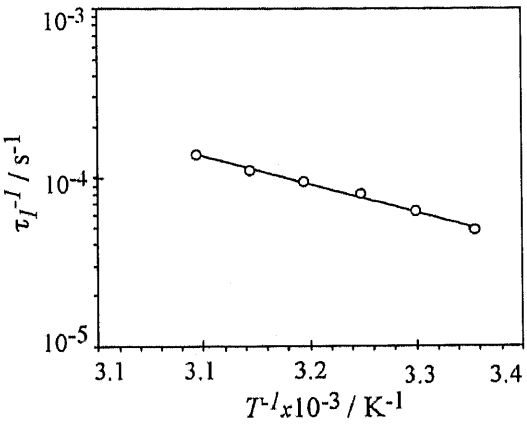


Figure 4-7: Variation of $\tau_1^{-1}$ as a function of the inverse of temperature of 1wt% EF122A aqueous solution.

### 4.3.3 Interfacial dilatational rheology

The interfacial surface dilatational elasticity $|E^*|$ of an air-liquid interface of area, A undergoing a periodic dilatation is given by the equation

$$|E^*| = \frac{d\gamma}{d\ln A} \tag{4-5}$$

where $d\gamma$ is the small change in surface tension due to small change in area $dA$. The interfacial elasticity is related to the ability of the perturbed interface to retain the equilibrium tension, which mainly depends on the kinetics of the exchange of the surfactant molecules between the bulk and interface. This kinetics is highly dependent on the dilatational frequency and nature of the surfactant molecules. When the interfacial dilatational frequency is high, the surfactant molecules have no time for bulk-interface exchange and the value of $\gamma$ deviates from the equilibrium value and consequently the magnitude of $|E^*|$ increases. At very fast dilatational frequency, however, the elasticity becomes independent of the oscillation frequency[22,23]. Figure 4-8 shows the variation of the modulus of surface dilatational elasticity as a function of oscillation frequency for EF122A and EF122B aqueous solutions at different

concentration at 25°C. In all measurements, the interface was allowed to attain equilibrium surface tension before inducing sinusoidal deformation.

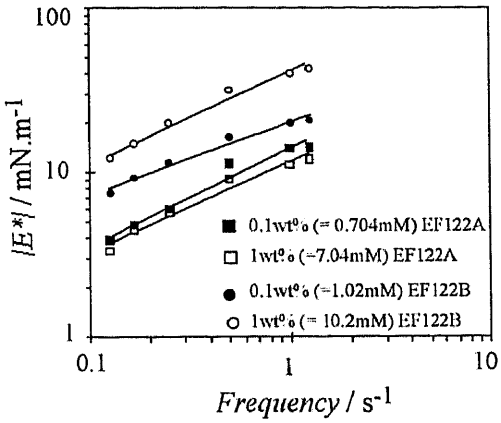


Figure 4-8: Plot of surface dilatational elasticity as a function of oscillatory frequency at various concentrations of aqueous solutions of EF122A and EF122B at 25°C.

Increasing the surfactant concentration increases the extent of adsorption of surfactant molecules at the interface and surface tension will not change appreciably compared to surface area of the interface and hence elasticity decreases. That is why the elasticity value at 1wt% is lower than 0.1wt% for EF122A although the difference between elasticity values is narrow. However, the opposite trend of increasing the surface elasticity value with the surfactant concentration is observed in the EF122B system. This result contradicts the general trend for the variation of elasticity with surfactant concentration. This anomalous behavior is attributed to the different micellar structure in 1wt% EF122B system. From the viscosity measurement it is found that the viscosity of 1wt% EF122B sample is nearly one hundred fifty times higher than that of pure water at 25°C. This indicates the formation of long entangled micelles and hence the diffusion of monomers from micellar reservoir is slower within time scale of measurement. This result is correlated with the dynamic surface tension behavior of 1wt% EF12B (Figure 4-2) and confirm the slow diffusion of monomers to the air-liquid interface.

**4.4 Conclusions**

The fluorinated surfactant EF122A shows significantly low values for both CMC and equilibrium surface tensions at CMC. The dynamic behavior of this system is characterized by fitting the two-terms exponentials to the dynamic surface tension data suggesting more than one relaxation mechanism. Due to fast diffusion of surfactant molecules to surface EF122A is more effective in reducing the surface tension of water compared with EF122B over short time. The surface dilatational

elasticity of air–liquid interface is high for EF122B system compared with EF122A system within the measured range of dilatational frequency (0.125-1.25Hz) and it is attributed to slow exchange of monomers between bulk and interface.

**References**


1 Kissa, E. *Fluorinated Surfactants and Repellants*, 2nd Ed., Marcel Dekker, New York, **2001**.

2 Hoffmann, H.; Würtz, J. *J. Mol. Liq.* **1997**, *72*, 191.

3 Kunieda, H.; Shinoda, K. *J. Phys. Chem.* **1976**, *80*, 2468.

4 Shinoda, K.; Hato, M.; Hayashi, T. *J. Phys. Chem.* **1972**, *76*, 909.

5 Ravey, J.C.; Stébé, M.J. *J. Colloids Surf. A,* **1994**, *84*, 11.

6 Würtz, J.; Meyer, J.; Hoffmann, H. *Phys. Chem. Chem. Phys.* **2001**, *3*, 3132.

7 Ravey, J.C.; Gherbi, A.; Stébé, M. *Prog. Colloid Polym. Sci.* **1988**, *76*, 234.

8 Eastoe, J.; Paul, A.; Rankin, A.; Wat, R.; Penfold, J.; Webster, J.R.P. *Langmuir* **2001**,*17*, 7873.

9 Matos, L.; Ravey, J.-C.; Serratrice, G. *J. Colloid Interface Sci.* **1989,** 128, 341.

10 Rodriguez-Abreu, C.; Kunieda, H. *J. Dispersion. Sci. Technol.* **2005**, *26*, 435.

11 Rodríguez, C.; Kunieda, H.; Noguchi, Y.; Nakaya, T. *J. Colloid Interface Sci.* **2001**, *242*, 255.

12 Asakawa, T.; Ishikawa, K.; Miyagishi, S. *J. Colloid Interface Sci.* **2001**, *240*, 365.

13 An, Y.-J.; Jeong, S.-W. *J. Colloid Interface Sci.* **2001**, *242*, 419.

14 Hirt, D.E.; Prud'Homme, R.K.; Miller, B.; Rebenefeld, L. *Colloid Surf.* **1990**, *44*, 101.

15 Frømyr, T.; Hansen, F.K.; Kotzev, A.; Laschewsky, A. *Langmuir* **1990**, *17*, 5256.

16 Zhmud, B.V.; Tiberg, F.; Kizling, J. *Langmuir* **2000**, *16*, 2557.

17 Kjellin, U.R.M.; Reimer, J.R.; Hansson, P. *J. Colloid Interface Sci.* **2003**, *262*, 506.

18 Patist, A.; Kanicky, J.R.; Shukla, P.K.; Shah, D.O. *J. Colloid and Interface Sci.* **2002**, *245*, 1.

19 Ward, A.F.H.; Tordai, L. *J. Chem. Phys.* **1946**, *14*, 453.

20 Theander, C.: Pugh, R. *J. Colloid Interface Sci.* **2001**, *239*, 209.

21 Danov, K.D.;Valkovska, D.S.; Kralchevsky, P.A. *J. Colloid Interface Sci.* **2002**, *251*, 18.

22 Wantke, K.-D.; Fruhner, H.; Fang, J.; Lunkenheimer, K. *J. Colloid Interface Sci.* **1998**, *208*, 34.

23 Wantke, K.-D.; Fruhner, H.; Örtegren, J. *Colloids Surf. A* **2003**, *221*, 185.

# Chapter 5: Phase Behavior in Aqueous Mixtures of Fluorinated Surfactant and Hydrophobic Fluorinated Polymer

## 5.1 Introduction

Fluorinated surfactants are known to possess remarkable thermal and chemical stability and can reduce the surface tension of water to very low values, therefore, they have several applications such as water and oil repellents for textiles, surface modifiers for plastic, paper and metal, in coating, for antifogging, in cosmetics, in foams and defoaming, in graphic imaging, in greases and lubricants, etc[1-6]. The replacement of hydrogen atoms by the highly electronegative fluorine strongly affects the properties of surfactants and particularly its hydrophobicity and its critical micellar concentration (cmc)[4]. The greater rigidity, volume, and hydrophobicity of fluorocarbon chains, relative to hydrocarbon chains, enhance the self-association of fluorinated surfactants into micelles, as well as into the liquid crystal mesophases and vesicles[1]. In contrast to the extensive knowledge on hydrocarbon type surfactants, the phase behavior of fluorinated surfactant has been much less explored. The structures formed by fluorinated surfactants are as various as with hydrogenated surfactants. However, they tend to prefer to form structures based on bilayers[5]. Among fluorinated surfactants perflurocarboxylic acids and their alkali-metal and (alkyl) ammonium salts are widely investigated compounds[2,4,7-11]. The anionic fluorinated alkyl carboxylates continue to attract attention due to their ability to form the lyotropic nematic phases. Monduzzi et al. reported the counterion effect on the phase behavior of perfluropolyether carboxylates in water[12-14]. In spite of the growing study of phase behavior of nonionic fluorinated surfactants in water[15-20] the incorporation of fluorinated oil into self–organized structures of fluorocarbon surfactant has rarely been considered[21]. Perfluoropolyether (PFPE) oils have been used as lubricants in many industrial applications and possess the main properties of fluorinated surfactants like thermal, chemical and biological inertness, and low compatibility with aqueous and hydrocarbon based systems. In this context, we aim to study the phase behavior and microstructure of aqueous mixture of fluorinated surfactant and fluorinated polymer.

## 5.2 Experimental

### 5.2.1 Materials

Perfluoropolyether oil [F-$(CF_2CF_2CF_2O)_n$-$CF_2CF_2COOH$] designated as $(C_3F_6O)_nCOOH$ was kindly supplied by Daikin Industries, Ltd. (Japan). The number average molecular weight of $(C_3F_6O)_nCOOH$ is 3600, which gives $n \approx 21$and polydispersity 1.14. The fluorinated surfactant $C_8F_{17}SO_2(C_3H_7)N(C_2H_4O)_{10}H$ designated as $C_8F_{17}EO_{10}$ was obtained as a gift from Mitsubishi Materials (Japan). The surfactant was purified by placing it under vacuum for several days in order to remove volatile components until weight became constant. $(C_3F_6O)_nCOOH$ was used as received. Millipore water was used in all the experiments.

### 5.2.2 Determination of phase diagrams

Various amounts of components were weighed and flame-sealed in ampoules. Samples were mixed using a vortex mixer and homogeneity was attained by repeated centrifugation through a narrow construction in sample tubes. The ampoules were then left in a temperature-controlled bath at 25°C for several days to bring the system at equilibrium. The phase state was determined by direct visual inspection and by crossed polarizers.

### 5.2.3 Small angle X-ray scattering (SAXS)

The structural characterization of liquid crystal was determined by a Nanoviewer SAXS of Rigaku, equipped with a CCD detector, operating at 40kV and 20mA. The samples were covered by plastic films (Mylar seal method). The interlayer spacing, d, of the liquid crystals was obtained from the first Bragg peak.

### 5.2.4 Rheological measurements

Rheological measurements were performed in an ARES7 Test Station (Rheometric Scientific) at 25 °C using a Couette fixture with a 33.3mm-long bob. Samples were equilibrated for at least 24 h before the measurements.

## 5.3 Results and discussion

### 5.3.1 Phase diagram of water/ $C_8F_{17}EO_{10}$/ $(C_3F_6O)_nCOOH$ system

The ternary phase diagram of water/ $C_8F_{17}EO_{10}$/$(C_3F_6O)_nCOOH$ system at 25°C is shown in Figure 5-1. In the water - $C_8F_{17}EO_{10}$ binary system, surfactant forms aqueous micellar solution ($W_m$), lamellar ($L_\alpha$), and surfactant liquid or reverse micellar solution ($O_m$) phases. The isotropic gel, hexagonal ($H_1$) and normal bicontinuous cubic ($V_1$) phases are also observed at temperature below 25°C[22].

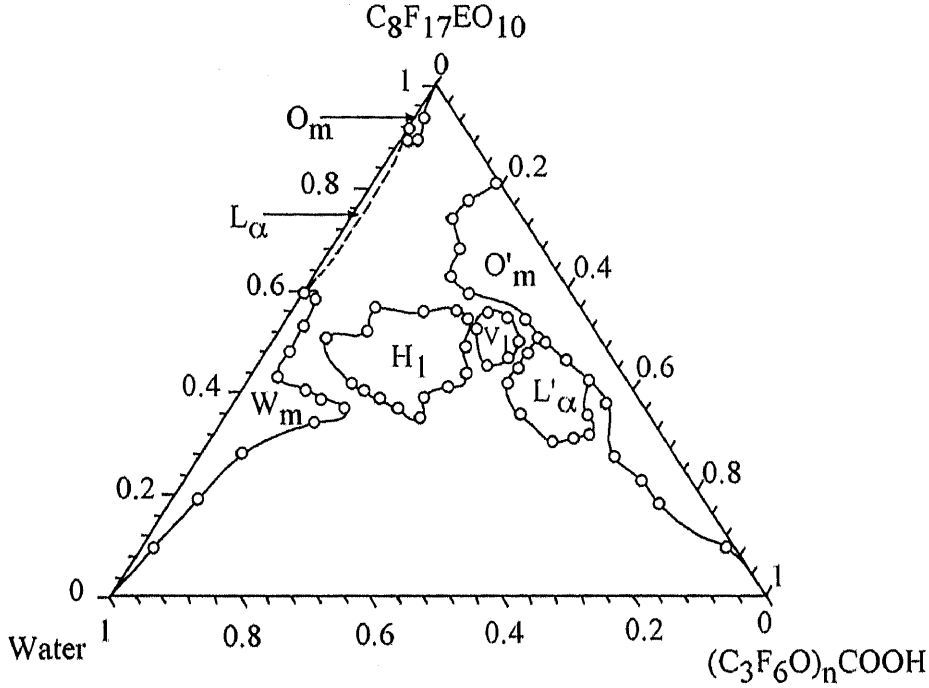


Figure 5-1: Phase diagram of water / $C_8F_{17}EO_{10}$ / $(C_3F_6O)_nCOOH$ system at 25°C. Only single phase regions are indicated. $W_m$: micellar solution; $H_1$: hexagonal phase; $L_\alpha$: surfactant rich lamellar phase; L L'$_\alpha$: polymeric oil rich lamellar phase; $O_m$: surfactant rich reverse micellar solution; O'$_m$: polymeric oil rich reverse micellar solution.

On the other hand, in the $C_8F_{17}EO_{10}$-$(C_3F_6O)_nCOOH$ axis, a miscibility gap is observed close to the $C_8F_{17}EO_{10}$, indicating low miscibility of $(C_3F_6O)_nCOOH$ in $C_8F_{17}EO_{10}$. This segregation is caused by the difference in molecular weight between the two components. In the ternary system hexagonal ($H_1$), isotropic highly viscous phase bicontinuous cubic ($V_1$) and an anisotropic polymeric oil - rich lamellar (L'$_\alpha$) are formed when polymeric oil [$(C_3F_6O)_nCOOH$] is added to the surfactant solution. The micellar region appears up to about 60 wt% of surfactant concentration. The maximum amount of polymeric oil that can be solubilized in the micellar solution is around 17 wt% at 45 wt% surfactant in water. However, the solubility of polymer in the surfactant lamellar phase ($L_\alpha$) is negligible, and phase separation takes place upon addition of a minute amount of polymeric oil. Hence, two kinds of lamellar phases exist, one rich in surfactant and the other rich in polymer in the water / $C_8F_{17}EO_{10}$ / $(C_3F_6O)_nCOOH$ system. This behavior has been previously found in several surfactant-polymer systems[23-26] and it is associated with packing restrictions as will be discussed later.

### 5.3.2 Microstructure of liquid crystals

The representative typical SAXS spectra for different liquid crystals are shown in Figure 5-2. The SAXS peak ratios are 1: √3: 2: √7 for hexagonal phase and 1:2 for polymeric oil – rich lamellar phases.

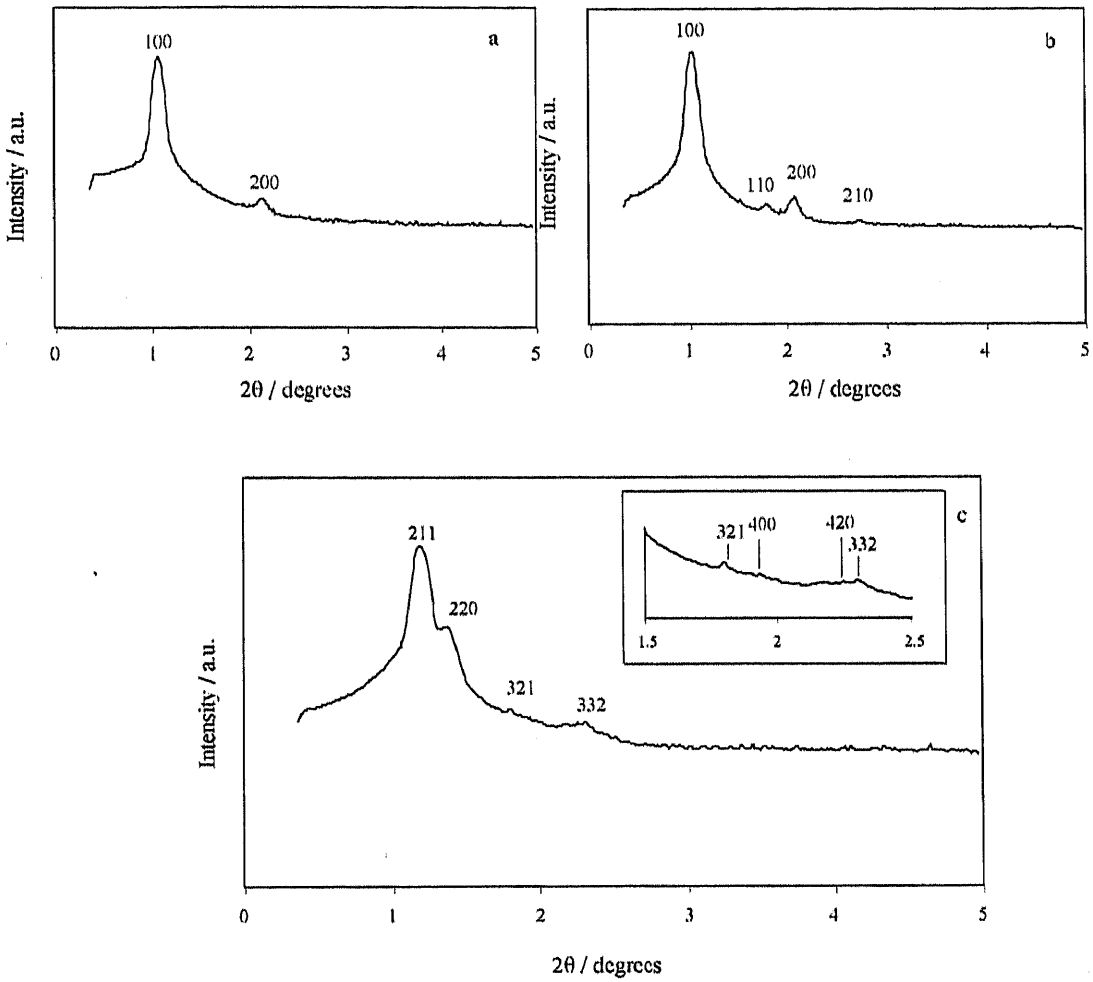


Figure 5-2: Representative SAXS patterns for (a) Lamellar phase at surfactant/water =75/25, *Wo* (weight fraction of $(C_3F_6O)_nCOOH$ in the system.)=0.5; (b) Hexagonal phase at surfactant/water=60/40,Wo=0.25; (c) Bicontinuous cubic phase at surfactant/water =75/25, Wo=0.30. The inset in (c) shows the higher order peaks in an expanded scale.

The SAXS peak ratios √6: √8: √14: √16: √20: √22 obtained from diffraction planes [h, k, l] = [211], [220], [321], [400], [420] and [332] respectively for the $V_1$ phase indicate that the cubic phase belongs to the Ia3d ($Q^{230}$) space group . This structure has been found previously in shorter nonionic fluorinated surfactant systems[15]. The indexing of the peaks is obtained from the plot of $(h^2 + k^2 + l^2)^{1/2}$ versus $1/d$ giving a straight line passing through the origin of coordinates (Figure 5-3).

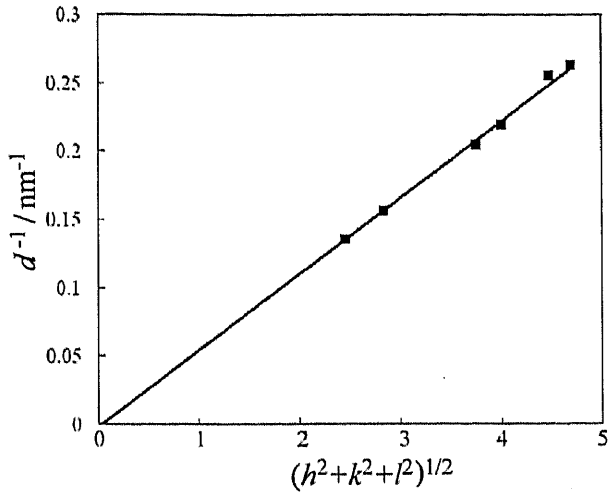


Figure 5-3: Indexing of SAXS peaks in 2(c) to a Ia3d ($Q^{230}$) cubic structure

From the inverse of the slope, the unit cell parameter is estimated to be 18 nm. SAXS measurements were performed along the lines defined by 60/40, 70/30, 75/25 of $C_8F_{17}EO_{10}$ / water ratios of Figure 5-1.

The values of the structural parameters $r'_H$, $d'_L$ and $a'_s$ are calculated and plotted as a function of polymeric oil content in Figure 5-4. Note that the solubility of $(C_3F_6O)_nCOOH$ in the surfactant-rich lamellar phase is very low so that a wide two-phase region in which two liquid crystal phases coexist is found in Figure 5-4 [(b)-(c)]. In mixed membranes of hydrophobically modified polymers and nonionic surfactants, it has been found that if the radius of gyration of polymer is comparable to or greater than one half of the interlamellar distance, phase separation into two coexisting lamellar phases generally occurs[27,28].

There is no available data on the radius of gyration of $(C_3F_6O)_nCOOH$, but can extrapolate previous data on lamellar phases of shorter perfluoropolyethers as a function of $n$ (14), and make a rough calculation to get a chain length of 5 nm for $(C_3F_6O)_nCOOH$, which is more than half the interlayer spacing of the lamellar phase in the binary surfactant-water system; hence, phase separation takes place. The other criteria to explain the limited miscibility of polymers in surfactant lamellar phases is the available area in the lamellar phase, which should be larger than the surface coverage of the polymer[27]. $(C_3F_6O)_nCOOH$ is expected to be rigid and hence its surface coverage should be low, so the surface area criteria seems not to be determinant for phase separation in the present system, as will be explained below.

For all single- phase regions of liquid crystals, $d'$, $r'_H$ and $d'_L$ and $a'_s$ increase with polymeric oil content. In the hexagonal phase the radius of hydrophobic core, $r'_H$, is longer than the hydrophobic chain length of $C_8F_{17}EO_{10}$ in its extended (helix)

conformation, which is estimated to be about 2 nm[15,16]. Hence hydrophobic chain $(C_3F_6O)_n$ of $(C_3F_6O)_nCOOH$ makes an oil pool in the cylindrical micelles. Note [Figure 5- 4 (b)] that a $H_1$-L'$_\alpha$ phase transition occurs when $r'_H$ almost reaches the length of $(C_3F_6O)_nCOOH$. This transition means that the curvature changes from positive to zero. This change is favored by the penetration of the $(C_3F_6O)_nCOOH$ molecules that produces an expansion of the effective average cross-sectional area $a'_s$ per amphiphile at the interface. At surfactant/water ratio =70/30, the L'$_\alpha$ can contain almost the same number of polymer and surfactant molecules.

At a 75/25 (surfactant/water) ratio, the phase sequence $H_1$-$V_1$-L'$_\alpha$ occurs by incorporating polymeric oil. Again, the curvature changes from positive to zero. The incorporation of polymeric oil also leads to a continuous swelling of the cubic phase and lamellar stacks since $d$ value increases with polymeric oil content as shown in Figure 5- 4(c).

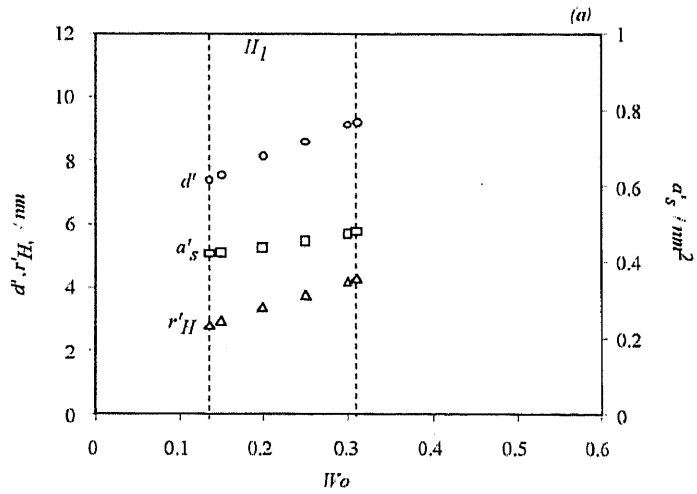

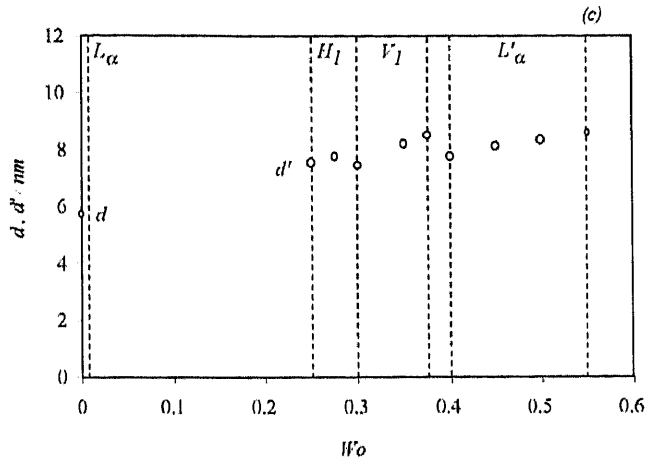


Figure 5-4: Change in microstructural parameters with $(C_3F_6O)_nCOOH$ content. The surfactant/water ratios are (a) 60/40; (b) 70/30; (c) 75/25. Circles: interlayer spacing ($d$ or $d'$); Triangles: Length of hydrophobic part of lamellar phase ($d_L$ or $d'_L$) radius of hydrophobic core in hexagonal phase ($r'_H$); Squares: effective surface area per amphiphile($a_s$ or $a'_s$).

From a different point of view, it can be seen moving left in Figure 5- 4(b) that $d'$ and the half thickness of the hydrophobic part $d'_L$ decrease monotonically by replacing polymeric oil with the surfactant. It means that the hydrophobic chains of polymeric oil are compressed in the direction vertical to the surface because $a_s$ is decreased by the mixing. There is a limit for hydrophobic chains of polymeric oil to be compressed up to $d'_L$ = 1.6 nm and hence, the polymer cannot be incorporated any more in the lamellar phase. The loss of conformational entropy prevents the polymer confinement in the membrane solution if there is not sufficient hydrophobic interaction between the polymer hydrophobes and the lamellar bilayers.

It is also observed that the polymeric oil is practically insoluble in the $C_8F_{17}EO_{10}$ $L_\alpha$ phase, because the half thickness of this lamellar phase is too small ($d'_L$ = 0.52nm at $W_O$ = 0 and surfactant / water =70/30) to include the hydrophobic chains of polymeric oil in the surfactant bilayer.

### 5.3.3 Rheological behavior

To obtain some insight on the microstructure in the dilute region, rheological measurements were carried out. As can be seen in Figure 5-5, at 5wt% of surfactant (0% of hydrophobic polymer), the system is already very thick, with a zero-shear viscosity more than four orders of magnitude higher than water. As $(C_3F_6O)_nCOOH$ is added, the zero-shear viscosity decreases dramatically, reaching the value of water when the concentration of $(C_3F_6O)_nCOOH$ is 1wt%. This behavior has been found in

solutions of worm-like micelles when long-chain oils are solubilized, and it is attributed to a rod-sphere transition[2,29]. As a matter of fact, worm-like micelles have been reported in several fluorinated surfactant systems[30-35], although they are not common in binary nonionic surfactant-water systems.

Results on shear-sweep measurements are shown in Figure 5-6. In the absence of $(C_3F_6O)_nCOOH$, strong shear thinning is observed, which is typical for worm-like micelles solutions aligned under shear[2].

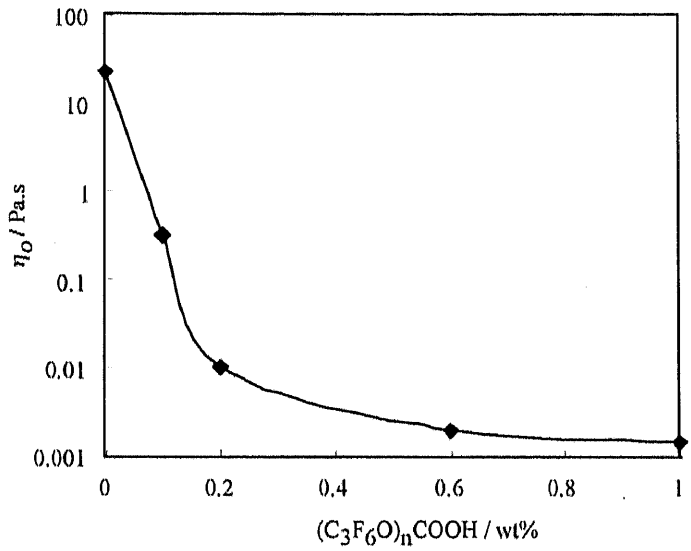


Figure 5-5: Zero-shear viscosity in water/$C_8F_{17}EO_{10}$/$(C_3F_6O)_nCOOH$ systems. The surfactant/water ratio is kept constant at 5/95. The line is only a visual guide.

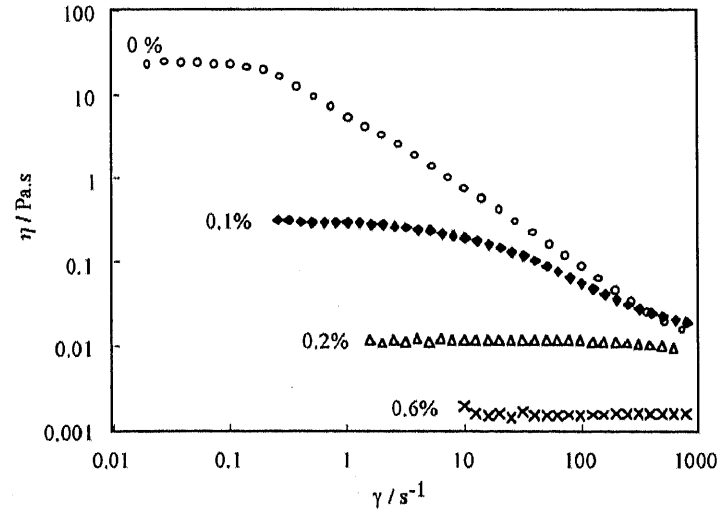


Figure 5-6: Viscosity as a function of shear rate in water/$C_8F_{17}EO_{10}$/$(C_3F_6O)_nCOOH$ systems. The surfactant/water ratio is kept constant at 5/95. The $(C_3F_6O)_nCOOH$ concentrations are shown for each set of data.

The viscosity decreases with shear rate following a power law. The presence of a viscosity plateau in the low-shear range is an indication of long relaxation times found in long, entangled aggregates[29]. The shear thinning and viscoelastic behavior tends to vanish as $(C_3F_6O)_nCOOH$ is added, and finally, the system becomes a Newtonian fluid, similar to solutions of spherical micelles. The rod-sphere transition induced by $(C_3F_6O)_nCOOH$ suggests a change in curvature driven by an increase in the specific surface area, in agreement with the SAXS results in the concentrated region.

**5.4 Conclusions**

Liquid-crystalline phases $H_1$, $V_1$, $L'_\alpha$ formed in $C_8F_{17}EO_{10}$ / $(C_3F_6O)_nCOOH$ / water system are essentially polymeric oil-rich liquid crystals. A considerable amount of surfactant is dissolved in the polymeric oil aggregate, whereas solubility of polymeric oil in the surfactant lamellar ($L_\alpha$) is insignificant and phase separation takes place upon addition of a trace amount of polymeric oil because of the large size difference between the two components. At low surfactant concentration, the transformation of the viscoelastic surfactant solution into a low viscosity Newtonian liquid with increasing solubilization of polymeric oil is attributed to a rod-sphere transition. On the other hand, at high surfactant concentration, the phase sequence $H_1$-$V_1$- $L'_\alpha$ occurs by incorporating polymeric oil, which suggests that the curvature changes from positive to zero.

**References**


1 Kissa, E. *Fluorinated Surfactants and Repellants*, 2nd Ed., Marcel Dekker, New York, **2001**.

2 Hoffmann, H.; Würtz, J. *J. Mol. Liq.* **1997**, *72*, 191.

3 Kunieda, H.; Shinoda, K. *J. Phys. Chem.* **1976**, *80*, 2468.

4 Shinoda, K.; Hato, M.; Hayashi, T. *J. Phys. Chem.* **1972**, *76*, 909.

5 Ravey, J.C.; Stébé, M.J. *Colloids Surf. A* **1994**, *84*, 11.

6 Würtz, J.; Meyer, J.; Hoffmann, H. *Phys. Chem. Chem. Phys.* **2001**, *3*, 3132.

7 Fontell, K.; Lindman, B. *J. Phys. Chem.* **1983**, *87*, 3289.

8 Hoffmann, H.; Reizlein, K. *Prog. Colloid Polym. Sci.* **1984**, *69*, 83.

9 Bucci, S.; Hoffmann, H.; Platz, G. *Prog. Colloid Polym. Sci.* **1990**, *81*, 87.

10 Downes, N.; Ottewil, G.A.; Ottewil, R.H. *Colloids Surf. A* **1995**, *102*, 203.

11 LoNostro, P.; Choi, S.M.; Ku, C.Y.; Chen, S.H. *J. Phys. Chem. B* **1999**, *103*, 5347.

12 Caboi, F.; Chittofrati, A.; Lazzari, P.; Monduzzi, M.J. *Colloids Surf. A* **1999,** *160*, 47.

13 Monduzzi, M.; Chittofrati, A.; Boselli, V. *J. Phys. Chem.* **1994**, *98*, 7591.

14 Mele, S.; Ninham, B.W.; Monduzzi, M. *J. Phys. Chem. B* **2004**, *108*, 1751.

15 Ropers, M.H.; Stébé, M.J. *Phys. Chem. Chem. Phys.* **2001**, *3*, 4029.

16 Blin, J.L.; Lesieur, P.; Stébé, M.J. *Langmuir* **2004**, *20*, 491.

17 Ropers, M.H.; Stébé, M.J.; Schmitt, V.J. *Phys. Chem. B* **1999,** *103*, 3468.

18 Ravey, J.C.; Stébé, M. -J. *Prog. Colloid Polym. Sci.* **1987,** *73*,127.

19 Kratzat, K.; Guittard, F.; Taffin de Givenchy, E.; Cambon, A. *Langmuir* **1996**, *12*, 6346.

20 Mathis, G.; P. Leempoel, P.; Ravey, P.; Selve, C.; Delpuech, J.J. *J. Am. Chem. Soc.* **1984**, *106*, 6162.

21 Ropers, M.H.; Stébé, M.J. *Langmuir*, **2003**, *19*, 3137.

22 Esquena, J.; Rodríguez, C.; Solans C.; Kunieda, H. *Micropor. Mesopor. Mater.* **2006**, *92*, 212.

23 Kaneko, M.; Matsuzawa, K.; Uddin, Md.H.; Lopez-Quintela, M.A.; Kunieda, H. *J. Phys. Chem. B* **2004**, *108*, 12736.

24 Kunieda, H.; Uddin, Md. H.; Furukawa, H.; Harashima, A. *Macromolecules* **2001**, *34*, 9093.

25 Uddin, Md. H.; Morales, D.; Kunieda, H. *J. Colloid Interface Sci.* **2005**, *285*, 373.

26 Aramaki, K.; Hossain, Md.K.; Rodriguez, C.; Uddin, Md.H.; Kunieda, H. *Macromolecules* **2003**, *36*, 9443.

27 Yang, B.-S.; Lal, J.; Richetti, P.; Marques, C.M.; Russel, W.B.; Prud'homme, R.K. *Langmuir* **2001**, *17*, 5834.

28 Demé, B.; Dubois, M.; Zemb, T.; Cabane, B. *J. Phys. Chem.* **1996**, *100*, 3828.

29 Rodríguez, C.; Aramaki, K.; Tanaka, Y.; López-Quintela, M.A.; Ishitobi, M.; Kunieda, H. *J. Colloid Interface Sci.* **2005**, *291*, 560.

30 Ravey, J.C.; Stebe, M.J.; *Physica B: Condensed Matter*. **1989**, *156-157*, 394.

31 Abe, M.; Tobita, K.; Sakai, H.; Kondo, Y.; Yoshino, N.; Kasahara, Y.; Matsuzawa, H.; Iwahashi, M.; Momozawa, N.; Nishiyama, K. *Langmuir* **1997,** *13*, 2932.

32 Wang, K.; Karlsson, G.; Almgren, M.; Asakawa, T.; *J. Phys. Chem. B* **1999**,

*103*, 9237.

33 Buhler, E.; Oelschlaeger, C.; Waton, G.; Candau, S.J. *J. Phys. Chem. B* **2004**, *108*, 11236.

34 Hoffmann, H.; Kalus, J.; Reizlein, K.; Ulbricht, W.; Ibel, K. *Colloid Polym. Sci.* **1982**, *260*, 435.

35 Angel, M.; Hoffmann, H. *Z. Phys. Chem.* **1984**, *139*, 153.

# Chapter 6: Viscoelastic Micellar Solutions in Nonionic Fluorinated Surfactant Systems

## 6.1 Introduction

Perfluorosurfactants behave in a manner similar to that of their hydrocarbon analogues. Above critical micelle concentration (cmc), they form micelles, threadlike micelles, vesicles, lamellar aggregates, and other various liquid crystalline structures in solution. Similar phase sequences are observed in fluorinated-surfactant and hydrocarbon -surfactant systems when solution conditions are changed, for example, when the surfactant concentration is changed. However, perfluorosurfactants are more hydrophobic and reduce the surface tension of an aqueous solution to an extent, which is unattainable with hydrocarbon surfactants. Similarly, they show a much lower cmc than hydrocarbon -chain surfactants of same length[1,2]. Atomic properties of fluorine (viz., its high electronegativity, its relatively large van der Waals radius, and less conformational freedom (mainly all-trans) of the fluorinated chain) produce bulky and stiff chains with their skeleton covered by a dense electro-rich environment. It is easier to pack fluorocarbon chain closely because the chains are in all-trans states and less entropy is lost. As a result, these surfactants have high chemical and thermal stability and therefore are useful in many practical applications where hydrocarbon surfactants would decompose.

The aggregate structures in fluorinated surfactants can be explained, like hydrocarbon surfactants, in terms of the value of packing parameter[3], $CPP = v/a_s l$, where $v$ is the volume hydrophobic part, $l$ is its length, and $a_s$ the average area of head group at the interface. However, the fluorocarbon chains are bulkier than the hydrocarbon chain with the volume of $-CF_2$ and terminal $-CF_3$ being 0.041 and 0.084 $nm^3$, respectively, compared with 0.027 and 0.037 $nm^3$, respectively, for hydrocarbon analogues[4]. Therefore, to form a spherical aggregate ($CPP \leq 1/3$), fluorinated surfactant with very large head groups are needed to balance the effect of the bulky fluorocarbon chain[5]. Therefore, cylindrical micelles are often observed at solution conditions where spherical micelles are expected in hydrocarbon surfactant systems. These cylindrical micelles often undergo enormous one-dimensional growth and form flexible threadlike aggregates called "wormlike micelles". This type of growth is attributed to effort of the system to reduce the high free-energy cost associated with

the formation of hemispherical end caps when the solution properties favor spontaneous curvature of cylinders. The system can reduce the free energy by reducing the number of free ends, that is, by end-to-end fusion of several short cylindrical aggregates to form a long aggregate. When the number density of the wormlike aggregates exceeds a certain threshold value, they entangle each other to form a transient network and exhibit viscoelastic properties.

The formation and properties of viscoelastic wormlike micelles have been studied extensively for hydrocarbon surfactants, mostly in long hydrophobic-chain ($C_{16}$ or longer) cationic surfactant in the presence of excess counterions[6-12] and, in some cases, even in absence of excess counterions if counterions are strongly bound at hydrophilic-hydrophobic interface[13-16]. Viscoelastic solutions of wormlike micelles have also been reported in cationic or anionic fluorinated surfactant aqueous systems even at a relatively short fluorocarbon chain length[17-19]. The effect of the concentrations of the counterions and the surfactant concentration on the rheological behavior and micellar growth is more or less similar in both types of surfactants[19]. There are reports of thermoresponsive viscoelasticity in some hybrid anionic surfactants containing both fluorocarbon and hydrocarbon chains in their molecules[20-23].

Only a few reports on the formation of viscoelastic wormlike micellar solution and the study of their rheological behavior are available in aqueous systems of nonionic hydrocarbon surfactants such as ethoxylated sterols[24-26] and sucrose alkanoates[27]. In these systems, interfacial curvature of the aggregates can be tuned to induce the sphere-rod transition and one-dimensional micellar growth via the adding of a lipophilic surfactant, such as polyoxyethylene alkyl ether or long chain monoglyceride. A similar tendency is observed in ionic surfactant solutions as well[28-32]. An aqueous solution of a surfactant with a cholesteric group as the hydrophobic part formed a viscoelastic solution at elevated temperatur[33]. However, not much is known about the formation and rheological behavior of the wormlike micelles in nonionic systems. Knowledge about the formation and rheological properties of nonoionic systems is important not only to obtain a better understanding of the underlying basic principle of the phenomenon, but also for practical applications, such as in cosmetics and toiletry products, because of the absence of charged species and improved mildness to the skin.

In this paper, we present our study on the temperature-induced viscosity growth in a water-surfactant binary system of a nonionic fluorinated surfactant, perfluoroalkyl sulfonamide ethoxylate at various concentrations. To our knowledge, this is the only nonionic surfactant known so far which forms a viscoselastic solution of wormlike micelles in a surfactant-water binary system[34], but little is known about its rheological behavior. In this study, the microstructural change in the aggregates as a function of temperature and composition is studied by rheometry and dynamic light scattering (DLS). The small-angle X-ray scattering (SAXS) technique has been used to obtain direct evidence of the shape change and the internal structure of the aggregates.

## 5.2 Experimental

### 5.2.1 Materials

The fluorinated surfactant perfluoroalkyl sulfonamide ethoxylate, $C_8F_{17}SO_2N(C_3H_7)(C_2H_4O)_{10}H$, designated as $C_8F_{17}EO_{10}$ was obtained from Mitsubishi Materials (Japan). The surfactant was purified by placing it under vacuum for several days to remove volatile components until the weight became constant. The surfactant was used without further purification. Millipore water was used in all the experiments.

$$C_8F_{17}SO_2N(C_3H_7)-(CH_2CH_2O)_{10}H$$

Scheme 1: Molecular structure of $C_8F_{17}EO_{10}$

### 5.2.2 Phase diagram

For the study of phase behavior, sealed ampoules containing required amount of reagents were homogenized and kept in a water bath for equilibration. Liquid crystalline samples were characterized by visual observation (through crossed polarizers) and also by SAXS.

### 5.2.3 Rheological measurements

Samples for rheological measurements were homogenized and kept in a water bath at 25°C for at least 24 h to ensure equilibration before performing measurements. The rheological measurements were performed in an ARES rheometer (Rheometric Scientific) using couette geometry for low viscosity solutions and cone-plate geometry for highly viscous solutions. The temperature was controlled using a circulating fluid from a temperature-controlled water bath. A sample cover provided with the instrument was used to minimize the change in sample composition by evaporation during the measurement. While studying the effect of temperature on the

rheological behavior, we maintained the samples at each temperature from 30 min (for samples of low viscosity) to 1 h (for samples of high viscosity) before the measurements, which was sufficient to attain a stability in the rheological parameters ($\eta$ and $G_o$), as suggested by a separate rheological measurement as a function of time. Frequency sweep measurements were performed in the linear viscoelastic regime of the samples, as determined previously by dynamic-strain sweep measurements. The zero-shear viscosity of the samples was determined either from a steady shear rate measurement of less viscous samples by extrapolating the viscosity (shear-rate curve to zero shear-rate) or from the values of $G_o$ and $\tau_R$ as obtained from oscillatory measurements.

### 6.2.4 SAXS

SAXS measurements on micellar solutions were performed by a SAXSess camera (Anton Paar) equipped with the PW3830 laboratory X-ray generator operating at 40 kV and 50 mA, a long-fine focus sealed glass X-ray tube ($K_\alpha$wavelength of 0.1542 nm) from PANalytical, focusing multiplayer optics, a block collimator for a slit collimation, a translucent beam stop, an image plate (IP) detector, and a temperature-controlled sample holder unit (TCS 120, Anton Paar). The sample was taken in a clean capillary, and the same capillary was repeatedly used for all measurements. The scattered intensity recorded on the IP was read by means of a Cyclone storage phosphor system (Perkin Elmer). Because of the translucent beam stopper, the raw scattering data always include a reduced primary intensity at a scattering vector $q = 0$. All the data were normalized to the same incident primary-beam intensity for the transmission calibration and were corrected for the background scattering from the capillary and the solvent. The absolute scale calibration was done using water as a secondary standard. The maximum resolution of the instrument, $q_{min}$, was ~0.08 $nm^{-1}$, which corresponds to ~40 and ~80 nm for the detectable maximum size of a particle and interlayer spacing, respectively.

The primary SAXS data were analyzed by the GIFT technique with the Boltzmann simplex simulated annealing (BSSA) algorithm. In the calculation, we used a model of the averaged structure factor for a hardsphere (HS) interaction, $S(q)^{av}$, which considers the Gaussian distribution of the interaction radius, $\sigma$, for individual monodisperse systems for polydispersity, $\mu$, and a Percus-Yevick (PY) closure

relation to solve Ornstein-Zernike (OZ) equation[35,36]. The detailed theoretical description on the method has been reported elsewhere[31,33].

### 6.2.5 DLS measurements

Dynamic light-scattering measurements were performed in homodyne light beating mode with vertically polarized light from a diode laser operated at 200 mW CW and 532 nm wavelength on an ALV SP-86 goniometer equipped with a photomultiplier detector operated in photon-count mode in the far field. The scattered light intensity's autocorrelation function *g(t)*,was accumulated by an ALV5000 correlator. Thermostated, >6h-annealed, samples taken in cylindrical glass cells were used in the measurement.

## 6.3 Results and discussion

### 6.3.1 Phase behavior

Phase diagram of $C_8F_{17}EO_{10}$/water binary system is shown in Figure 6-1. This is a typical phase diagram of nonionic surfactants such as polyoxyethylene alkylethers ($C_mEO_n$)[37], with a close resemblance to the phase diagram of $C_{12}EO_6$.

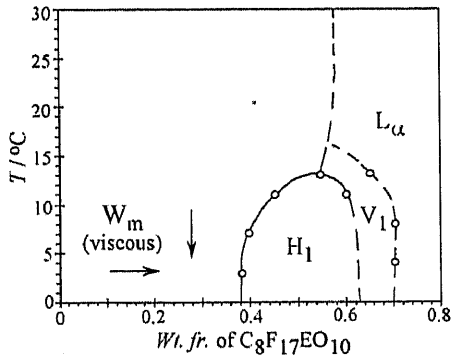


Figure 6-1: Partial phase diagram of $C_8F_{17}EO_{10}$/water binary system. $W_m$ stands for micellar solution and $H_1$, $V_1$ and $L_\alpha$ stand for hexagonal, bicontinuous cubic and lamellar liquid crystalline phases. The arrows in the $W_m$ domain show the directions of viscosity increase for the systems at surfactant concentration of 15wt% and above. At lower concentrations, viscosity increases and then decreases with increasing temperature. For detail see Figure 6-5.

At low-temperature, a micellar solution is formed over a wide range of compositions (up to ~38wt% at 5 °C). With a further increase in surfactant concentration, hexagonal ($H_1$), bicontinuous cubic ($V_1$) and lamellar ($L_\alpha$) liquid crystalline phases are formed successively. Micellar solutions at low temperature become increasingly viscous with increasing surfactant concentration, and at compositions near the $H_1$ phase, a highly viscous or gel-like solution is formed. However, the SAXS pattern shows a broad scattering band (data not shown), which rules out the possibility of the presence of the discontinuous cubic ($I_1$) phase. Moreover, the fact that the viscosity of the solution

gradually increases with increasing concentration also indicates that the $I_1$ phase is not present. In fact, the formation of globular micelles is not favorable because of bulky and stiff fluorinated chain unless the head group is very big. With increasing temperature, the viscosity of the solution gradually decreases, and ultimately, a less viscous easily flowing isotropic solution is formed. At higher temperatures, a phase separation occurs which is typical of nonionic surfactant systems. The phase diagram of this system over wide range of temperatures and compositions has been reported recently[38]. Although the present diagram is essentially similar to the reported diagram, the $H_1$ melts at lower temperature in the present diagram. We believe that the discrepancy is related to the purity of the surfactant sample because small amount of impurities affect the phase behavior significantly.

### 6.3.2 Steady-shear rheological behavior

Figure 6-2 shows the steady shear rate ($\dot{\gamma}$) versus viscosity ($\eta$) curves for 1wt% surfactant solution at different temperatures. At low temperature (5 °C), $\eta$ is independent of $\dot{\gamma}$ ( i.e., Newtonian flow behavior is observed up to $\dot{\gamma} \approx 100\ s^{-1}$). At higher values of $\dot{\gamma}$ (>100 $s^{-1}$) the viscosity decreases with increasing $\dot{\gamma}$, and this "shear thinning" behavior can be described by the power law: $\eta \propto \dot{\gamma}^{-a}$. This behavior is typical of wormlike micelles. Note that the viscosity of the surfactant solution is significantly higher than that of water or micellar solutions generally observed in surfactants solutions at such a low concentration of 1wt%. Therefore, cylindrical micelles are expected to be present even at low temperatures. Upon an increase of the temperature up to 35 °C, the plateau value of $\eta$ at low $\dot{\gamma}$ (and hence $\eta_o$), increases, and the shear thinning also begins at a lower-shear rate, with nearly similar value of exponent in the power law. It suggests that the system is getting more "structured" with increasing temperature. When the temperature is increased further to 45 °C, $\eta$ at low shear rate (or $\eta_o$) decreases, and the critical shear rate shifts again to higher $\dot{\gamma}$ values but $\eta$ decreases more steeply with $\dot{\gamma}$ (larger $a$ in the power law) than was observed at lower temperatures. A comparison of the steady shear-rate curves at 25 and 45 °C shows that, although the viscosity at low-shear rate is nearly same plateau value, the shear-thinning behavior at higher shear-rate is not similar, which might be the result of a difference in the structure of the system at the respective temperatures. Rheological measurement was carried out only up to 55 °C because phase separation occurs at higher temperature.

The increase in $\eta_o$ with temperature in the nonionic surfactant can be understood in terms of the decrease in $a_s$ or the decrease in the interfacial curvature of aggregates because of the progressive dehydration of the EO chain. This would induce a sphere-rod transition in the aggregate shape or induce one-dimensional growth if the rodlike aggregates are already formed. The formation of end caps in the cylindrical aggregates becomes unfavorable with increasing temperature because of the high free-energy cost associated with the formation of hemispherical ends when the surfactant molecules prefer the spontaneous curvature of a cylinder. The aggregate tends to minimize the energy cost by forming fewer long aggregates instead of several short aggregates. Therefore, the trend observed up to 35 °C is consistent with that view. However, above 35 °C a turning point occurs, and the viscosity begin to decrease as if the micellar length changes in opposite direction for some reason, such as an increase in the extent of micellar scission kinetics.

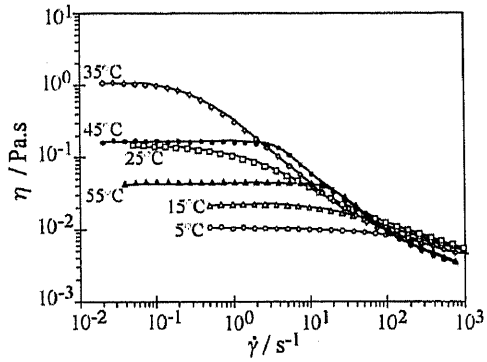


Figure 6-2: Steady shear-rate ($\dot{\gamma}$) vs viscosity ($\eta$) curves of 1wt% surfactant system at various temperatures.

A more convincing explanation is that with increasing temperature, the energy cost of the free ends of the micelles become higher, and therefore, the free ends would fuse at the cylindrical part of its own or of another micelles, thus forming micellar joints, or branching[9,39]. Such joints reduce the viscosity because; when a stress is applied the micellar joint can slide along the cylindrical body (contour) thereby allowing a fast stress relaxation process. Since the surfactant molecules in the aggregate are not chemically connected, the surfactant are expected to form this type of saddle-shaped interconnection readily if they do not strongly resist a negative Gaussian curvature. Micellar connections or branching have been detected by cryogenic transmission electron microscopy (cryo-TEM) in some surfactant systems, especially in the region where the viscosity decreases after the maximum[40-43]. In recent years, a theoretical

basis for the formation of branching and network, supported by experimental evidences, has been provided [44-46].

### 6.3.3 SAXS

To study the variation of microstructural changes in the shape and size of aggregates as a function of temperature, SAXS measurements were performed on 1wt% surfactant solution at different temperatures (viz., 15, 35, 45 and 55 °C). As it can be seen from Figure 6-2 (and also from Figure 6-5), these temperatures correspond to the different regions of viscosity temperature curves, namely, viscosity-growth region, viscosity-maximum region, viscosity-decline region after the maximum and near the phase boundary, respectively. Figure 6-3 shows the $I(q)$-$q$ curves after the correction for instrumental broadening (desmearing). The absence of a peak or maximum in the low-$q$ region indicates a negligible interparticle interaction. In fact, the analysis of data without considering structure factor (using the IFT method) gave nearly identical results. The decay of $I(q)$ at $\sim q^{-1}$ in the low-$q$ region suggests that the aggregates have rodlike local structures at 15, 35 and 45 °C. However, at 55 °C, a very small but noticeable increase in the slope in the $q < 0.7$ nm$^{-1}$ region was observed which suggests that the aggregate shape is mainly cylindrical but a lamellar like structure is gradually developing. Lamellarlike aggregates are characterized by $I(q)$ decaying at $\sim q^{-2}$ in the low-$q$ region. The structural change with increasing temperature is more evident from the corresponding PDDF curves shown in Figure 6-3. The pattern of the PDDF plots at 15, 35 and 45 °C are typical of rodlike particles. The PDDFs of the aggregates show that the $D_{max}$ increases with increasing temperature but the cylindrical cross-sectional diameter of the rodlike aggregates is almost constant (~ 5.8 nm). Note that the measured value of $D_{max}$ is biased by the maximum of resolution (or $q_{min}$) of the measurement, and it may not provide the actual length of the micelles, which are believed to have their contour lengths in several hundred nanometers or even micrometer range. Nevertheless, the trends in the variation of $D_{max}$ values as obtained from SAXS measurements can be taken as the evidence of micellar growth. Further information on the structure of the aggregates can be obtained from the SAXS data. Figure 6-4 shows the representative cross-sectional PDDF, $p_c(r)$, considering the long cylindrical shape of the aggregate and the radial contrast profile, $\Delta\rho_c(r)$, of the cross-section as obtained by deconvolution of $p_c(r)$.

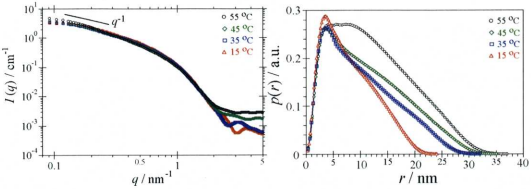


Figure 6-3: Scattered intensity, $I(q)$, from SAXS measurement of 1wt% surfactant solution at different temperatures (*a*). Corresponding pair distance distribution functions, $p(r)$, are shown in (*b*).

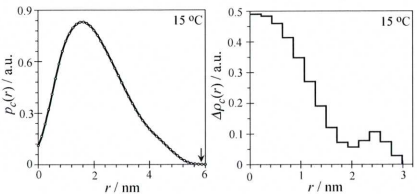


Figure 6-4: Cross sectional PDDF, $p_c(r)$ and contrast profile, $\Delta\rho_c(r)$ as obtained from the deconvolution of $p_c(r)$ for 1% surfactant system at 15 °C. Scattering intensity curve is shown in Figure 6-3.

The cross-sectional radius of the aggregate is estimated to be ~2.95 nm, which corresponds to a half of the value of $r$ for $p_c(r)$=0 at large $r$ (shown by an arrow in Figure 6-4). An extended length of 1.7 nm is estimated for $C_8F_{17}$–S–N moiety with a rigid fluorocarbon chain. This value is consistent with the experimental value of 1.8 nm reported for the radius of the hydrophobic core of cylindrical aggregates ($H_1$ phase) formed by a perfluorosurfactant $C_8F_{17}C_2H_4EO_9$,[47] which has a hydrophobic moiety of a length comparable to that of the surfactant of present study. With this, ~ 1.2 nm is left for the length of hydrophilic chain ($EO_{10}$) of the surfactant. The lengths of $EO_{10}$ chain is 1.8-2.0 and 3.5 nm in meander and zig-zag configurations, respectively. A zig-zag confirmation has been suggested for EO chains of less than 18-20 EO units. The estimated length of an $EO_{10}$ chain with a zig-zag configuration is nearly three times longer than the value estimated from the PDDFs. Even if we assume a meander configuration, the length of the EO chain obtained from the PDDFs is not consistent with the reported length. Note that the zig-zag conformation can not

be ruled out just because of the observed discrepancy in the EO chain length because the contrast of EO chain is low and it gradually decreases further when the EO units extend toward the solvent (water). An increase in the extent of hydration further decreases the contrast and makes the estimation of the correct length of the EO chain impossible. The extended part of the $p_c(r)$ curve in the higher-$r$ region (Figure 6-4) probably comes from the fading contrast profile outside the fluorinated core, although a noncircular cross-section may also introduces asymmetry in $p_c(r)$ plot. If a circular cross-section of the cylindrical aggregates is assumed, a contrast step profile was obtained by deconvolution, and the result is shown in Figure 6-4. The fluorocarbon core has a high electron density, and therefore, shows a high contrast. A minimum in the contrast profile is observed around $r = 2$ nm. It is reasonable because the $-C_3H_7$ moiety of the low- electron density might have balanced the positive contribution of N, S and O, bringing the overall contrast profile to a low value. With increasing $r$ values, the contrast profile improves slightly which is due to EO chain, but it fades out gradually and eventually approaches to zero at a value of $r$.

The results of SAXS measurements, especially the constant cross-sectional diameter and increasing $D_{max}$, provide important information about the microstructural changes. The continuity in the one dimensional micellar growth even above 35 °C, which is the $T_{\eta max}$ for the system, confirms that the decay of the viscosity above this temperature is not caused by decreases in the length of the cylindrical aggregates. With a further increase in temperature to 55 °C, the $D_{max}$ continues to increase, but more important, there is the significant change in the pattern of $p(r)$ observed in the middle-$r$ region (Figure 6-3). Here, a sharp decay of $p(r)$ immediately after the maximum has healed, and a significant bulge in upward direction has developed in that region. In fact, careful analysis of the evolution of $p(r)$ curves reveals that indication of such a change has already begun at 45 °C, although to a small extent. Such a change in the $p(r)$ would suggest a gradual evolution of the local structure toward a lamellar pattern[48]. With a gradual evolution of lamellar structure (with increasing temperature), we can expect that the bulge at the intermediate-$r$ region would grow and, ultimately, that the maximum in the low-$r$ region would completely disappear and the $p(r)$ curve would transform to a bump with a broad maximum in the intermediate-$r$ region, which is a typical pattern for a flat structure. SAXS measurements were not carried out at higher temperature. Therefore, evidence of

evolution of the aggregate shape to form a locally flat structure is not available. Even from the scattering pattern from SAXS and corresponding $p(r)$ curves, it is not possible to distinguish among different structures such as vesicles, lamellar liquid crystalline ($L_\alpha$) phase or sponge ($L_3$) phase.

One-dimensional micellar growth with increasing temperature, evolution of low-curvature structures at elevated temperature as obtained by SAXS measurements, and the results of the steady-shear rate rheological measurements may be attributed to the formation of micellar joints or branching. At branching points, the mean local curvature is zero. Probably the number and size of those points grows sharply with increasing temperature at $T > T_{\eta\text{-max}}$. In dilute solutions of several ionic as well as hydrophilic nonionic surfactants successive addition of lipophilic nonionic surfactant such as $C_{12}EO_3$ induces one dimensional micellar growth and causes the viscosity to sharply increase to a maximum and then decrease. Ultimately, a two-phase region consisting of aggregates with low curvature ($L_\alpha$ phase or vesicles) and micellar solution appears. Still it is not clearly understood how wormlike micelles transform to structures with very low curvature. Most probably, formation of micellar joints and the growth of the joints to a bilayer structure is the mechanism. It is reasonable to expect a similar type of structural evolution in the present system because increasing temperature is equivalent to addition of lipophilic surfactant because both decrease the interfacial curvature of the aggregates.

### 6.3.4 Effect of surfactant concentrations on zero shear viscosity

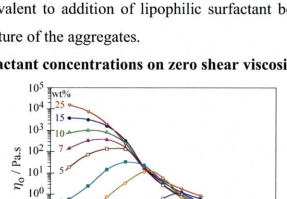


Figure 6-5: Variation of zero shear viscosity ($\eta_0$) as a function of temperature at different concentrations (in wt%) of surfactant in water.

Figure 6-5 shows the variation of $\eta_0$ as a function of temperature at different compositions, including the 1wt% surfactant system described above. At 0.5wt% surfactant concentration, the viscosity of the solution is low, and a gradual but small

increase in viscosity is observed with increasing temperature up to 40 °C; then it decreases with a further increase in temperature and ultimately a phase separation takes place. With a slight increase in surfactant concentration (1wt%), the increase in viscosity with an increase in temperature is clearly visible, with an increase of about 2 orders of magnitude in viscosity upon increasing temperature from 5 to 35 °C. With a further increase in temperature, the viscosity decreases. On the other hand, with an increase in the surfactant composition, the trend of the viscosity-temperature curve is essentially similar but the temperature for the viscosity maximum ($T_{\eta\text{-max}}$) gradually shifts to a lower value, and there is a significant increase in viscosity at temperature below $T_{\eta\text{-max}}$. At a high concentration of surfactant, highly viscoelastic solutions are formed at low temperatures. At a surfactant concentration of 25wt%, the viscosity decreases with increasing temperature from 5 °C, and judging from the trends of curves, $T_{\eta\text{-max}}$ is well below 5 °C but the behavior is essentially the same as that observed at lower concentrations. As can be seen from viscosity-temperature curves, the viscosity of the micellar solution is very sensitive to the concentrations at low temperatures but at and above 25 °C, the viscosity is nearly same over wide range of concentration (2-25wt%).

With increasing surfactant concentration, the degree of hydration of the EO chain decreases, and consequently, the aggregation number increases, in addition to the increase in the number density of the aggregates. The decrease in the hydration would decrease the spontaneous curvature of the aggregate and, therefore, induce a large energy cost for end-cap formation. These factors would favor one-dimensional micellar growth, and, therefore, increase the viscosity. Therefore, the effect of increasing surfactant concentration is similar to that of increasing temperature. Upon an increase of the surfactant concentration, the formation of micellar joints is expected to take place at lower temperature, which can explain the gradual shift of $T_{\eta\text{-max}}$ toward lower temperature.

### 6.3.5 Oscillatory-shear rheological measurement

Oscillatory-shear (frequency-sweep) measurements were performed on the viscoelastic samples formed around the viscosity maximum. Figure 6-6 shows a plot of the elastic modulus ($G'$) and loss modulus ($G''$) as a function of oscillatory-shear frequency ($\omega$) for a sample of a 10% surfactant system at 15, 20 and 25 °C.

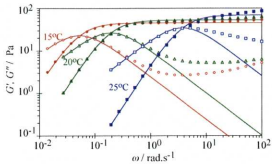


Figure 6-6: Variation of elastic modulus, $G'$ (filled symbols) and viscous modulus, $G''$ (open symbols as a function of oscillatory shear frequency ($\omega$) as obtained by frequency in 10% surfactant system at different temperatures. Fittings to the Maxwellian equations are shown by solid lines.

The result shows that sample is viscoelastic in the timescale of measurement: $G'$-$G''$ crossover occurrs in the low frequency region at 15 °C. In the low-$\omega$ region, the data points of $G'$ and $G''$ could be fitted to Maxwell equations, but in the high-$\omega$ region, the experimental data deviate from the model, which is generally considered to be caused by faster relaxation processes, such as Rouse modes. Maxwellian-type oscillatory rheological behavior of viscous micellar solutions, such as that shown in Figure 6-6, can be related to the transient network formed by the entanglement of wormlike micelles. The data at lower temperatures have not been shown here for the sake of clarity, but they follow a similar trend. It can be seen from the figure that with increasing temperature the plateau value of $G'$ increases which corresponds to an increase in network density. The $G'$-$G''$ crossover frequency shifts to the high-frequency region that suggests faster relaxation processes resulting from the formation of micellar joints, but the network density also increases as indicated by an increase in $G'$ plateau.

The rheological parameters $G_o$ and $\tau_R$ may be obtained by fitting of the experimental data from frequency-sweep measurements, especially the data in low frequency region, to the Maxwell equations. As in the case of the system described in Figure 6-6, $G'$ at the high-$\omega$ region (say $G'_\infty$) usually does not attain a perfect plateau as predicted by Maxwell equations. Instead, $G'_\infty$ is often higher than the value of $G_o$ given by the Maxwell model. Therefore, the values of $G_o$ estimated from Maxwell equations should be considered as the lower limit for the shear modulus. Figure 6-7 shows the variation of $G_o$ and $\tau_R$ as a function of temperature at different surfactant concentrations. It can be seen that $G_o$ increases monotonically with increasing temperature, which may be taken as the evidence of a one-dimensional micellar growth and, consequently, of an increase in the density of the entanglements of the

wormlike micelles with increasing temperature at all concentrations. However, the extent of the increase of $G_0$ with temperature decreases with increasing surfactant concentration. At a 3wt% surfactant concentration, $G_0$ increases by 1 order of magnitude when temperature changes by 20°C, whereas at 25wt% the change is significantly small. At high concentrations, $G_0$ could not be ascertained at higher temperature because the $G'$-$G''$ crossover occurs very near or above the upper working limit of $\omega$ of the instrument. Nevertheless, it can be expected from the trend that the behavior is likely to be similar at higher temperatures as well.

On the other hand, the $\tau_R$ of the viscoelastic solutions at low concentrations, for example, in a 3wt% surfactant system, first increases swiftly with increasing temperature, reaches the maximum value at ~20 °C, and then decreases (Figure 6-7). Upon an increase of the surfactant concentration from 3wt% to 5wt% and above, the trend remains essentially same, but the position of the $\tau_R$ maximum gradually shifts to lower temperature. At higher concentrations of surfactants (*e.g.*, at 10 and 15 wt%), the $\tau_R$ maxima are around 5 °C. At a surfactant concentration of 25wt%, no maximum is seen but $\tau_R$ decreases from 5 °C. However, judging from the trends of the $\tau_R$-$T$ curves, the $\tau_R$-maxima for these concentrations is expected to fall below 5°C. Nevertheless, $\tau_R$ approaches a very large value (e.g., ~ 67 s) for a 25wt% system at 5 °C, which corresponds to the presence of very long micelles.

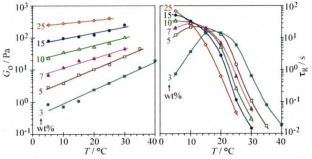


Figure 6-7: Variation of shear modulus ($G_o$) and stress relaxation time ($\tau_R$) as a function of temperature at different surfactant concentrations (in wt%).

The observed trend in $\tau_R$ clearly shows that with increasing temperature some structural changes occur in the network, which allows the system to release the stress quickly. The shortening of micelles is ruled out because the monotonous increase in $G_0$ clearly indicates that network density increases with temperature. These results are consistent with the formation of micellar joints or branching because sliding of the branching point along the micellar length can provide a fast stress relaxation mechanism.

The scaling relationship of different rheological parameters with volume fraction of surfactant ($\phi$) is based on the uncharged polymer solution. The validity of scaling relationships to the wormlike micellar system has been tested only in the systems of ionic surfactants in the presence of counterions. The present nonionic surfactant system would be an appropriate system to check the validity of the scaling relationships. Figure 6-8 shows the variation of $\eta_o$, $G_o$, and $\tau_R$ with the weight fraction of surfactant in system ($w$) at fixed temperature (5 °C). Since $w$ is proportional to $\phi$, the exponents of the scaling relationships can be evaluated from such plots. Note that systems with branched micelles have lower values of viscosity and relaxation time than those of the systems of unbranched micelles, and therefore, exhibit different scaling behavior. Hence, the data points corresponding to 25wt% system have not been included in the plot shown in Figure 6-8. The exponents of $\eta_o$ and $G_o$ evaluated from the experimental data are larger than the theoretical values, whereas the exponent of $\tau_R$ is very close to the theoretical value. The exponents of the power laws decrease with increasing temperatures. Scaling relationships with lower values of exponents (viz., $\eta_o \approx w^{3.4}$, $G_o \approx w^{2.9}$, and $\tau_R \approx w^{0.4}$ at 10 °C and $\eta_o \approx w^{2.2}$, $G_o \approx w^{2.5}$, and $\tau_R \approx w^{-0.3}$ at 15 °C ) come from the increase in the number density of the micellar joints and gradual shift toward the formation of saturated network.

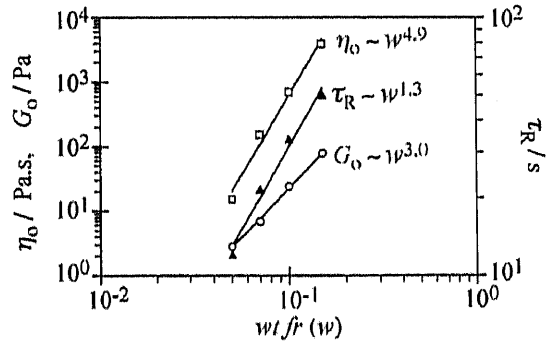


Figure 6-8: Variation of $\eta_o$, $G_o$ and $\tau_R$ as a function of surfactant weight fraction ($w$) at 5 °C. The scaling relations of each of the parameters are shown next to the corresponding data series. For the scaling relations at other temperatures see text.

Figure 6-9 shows the variation of $G''_{min}/G_o$ with temperature at surfactant concentrations of 7, 10 and 15wt%. At higher temperature (>20 °C) and lower surfactant concentrations, not enough data points are available because the minima in the $G''$ could not be obtained within the frequency range of measurement, and therefore, $G''_{min}/G_o$ are not available. At a surfactant concentration of 7wt%, the parameter decreases with increasing temperature up to 15 °C, which corresponds

approximately to $T_{\eta\text{-max}}$ for the series, and then increases. The minimum becomes increasingly shallow with increasing concentration and shifts gradually to the lower temperature. The minimum corresponds to the related minimum in the $l_e/L$. The parameter $l_e$ and, from there, $L$ can be estimated, provided that $l_p$ is known. However, $l_p$ is not available for the fluorinated nonionic surfactant system. If we assume that $l_e$ is approximately constant within the range of temperature (5-20 °C), the minimum in $G''_{min}/G_o$ correspond to the maximum in $L$.

The variation of $G''_{min}/G_o$ as a function of weight fraction of surfactant at 5 °C, as well as at higher temperatures (10 and 15 °C), is shown in the inset of Figure 6-9. It can be seen that power-law exponents are temperature dependent. The magnitude of the exponent decreases with increasing temperature, and it approaches to zero at 20 °C; although the plot at this temperature is not shown in the inset for the sake of clarity, it is clearly evident from the $G''_{min}/G_o - T$ plot. The decrease in the exponent is related to the formation of micellar joints or branching[49]. The experimental values of the power-law exponent at 10 °C and 15 °C are very close to the theoretical values proposed for linear and saturated aggregates, respectively[10,50-52]but at 5 °C experimental value is higher than the predicted value.

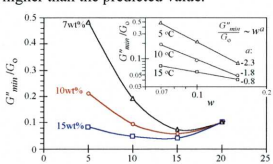


Figure 6-9: Variation of $G''_{min}/G_o$ as a function of temperatures at different surfactant concentration. The plot of $G''_{min}/G_o$ as function of the weight fraction of surfactant, $w$, at different temperature is shown in the inset.

### 6.3.6 DLS

DLS is commonly used as a complementary technique for the study of viscoelastic solutions. As shown in Figure 6-10, in the present system, the normalized autocorrelation function, $g(t)$, shows several decays that can be attributed to different relaxation processes, as typically found in worm-like micellar systems. At 15 °C, $g(t)$ becomes zero at very long times, almost out of the experimental window, indicating that the system is somewhat "frozen" and nearly nonergodic. In fact, slow relaxation times diverge at the gel point[53]. However, the time for which $g(t) = 0$ tends to shift to

lower values as temperature is increased over 25 °C, indicating faster relaxation, which is in agreement with the change of viscoelatic properties with temperature presented in previous sections. At 45 °C, near the surfactant cloud point at the given concentration, the shift of the fast decay to the right becomes evident. A similar behavior has been found in other nonionic wormlike micelles[48], and was attributed to the formation of structures with low curvature. But in the present case, there is an additional factor, which is the onset of attractive interactions as nonionic surfactants approach the cloud poin[54]. The general trend of Figure 6-10 is different from other nonionic micellar systems which form globular micelles at low temperatures and give $g(t)$ values that can be closely fitted by single exponentials[48].

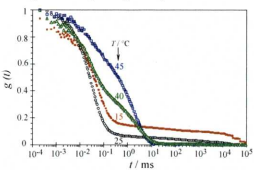


Figure 6-10: Normalized autocorrelation function $g(t)$ for different temperatures in 5 wt% EF122B aqueous systems. The detection angle is 90 degrees.

As can be seen in Figure 6-11a for two representative temperatures, the CONTIN analysis of $g(t)$ gives three relaxation modes, similar to other systems in which worm-micelles are present[27,55-58]. At temperatures below 25 °C, it is difficult to define precisely the distribution peak corresponding to the slow mode because the associated relaxation time is very long and falls out of the experimental limit. At low temperatures, the fastest mode is also the one with the highest contribution to the distribution of relaxation times. It was found that the inverse of the relaxation time associated with this mode changes linearly with the square of the scattering vector, namely, $\tau^{-1} = Dq^2$, where $D$ is the diffusion coefficient. In other words, the fastest mode is diffusive, and may be attributed to the diffusion of micelles. Moreover, the peak maximum of this mode corresponds to a hydrodynamic length (estimated by the Stokes-Einstein equation) that shows some increase (from 4 to 6 nm) with temperature from 15 to 40 °C. It is known that nonentangled nonionic micelles show strong micellar growth as temperature is increased[54,59,60]. It is interesting to note that the mentioned length is similar to that obtained for the cross sectional diameter of micelles according to SAXS calculations. With consideration of the polydispersity of

the wormlike micellar systems, it has been argued that fast modes in wormlike micellar systems might correspond to the diffusion of aggregates with low-axial ratios, which coexist with long micelle[27,55]. This coexistence has already been confirmed for ionic fluorosurfactants by Transmission Electron Microscopy (TEM)[17] and inferred from DLS measurements[61]. Accordingly, small aggregates would have a size close to the diameter of hemispherical endcaps of worm-like micelles.

The other two modes (medium and slow) at low temperatures do not follow the linear $\tau^{-1}$ vs $q^2$ relationship, and therefore they cannot be considered diffusive. This in agreement with previous reports on wormlike micelles[57,58]. The range of distribution times covered by the medium mode are in the same scale of the lifetime of transient connections between wormlike micelles found by Kato[62] and other authors[57,58]. The medium mode is theoretically predicted for entangled polymer solutions and has been assigned to the Rouse mode[63], which is estimated to be smaller than the slow reptational mode, as is in the present case at low temperatures. However, this is not always the case[57]. From the position of the medium mode, values of hydrodynamic length ranging from 1 to 2 μm are estimated, namely, the change with temperature is not very large. However, as temperature is increased, the medium mode prevails over the fastest mode and the third mode tends to disappear. To better illustrate this point, the relative the contributions of fast ($A_f$), medium ($A_m$), and slow ($A_s$) modes to the distributions of relaxation times as a function of temperature are plotted as $A_m / A_f$ and $A_s / A_m$ in Figure 6-11b.The fact that the medium mode is by far the most significant at high temperatures, as expressed by the increase in $A_m / A_f$ ratio, indicates that it is related to large structures, probably having junctions that are not stable enough to generate a slow relaxation mode. This would be in agreement with the formation of branched aggregates and the resultant loss of viscoelastic properties at high temperatures. Note the sharp increase of the $A_f / A_m$ ratio as the system approaches the cloud point and the onset of micellar interactions.

On the other hand, the decrease in the contribution of the fast mode could indicate that small aggregates have been converted to larger ones with the increase in temperature. Another possibility is that this mode is also related in some way to the micellar end caps, the number of which would decrease as micellar joints and branches are formed to decrease the energy penalty derived from the unfavorable curvature of those caps.

Although it should be mentioned again that there are some inaccuracies in the determination of the amplitude and position of the distribution peak related to the slow mode at low temperatures because of the time scale of the experiment, there is a correlation between the decrease in $A_s$ / $A_m$ ratio and the decrease in viscosity and the loss of viscoelastic properties as temperature is increases, which supports the assignment of this mode to the presence of long range networks[64].

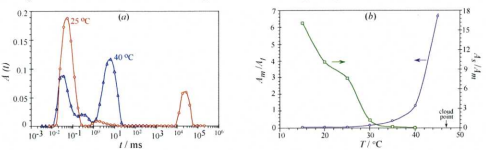


Figure 6-11: (a) Distribution of relaxation times estimated by CONTIN method in 5 wt% EF122B aqueous system at different temperature. The detection angle is 90 degrees. (b) Relative contributions of fast ($A_f$), medium ($A_m$), and slow ($A_s$) modes to the distributions of relaxation times as a function of temperature. The continuous lines are only for visual guide.

### 6.4 Conclusions

Fluorinated surfactants tend to form aggregates with low curvature, such as cylindrical aggregates, at a solution conditions where hydrocarbon surfactants would form spherical aggregates. A nonionic fluorinated surfactant, perfluoroalkyl sulfonamide ethoxylate, forms flexible cylindrical aggregates in water even at low-surfactant concentrations and low temperature, and with an increase in the surfactant concentration, these cylindrical micelles undergo one-dimensional growth and form very long and flexible wormlike micelles which entangle and form a network making viscoelastic solution. The dynamic rheological behavior can be described by the Maxwell model at low-shear frequency, which is typical behavior of wormlike micellar solution. With successive increase in the surfactant concentration, the aggregates loose the flexibility and transform into hexagonal liquid crystalline phase. An increase in the temperature of the nonionic surfactant system reduces the interfacial curvature and induces micellar growth, which is mainly attributed to the progressive increase in the energy cost for the formation of the hemispherical end caps of the aggregates. Therefore, the viscosity increases with temperature. Above a certain temperature, viscosity begins to decrease, not because of the shrinking of micelles but because the system tends to eliminate the free ends by forming micellar

joints in the network and such changes in the microstructure result in a decrease in the viscosity and stress relaxation time, but the network structure is retained. Variation of the rheological parameters is in agreement, and SAXS provides a direct evidence of such microstructural changes. The temperature at which the viscosity begins a decline shifts gradually toward lower values when the surfactant concentration increases because both have similar effects on the interfacial curvature. The rheological parameters, $\eta_o$ and $G_o$, show scaling relationships with surfactant concentrations with exponents greater than the values predicted by the living-polymer model, but the exponent of $\tau_R$ is in agreement with the theory. Finally, DLS measurements indicate the presence of fast relaxation modes, associated with micelles, and medium and slow modes, associated with transient networks. The disappearance of the slow mode and the predominance of the medium mode as temperature is increased give support to the conclusions derived from SAXS and rheometry.

**References**


1 Shinoda, K.; Hato, M.; Hayashi, T. *J. Phys. Chem.* **1972**, *76*, 909.

2 Kunieda, H.; Shinoda, K. *J. Phys. Chem.* **1976**, *80*, 2468.

3 Israelachvili, J. N.; Mitchell, D. J.; Ninham, B. W. *J. Chem. Soc. Faraday Trans.* 2, **1976**, *72*, 1525.

4 Tanford, C. The Hydrophobic Effect: Formation of Micelles and Biological Membranes, 2nd ed.; John Wiley & Sons: New York, **1980**.

5 El Moujahid, C.; Ravey, J. C.; Schmitt, V.; Stébé, M. J. Colloid Surf. A **1998**, *136*, 289.

6 Rehage, H.; Hoffmann, H. *J. Phys. Chem.* **1988**, *92*, 4712.

7 Kern, F.; Lemarechal, P.; Candau, S. J.; Cates, M. E. *Langmuir* **1992**, *8*, 437.

8 Clausen, T. M.; Vinson, P. K.; Minter, J. R.; Davis, H. T.; Talmon, Y.; Miller, W. G. *J. Phys. Chem.* **1992**, *96*, 474.

9 Khatory, A.; Kern, F.; Lequeux, F; Appell, J.; Porte, G.; Morie, N.; Ott, A.; Urbach, W. *Langmuir* **1993**, *9*, 933.

10 Khatory, A.; Lequeux, F; Kern, F.; Candau, S. J. *Langmuir* **1993**, *9*, 1456.

11 Berret, J.-F.; Appell, J.; Porte, G. *Langmuir* **1993**, *9*, 2851.

12 Lin, Z.; Cai, J. J.; Scriven, L. E.; Davis, H. T. *J. Phys. Chem.* **1994**, *98*, 5984.

13 Soltero, J. F. A.; Puig, J. E.; Manero, O.; Schulz, P. C. *Langmuir* **1995**, *11*, 3337.

14 Soltero, J. F. A.; Puig, J. E.; Manero, O. *Langmuir* **1996**, *12*, 2654.

15 Narayanan, J.; Manohar, C.; Kern, F.; Lequeux, F.; Candau, S. J. *Langmuir* **1997**, *13*, 5235.

16 Hassan, P. A.; Candau, S. J.; Kern, F.; Manohar, C. *Langmuir* **1998**, *14*, 6025.

17 Wang, K.; Karlsson, G.; Almgren, M.; Asakawa, T. *J. Phys. Chem. B* **1999**, *103*, 9237.

18 Knoblich, A.; Matsumoto, M.; Murata, K.; Fujiyoshi, Y. *Langmuir* **1995**, *11*, 2361.

19 Hoffmann, H.; Würtz, J. *J. Mol. Liquids* **1997**, *72*, 191.

20 Abe, M.; Tobita, K.; Sakai, H.; Kondo, Y.; Yoshino, N.; Kasahara, Y.; Matsuzawa, H.; Iwahashi, M.; Momozawa, N.; Nishiyama, K. *Langmuir* **1997**, *13*, 2932.

21 Tobita, K.; Sakai, H.; Kondo, Y.; Yoshino, N.; Iwahashi, M.; Momozawa, N.; Abe, M.; *Langmuir* **1997**, *13*, 5054.

22 Tobita, K.; Sakai, H.; Kondo, Y.; Yoshino, N.; Kamogawa, K.; Momozawa, N.; Abe, M.; *Langmuir* **1998**, *14*, 4753.

23 Danino, D.; Weihs, D.; Zana, R.; Orädd, G.; Lindblom, G.; Abe, M.; Talmon, Y. *J. Colloid Interface Sci.* **2003**, *259*, 382.

24 Acharya, D. P.; Kunieda, H. *J. Phys. Chem. B* **2003**, *107*, 10168.

25 Acharya, D. P.; Hossain, Md. K.; Jin-Feng, Sakai, T.; Kunieda H. *Phys. Chem. Chem. Phys.* **2004**, *6*, 1627.

26 Naito, N.; Acharya, D. P.; Tanimura, K.; Kunieda, H. *J. Oleo Sci.* **2004**, *53*, 599.

27 Maestro, A.; Acharya, D.P.; Furukawa, H.; Gutiérrez, J. M.; López-Quintela, M. A.; Ishitobi, M.; Kunieda, H. *J. Phys. Chem. B* **2004**, *108*, 14009.

28 Herb, C. A.; Chen, L. B.; Sun, W. M. In *Structure and Flow in Surfactant Solutions*; Herb, C. A.; Prud'homme, R. K., Eds.; ACS Symposium Series 578, American Chemical Society, Washington, DC, **1994**, 153.

29 Rodriguez, C.; Acharya, D. P.; Hattori, K.; Sakai, T.; Kunieda, H. *Langmuir* **2003**, *19*, 8692.

30 Acharya, D. P.; Hattori, K.; Sakai, T.; Kunieda, H. *Langmuir* **2003**, *19*, 9173.

31 Acharya, D. P.; Sato, T.; Singh Y.; Kunieda, H. *J. Phys. Chem B* **2006**, *110*, 754.

32 Acharya, D. P.; Shiba, Y.; Aratani, K.-i. Kunieda, H. *J. Phys. Chem. B.* **2004**, *108*, 1790.

33 Sato, T.; Hossain, Md. K.; Acharya, D. P.; Glatter, O.; Chiba, A.; Kunieda, H. *J. Phys. Chem. B* **2004**, *108*, 12927.

34 Sharma, S. C.; Kunieda, H.; Esquena, J.; Rodríguez Abreu, C. *J. Colloid Interface Sci.* **2006**, *299*, 297.

35 Pusey, P. N.; Fijnaut, H. M.; Vrijm, A. *J. Chem. Phys.* **1982**, *77*, 4270.

36 Salgi P.; Rajagopolan, R. *Adv. Colloid Interface Sci.* **1993**, *43*, 169.

37 Mitchell, D. J.; Tiddy, G. J. T.; Waring, L.; Bostock, T.; MacDonald, M. P. *J. Chem. Soc. Faraday Trans. I* **1983**, *79*, 975.

38 Esquena, J.; Rodríguez, C.; Solans C.; Kunieda, H. *Micropor. Mesopor. Mater.* **2006**, *92*, 212.

39 Candau, S. J.; Oda, R. Colloid Surf. A: Physicochem. Eng. Aspects **2001**, *183-185*, 5.

40 Lin, Z. *Langmuir* **1996**, *12*, 1729.

41 Danino D.; Talmon, Y.; Levy, H.; Beinert, G.; Zana, R. *Science* **1995**, *269*, 1420.

42 In M.; Aguerre-Chariol, O.; Zana, R. *J. Phys. Chem. B* **1999**, *103*, 7747.

43 Zana, R. *Adv. Colloid Interface Sci.* **2002**, *97*, 205.

44 Zilman, A. G.; Safran, S. A. *Phys. Rev. E* **2002**, *66*, 051107.

45 Dan, N.; Safran, S. A. *Adv. Colloid Interface Sci.* **2006**, in press.

46 Zilman, A.; Safran, S. A.; Sottmann, T.; Strey, R. *Langmuir* **2004**, *20*, 2199.

47 Blin, J. L.; Lesieur, P.; Stébé, M. J. *Langmuir* **2004**, *20*, 491.

48 Moitzi, C.; Freiberger, N.; Glatter, O. *J. Phys. Chem. B* **2005**, *109*, 16161.

49 Kern, F.; Lequeux, F.; Zana, R.; Candau, S. J. *Langmuir* **1994**, *10*, 1714.

50 Drye, T. J.; Cates, M. E. *J. Chem. Phys.* **1993**, *98*, 9790.

51 Lequeux, F. *Europhys. Lett.* **1992**, *19*, 675.

52 Majid, L. J. *J. Phys. Chem. B* **1998**, *102*, 4064.

53 Munch, J. P.; Ankrim, M.; Hild, G.; Candau, S. *J. Phys Lett.* **1983**, *44*, 73.

54 Glatter, O.; Fritz, G.; Lindner, H.; Brunner-Popela, J.; Mittelbach, R.; Strey, R.; Stefan U. Egelhaaf, S. U. *Langmuir* **2000**, *16*, 8692.

55 Rodriguez-Abreu, C.; Aramaki, K.; Tanaka, Y.; Lopez-Quintela, M.A.; Ishitobi, M.; Kunieda, H. *J. Colloid Interface Sci.* **2005**, *291*, 560.

56 Duval, M.; Waton, G; Schosseler, F. *Langmuir* **2005**, *21,* 4904.

57 Buhler, E.; Oelschlaeger, C.; Waton, G.; Candau, S. J. *J. Phys. Chem. B* **2004**, *108,* 11236.

58 Buhler, E.; Munch, J. P.; Candau, S. J. *J. Phys. II Fr.* **1995**, *5*, 765.

59 Imanishi, K.; Einaga,Y. *J. Phys. Chem. B* **2005**, *109,* 7574.

60 Brown, W.; Rymdiin, R. *J. Phys. Chem.* **1987**, *91,* 3565.

61 Oelschlaeger, Cl,; Waton, G.; Buhler, E.; Candau, S. J.; Cates, M.E. *Langmuir* **2002**, *18,* 3076.

62 Kato,T.; Nozu, D. *J. Mol. Liq.* **2001**, *90* ,167.

63 Semenov, A. N. *Physica A* **1990**, *166*, 263.

64 Blanco, M.C.; Leisner, D.; Vazquez, C.; Lopez-Quintela, M.A. *Langmuir* **2000**,*16,* 8585.

## Chapter 7: Conclusions

Fluorinated amphiphiles are known to possess unique properties. They are chemically and thermally more stable and have lower intermolecular interactions, hence display lower surface tension than any of their hydrocarbon counterparts. In contrast to the extensive knowledge on hydrocarbon type amphiphiles, the phase behavior of fluorinated amphiphiles has been much less explored. The highly diversified industrial uses of fluorinated amphiphiles continue to be rich area of study. In this context, a systematic study on the interfacial properties of aqueous solutions of fluorinated amphiphiles, phase behavior of fluorinated amphiphiles or mixed fluorinated amphiphiles in water and temperature induced viscosity growth in a water-surfactant binary system of a nonionic fluorinated surfactant at various concentrations was carried out.

In chapter 3, it was clarified that cloud temperature of amphiphilic fluorinated random copolymers aqueous solutions depends upon the fluorocarbon chain length, the polyoxethylene chain length and the ratio of the numbers of polyoxyethylene to fluorocarbon chain lengths. The copolymers become increasingly surface active as fluorocarbon chain length as well as polyoxyethylene chain length decrease.

In chapter 4, it was shown that nonionic fluorocarbon surfactant shows significantly low values for both CMC and surface tension at CMC. The dynamic behavior of such surfactant system can be characterized by more than one relaxation mechanism. High elasticity of the air-liquid interface for more hydrophobic nonionic fluorocarbon surfactant can be seen.

In chapter 5, the phase behavior and microstructure of aqueous mixture of fluorinated surfactant and fluorinated polymeric oil was understood. A considerable amount of surfactant can be solubilized in the polymer aggregates whereas polymer molecules are practically insoluble in the surfactant lamellar phase because of the large size difference between the two components. The transformation of the viscoelastic surfactant solution into low viscosity Newtonian liquid with increasing solubilization of the polymeric oil is attributed to a rod-sphere transition.

In chapter 6, it was shown that nonionic fluorinated surfactant forms flexible cylindrical aggregates in water even at low surfactant concentrations and low temperature, and with increasing surfactant concentration these cylindrical micelles

undergo one-dimensional growth and form very long and flexible wormlike micelles which entangle and form a network making viscoelastic solution. An increase in temperature of the nonionic surfactant system reduces the interfacial curvature, induces micellar growth and hence viscosity increases with temperature. Above a certain temperature, the system tends to eliminate the hemispherical end caps of the aggregates by forming micellar joints in the network and such changes in the microstructure result in a decrease in the viscosity.

In summary, the cause of decreasing hydrophobicity of amphiphilic fluorinated copolymers with decreasing fluorocarbon chain length should be addressed precisely. Low miscibility of fluorinated polymeric oil in fluorinated surfactant is caused by the difference in molecular weight between the two components. The rheological behavior of the viscoelastic micellar solution of nonionic fluorinated surfactant can be controlled by tuning the temperature.

**Scientific Publications**

**A. Papers used in this thesis**

1. Phase Behavior and Surface Tensions of Amphiphilic Fluorinated Random Copolymer Aqueous Solutions. **Suraj Chandra Sharma**, Durga P. Acharya, Miguel García-Roman, Yasuo Itami, and Hironobu Kunieda. *Colloids Surf. A* **2006**, *280*, 140-145.
2. Interfacial Properties of Aqueous Nonionic Fluorocarbon Surfactant Solutions. **Suraj Chandra Sharma**, Lok Kumar Shrestha, and Kenji Aramaki. *J. Dispersion Sci. & Technol.* (Accepted for publication)
3. Phase Behaviors and Preparation of Mesoporous Silica in Aqueous Mixtures of Fluorinated Surfactant and Hydrophobic Fluorinated Polymer. **Suraj Chandra Sharma**, Hironobu Kunieda, Jordi Esquena, and Carlos Rudríguez-Abreu. *J. Colloid Interface Sci.* **2006**, *299*, 297-304.
4. Viscoelastic Micellar Solutions in Nonionic Fluorinated Surfactant Systems. Durga P. Acharya, **Suraj Chandra Sharma,** Carlos Rudríguez-Abreu, and Kenji Aramaki. *J. Phys. Chem. B* **2006**, *110*, 20224-20234.

**B. Other publications (not used in the thesis)**

1. Aqueous foam stabilized by dispersed surfactant solid and lamellar crystalline phase. Lok Kumar Shrestha, Durga P. Acharya, **Suraj Chandra Sharma**, Kenji Aramaki, Hiroshi Asaoka, Keiichi Ihara, Takeshi Tsunehiro and Hironobu Kunieda. *J. Colloid Interface Sci.* **2006**, *301*, 274-281.
2. Formation of lamellar silica from lyotropic liquid crystals of dodecyl benzene sulfonic acid. Carlos Rodríguez, **Suraj ChandraSharma** and Kenji Aramaki. *J. Dispersion Sci. & Technol.* (Accepted for publication)

**Presentation of Scientific Papers in Conferences:**

1. **Suraj Chandra Sharma**, Durga P. Acharya, Kenji Aramaki and Hironobu Kunieda. "Formation of Viscoelastic Micellar Solution in Nonionic Fluorinated Surfactant Solution." The 59$^{th}$ Divisional Meeting on Colloid and Interface Chemistry, The Chemical Society of Japan, International Symposium, September 13-15, 2006, Hokkadio University, Sapporo, Japan.
2. **Suraj Chandra Sharma**, Durga P. Acharya, Kenji Aramaki and Hironobu Kunieda. "Phase and Rheological Behavior of Viscoelastic Wormlike Micellar Solutions Formed in Nonionic Fluorinated Surfactant-Water System." The 16$^{th}$

International Symposium on Surfactants in Solution, June 4-9, 2006, Seoul, Korea.

3. **Suraj Chandra Sharma**, Carlos Rodriguez, Kenji Aramaki and Hironobu Kunieda. "Phase and Rheological Behavior in Aqueous Mixtures of Fluorinated Surfactant and Hydrophobic Fluorinated polymer."Annual Meeting of The Chemical Society of Japan, March 27-30, 2006, Nihon University, Tokyo, Japan.
4. **Suraj Chandra Sharma**, Durga P. Acharya, Yasuo Itami and Hironobu Kunieda. "Phase Behavior, Equilibrium and Dynamic Surface Tension Properties of Aqueous Solution of Amphiphilic Fluorinated Random Copolymers." The 58$^{th}$ Divisional Meeting on Colloid and Interface Chemistry, The Chemical Society of Japan, September 8-10, 2005, Utsunomiya University, Utsunomiya, Japan.

## Acknowledgement

I would like to pay rich tributes to late Prof. Hironobu Kunieda for his guidance, encouragement and inspiration during the initial stage of my Ph.D. course. I am pleased and honored to have worked with my supervisor Associate Prof. Kenji Aramaki, Graduate School of Environment and Information Sciences, Yokohama National University. I would like to thank him deeply from my heart for his advice and support. I am thankful to the Ministry of Education and Culture, the government of Japan for providing scholarship during the period of study.

I am also grateful to Professors Takao Hara, Takeshi Meguro, Atsushi Suzuki, Ken-ichi Kurumada for participating in the evaluation committee and for revising and correcting this thesis.

Carlos Rudríguez-Abreu needs to be thanked for many discussions on variety topics regarding my work. Thanks to my all group colleagues, for the co-operation extended toward me.